NASA/TM-20210000913

A Summary of Normal Incidence Tube Tests of NASA's Bio-Inspired Broadband Acoustic Absorber

L. Danielle Koch, Peter J. Bonacuse, J. Chris Johnston, Maria A. Kuczmarski, and Christopher J. Miller
Glenn Research Center, Cleveland, Ohio

Michael G. Jones
Langley Research Center, Hampton, Virginia

June 2021

NASA STI Program . . . in Profile

Since its founding, NASA has been dedicated to the advancement of aeronautics and space science. The NASA Scientific and Technical Information (STI) Program plays a key part in helping NASA maintain this important role.

The NASA STI Program operates under the auspices of the Agency Chief Information Officer. It collects, organizes, provides for archiving, and disseminates NASA's STI. The NASA STI Program provides access to the NASA Technical Report Server—Registered (NTRS Reg) and NASA Technical Report Server—Public (NTRS) thus providing one of the largest collections of aeronautical and space science STI in the world. Results are published in both non-NASA channels and by NASA in the NASA STI Report Series, which includes the following report types:

- TECHNICAL PUBLICATION. Reports of completed research or a major significant phase of research that present the results of NASA programs and include extensive data or theoretical analysis. Includes compilations of significant scientific and technical data and information deemed to be of continuing reference value. NASA counter-part of peer-reviewed formal professional papers, but has less stringent limitations on manuscript length and extent of graphic presentations.

- TECHNICAL MEMORANDUM. Scientific and technical findings that are preliminary or of specialized interest, e.g., "quick-release" reports, working papers, and bibliographies that contain minimal annotation. Does not contain extensive analysis.

- CONTRACTOR REPORT. Scientific and technical findings by NASA-sponsored contractors and grantees.

- CONFERENCE PUBLICATION. Collected papers from scientific and technical conferences, symposia, seminars, or other meetings sponsored or co-sponsored by NASA.

- SPECIAL PUBLICATION. Scientific, technical, or historical information from NASA programs, projects, and missions, often concerned with subjects having substantial public interest.

- TECHNICAL TRANSLATION. English-language translations of foreign scientific and technical material pertinent to NASA's mission.

For more information about the NASA STI program, see the following:

- Access the NASA STI program home page at http://www.sti.nasa.gov

- E-mail your question to help@sti.nasa.gov

- Fax your question to the NASA STI Information Desk at 757-864-6500

- Telephone the NASA STI Information Desk at 757-864-9658

- Write to:
  NASA STI Program
  Mail Stop 148
  NASA Langley Research Center
  Hampton, VA 23681-2199

NASA/TM-20210000913

A Summary of Normal Incidence Tube Tests of NASA's Bio-Inspired Broadband Acoustic Absorber

L. Danielle Koch, Peter J. Bonacuse, J. Chris Johnston, Maria A. Kuczmarski, and Christopher J. Miller
Glenn Research Center, Cleveland, Ohio

Michael G. Jones
Langley Research Center, Hampton, Virginia

National Aeronautics and
Space Administration

Glenn Research Center
Cleveland, Ohio 44135

June 2021

Acknowledgments

NASA's Advanced Air Transport Technology (AATT) project supported this work. Thanks, too, to Carl Blaser at NASA Glenn Research Center for his assistance with the design of the fully three-dimensional geometries with baseplates.

This work was sponsored by the Advanced Air Vehicle Program at the NASA Glenn Research Center

Level of Review: This material has been technically reviewed by technical management.

Available from

NASA STI Program
Mail Stop 148
NASA Langley Research Center
Hampton, VA 23681-2199

National Technical Information Service
5285 Port Royal Road
Springfield, VA 22161
703-605-6000

This report is available in electronic form at http://www.sti.nasa.gov/ and http://ntrs.nasa.gov/

A Summary of Normal Incidence Tube Tests of NASA's Bio-Inspired Broadband Acoustic Absorber

L. Danielle Koch, Peter J. Bonacuse, J. Chris Johnston, Maria A. Kuczmarski, and Christopher J. Miller
National Aeronautics and Space Administration
Glenn Research Center
Cleveland, Ohio 44135

Michael G. Jones
National Aeronautics and Space Administration
Langley Research Center
Hampton, Virginia 23681

Abstract

Motivated by the need to reduce noise pollution from aircraft engines, NASA has continued to design, manufacture and test recently patented structures that mimic the geometry and the broadband and low frequency acoustic absorption of assemblies of natural reeds. This report documents a screening test, which is a precursor to more controlled modelling experiments. The purpose of this experiment was to identify variables and prototype design features that might play a dominant role in the acoustic performance of these structures. To date, 24 prototypes, each with an overall shape of a cube (nominally 50 by 50 by 50 mm), were designed and additively manufactured from thermoplastics using a Fused Filament Fabrication technique. The prototypes were tested in the NASA Glenn and Langley Normal Incidence Tubes to experimentally determine the acoustic absorption as a function of frequency from 400 to 3000 Hz. Results indicate that a variety of structures exhibit substantial acoustic absorption in that frequency range, with an average absorption coefficient greater than 0.6, especially in the frequency range of 400 to 1000 Hz. Six basic prototype designs were chosen to inform future modeling research. Results of these experiments can be used to evaluate existing physics-based models of the interaction of sound waves with these structures or to develop new models. Validated physics-based models of these structures can help engineers optimize the designs for different commercial noise control applications.

1.0 Introduction

Transportation is a dominant source of anthropogenic noise. Since 1960, the number of vehicles used in the United States has roughly tripled according to the United States Bureau of Transportation (Table 1 and Figure 1) (Ref. 1). Just as artificial lights brighten the night sky impairing our view of space, transportation noise raises background sound levels preventing us from hearing the natural sounds of Earth. Maps that estimate the impact of artificial lights (Ref. 2) do resemble the maps that estimate the effect of anthropogenic noise, documenting the consequences of modern human activity across the world (Ref. 3). This co-location of sources of light and sound pollution is understandable, since a common use of artificial light is to illuminate transportation corridors. Noise from vehicles and locomotives is concentrated along roads and railways. Noise from aircraft is concentrated along flight paths near airports but can also impact large areas of rural and protected, road-less wilderness areas. Interactive maps available on the internet, such as the National Transportation Noise Map can estimate and illustrate transportation noise. An example of the map of transportation noise for the Cleveland, Ohio, area is shown in Figure 2 (Ref. 4).

Transportation noise is determined by the sounds produced by individual vehicles, the number of vehicles in operation, the operating conditions of the vehicles, as well as terrain and atmospheric conditions. Focusing in on the air transportation system, in 2018 approximately 7000 commercial aircraft were operated in the United States, nearly one quarter of the world's commercial aircraft , according to the 2018 Annual Report of the International Civil Aviation Organization (ICAO) Council and the United States Bureau of Transportation Statistics (Figure 3) (Refs. 5 and 1). Looking towards the future, the number of aircraft is expected to increase to meet the demand of a rapidly growing world population, while the cost of aircraft fuel is simultaneously expected to increase as non-renewable energy sources become less available (Ref. 6). We are seeking efficient, economically-viable technology that helps reduce the environmental impact of aircraft, reducing pollutants while increasing safety.

ICAO's Noise Policy(Ref. 7) recommends four different approaches that should be explored to reduce aviation related noise pollution: a) identifying and reducing noise sources, b) careful land-use planning around airports, c) using aircraft operational procedures to reduce take-off and landing noise, and as a last resort, d) operating restrictions or curfews.

One way to reduce individual aircraft noise is to install acoustic liners in the duct walls of an aircraft engine that can absorb sounds produced by the engine components before that sound has a chance to propagate to observers on the ground. Acoustic liners in aircraft engines need to absorb sound over a wide frequency range and be able to survive the harsh environment within the engine where the liners are exposed to high-speed airflow, high temperatures, and sprays of water, oil, ice, and debris. Acoustic absorbers that are placed in the comparatively benign environment within the fuselage can be used to protect the health and safety of crew and passengers (Ref. 8).

A variety of acoustic absorbers for aviation applications have been investigated at NASA. NASA has studied multi-layer perforate-over-honeycomb structures that are strong, lightweight, and highly effective broadband acoustic absorbers (Ref. 9). Foam metals have also been studied, with the goal of developing practical multi-use liners that can act as a fan containment as well as an acoustic absorber if placed over a rotor (Refs. 10 and 11). There are ongoing efforts to build broadband acoustic liners from ceramic materials that can absorb the low frequency sounds generated by the machinery in the hot sections of turbofan engines (Ref. 12).

Recently, tests at NASA Glenn and NASA Langley have demonstrated that 2-in. thick bundles of plastic tubes that resemble the irregular geometry of natural reeds are effective at absorbing sounds in the 400 to 3000 Hz range, and particularly below 1000 Hz (Refs. 13 to 15). Many of these prototypes have an average acoustic absorption coefficient greater than 0.6.

This concept has now been described in United States Patent 10,460,714 (Ref. 16). This work was inspired by an observation of the acoustic absorption of natural reeds reported by Oldham, et al. in 2011(Ref. 17).

Six basic prototype designs and nine variants of those designs were designed, manufactured, and tested. A brief description of the acoustic experiments conducted in NASA's normal incidence impedance tubes is given and test results are discussed, in an attempt to determine if any of the designs or their variants showed promise or warranted further consideration. This report serves as a type of catalog with prototype number and normal incidence tube data are presented and compared. Detailed information about prototype geometries is available at this time by contacting the NASA Glenn Technology Transfer Office. In the conclusion section, recommendations for future modeling and prototyping are given.

More controlled, parametric tests using design-of-experiments techniques can be used to determine which variables or combination of variables are important to the acoustic absorption. Results from these tests can be used to evaluate existing physics-based models or to develop new models. Physics-based

models that can describe the interaction of sound waves with these structures can help engineers design and optimize acoustic absorbers for specific applications.

2.0 Description of Prototypes

The nature of this work was exploratory. It can be thought of as both as a design-for-additive manufacturing exercise and a precursor to future efforts to identify physics-based models of the acoustic performance of these structures. Twenty-four prototypes of acoustic absorber structures that mimic natural reeds were designed, manufactured, and tested at NASA. These 24 prototypes were made from six basic designs and nine design variants. The tested combinations of the basic prototype designs and variations are labelled in Table 2. Some of the prototypes consisted of loose parts that need a retainer to hold their shape such as the one shown in Figure 4. Other prototypes were self-supporting and did not need a retainer to hold their shape such as the one shown in Figure 5. Loose and Fixed style prototypes were developed considering the wide variety of noise control constraints and needs in industrial and commercial products. Most designs were printed using ASA thermoplastic on NASA's GRC's Stratasys Fortus 400 mc Fused Deposition Modeler. The Ultem 1010 sample was printed on NASA Langley's Stratasys 900(Ref. 18).

For comparison, two modern styles of acoustic absorbers were chosen. The first baseline, melamine foam 50.8 mm (2 in.) thick, represented technology in common use for architectural noise control. The second baseline, a double-degree-of-freedom (DDOF) Perforate-Over-Honeycomb (POHC) liner, represented noise reduction technology used in turbofan engines. An illustration this type of liner is shown in Figure 6. For this test, the baseline DDOF liner was 38.1 mm (1.5 in.) deep and consisted of several layers. An aluminum perforate sheet that was 1.02 mm (0.04 in.) thick was perforated with 6.35 mm (0.25 in.) diameter round holes to achieve 39% porosity. A wire mesh was tack welded to the honeycomb side of the perforate sheet, which is not shown in the illustration. The wire mesh septum had a DC flow resistance of 400 MKS Rayls and was placed 1.52 mm (0.60 in.) from the rigid backplate.

3.0 Description of Tests

Tests were performed in NASA Glenn Research Center (GRC) and Langley Research Center (LaRC) normal incidence tubes, though not every prototype was tested at both locations. Standardized techniques described by ISO-10534-2 were used (Ref. 19). Figure A.1 to Figure A.77 in Appendix A contain groupings of plots for each prototype, and images for some of the prototypes. For example, Figure A.1 is a plot of acoustic absorption coefficient versus frequency for prototype ASA-2.0. Figure A.2 is a plot of normalized resistance and normalized reactance versus frequency for prototype ASA-2.0. Figure A.3 is a plot of acoustic absorption coefficient versus normalized resistance and normalized reactance. Figure A.4 is a photograph of the ASA-2.0 prototype.

Key observations are listed below and are discussed later in this section. In all of the plots, the measured absorption from three baseline samples are included for comparison: a double-degree-of-freedom perforate-over-honeycomb liner and melamine, and previously published test results of natural reeds tested by Oldham, et al. (Ref. 17) LaRC tested at two sound pressure levels, 120 and 140 dB and GRC tested at 105 dB. Data shown in this corresponds to the 140-dB dataset with a broadband source, since there was little difference between measured absorption for the different levels.

The NASA Langley Normal Incidence Tube (NIT) is a 50.8 by 50.8 mm (2.00 by 2.00 in.) waveguide that contains six 120-W compression drivers to generate a plane-wave sound field that impinges on the surface of the liner and combines with reflections from the liner to create a standing wave pattern. The tube is oriented vertically, with the sample installed at the bottom of the tube. The Two-Microphone

Method (TMM) (Ref. 20 and 21) is used to measure the complex acoustic pressures at two prescribed distances from the liner surface such that the frequency dependence of the no-flow acoustic impedance of the liner can be computed. Broadband noise tests are conducted to measure results at frequencies of 0.4 to 3.0 kHz, with source overall sound pressure levels (OASPLs) of 120 and 140 dB at the reference microphone. Two amplitudes are used so that test liner nonlinearities can be evaluated by determining whether the impedance is a function of the reference SPL.

The NASA GRC normal incidence impedance tube is shown schematically in Figure 7. As shown, the GRC tube is positioned horizontally on a laboratory bench with the speaker on one end and the sample on the other. An equivalent tube is available with a round cross-section. The square tube was used for these experiments since it was easier to install the prototypes that resembled slender reeds and it allowed samples to be interchanged between the LaRC and GRC tubes.

4.0 Discussion of Test Results

Results of the normal incidence impedance tube tests indicate that a variety of bio-inspired acoustic absorber prototypes exhibit desirable acoustic absorption. To help make sense of the large dataset, the acoustic absorption coefficients were averaged over two frequency ranges to get a sense of the broadband and low frequency acoustic performance of these samples: between 500 to 3000 Hz and between 500 to 1000 Hz. Figure 8 shows the average acoustic absorption for the baseline double-degree-of-freedom (DDOF) perforate over honeycomb liner and the melamine compared to the six basic prototype designs: ASA-2.0, ASA-2.1, ASA-2.7, ASA-2.14, ASA-2.19, and ASA-2.21. The data in Figure 8 are arranged in order of descending values of the average absorption between 500 and 3000 Hz.

To view the data another way, the variation of acoustic absorption with frequency for each of the six basic prototype designs are shown in Figure 9. Figure 9 also includes data for the melamine and double degree of freedom liner and the data for natural reeds reported by Oldham (Ref. 17). In this plot we can see that prototypes ASA-2.0, ASA-2.19 and ASA-2.21 absorb sound similar to the natural reeds with a strong peak in absorption in the 500 to 1000 Hz range. All prototypes absorbed more sound than the natural reeds above 1000 Hz, with an average acoustic absorption coefficient greater than 0.6, though not more than the melamine and double degree of freedom liner. These promising observations prompted us to explore a number of design variations to these six basic prototype designs to try to improve the acoustic and structural performance of this concept.

Nine variants to these designs were explored through our attempts to design and fabricate these kinds of structures for the first time (Table 2). Again, this experiment can be considered a screening test, looking for realizable design parameters that can be varied more methodically in future experiments. By developing physics-based models for these structures, we may someday be able to optimize the structures for a set of design constraints. We will step through the data to see what was learned from tests of these variants, and to see if any of these design changes might be promising enough for future research.

4.1 Variant 1

Four prototypes featured design Variant 1. ASA-2.11 was created by applying design Variant 1 to basic prototype design ASA-2.0; ASA-2.4 and ASA-2.5 were created by applying design Variant 1 to basic prototype design ASA-2.1; ASA-2.17 was created by applying design Variant 1 to basic prototype design ASA-2.14. The prototypes with Variant 1 did not perform as well as the basic designs, as shown in Figure 10 which compares averages for the acoustic absorption in two frequency ranges. The data in Figure 10 are arranged in pairs of basic design and the design variant, so that trends can be highlighted. Figure 11 shows acoustic absorption coefficient as a function of frequency for the prototypes with

Variant 1 compared to the baselines. However, there was one exception. While ASA-2.11 did not perform as well as ASA-2.0, the average low frequency absorption of ASA-2.11 was still slightly greater than the baselines between 500 to 1000 Hz.

4.2 Variant 2

Three prototypes featured design Variant 2. ASA-2.18 was created by applying design Variant 2 to basic design ASA-2.0; ASA-2.8 was created by applying design Variant 2 to basic design ASA-2.1; ASA-2.15 was created by applying design Variant 2 to basic design ASA-2.14. Figure 12 compares averages for the acoustic absorption in two frequency ranges. The data in Figure 12 are arranged in pairs of basic design and the design variant, so that trends can be highlighted. Figure 13 shows acoustic absorption coefficient as a function of frequency for the prototypes with Variant 2 compared to the baselines.

Figure 12 and Figure 13 show that designs with Variant 2 might increase the absorption for frequencies below 1000 Hz. Data from ASA-2.8 shows that by adding Variant 2 to the design of ASA-2.1, the peak absorption frequency might be shifted to lower frequencies without increasing overall sample depth. Likewise, data from ASA-2.15 shows that by adding Variant 2 to the design of ASA-2.14 the peak absorption frequency might be shifted to lower frequencies without increasing overall sample depth. We cannot definitively attribute the changes in acoustic absorption with Variant 2 from the data in this experiment since other factors were not sufficiently controlled during the test. More data is needed in this area.

4.3 Variant 3

Two prototypes featured design Variant 3. ASA-2.6 was created by applying design Variant 3 to basic design ASA-2.1; ASA-2.16 was created by applying design Variant 3 to basic design ASA-2.14. Figure 14 compares averages for the acoustic absorption in two frequency ranges to get a sense of the broadband and low frequency acoustic performance of these samples: between 500 to 3000 Hz and between 500 to 1000 Hz. The data in Figure 14 are arranged in pairs of basic design and the design variant, so that the effect of the variant can be highlighted. Figure 15 shows acoustic absorption coefficient as a function of frequency for the prototypes with Variant 3.

Variant 3 was created to try to improve the strength, durability and acoustic absorption of the prototypes. Comparison between ASA-2.1 and ASA-2.6 shown in Figure 14 and Figure 15 indicates Variant 3 may improve the acoustic performance of the basic designs. We cannot definitively attribute the changes in acoustic absorption with Variant 3 from the data in this experiment, however, since we believe there were other factors in the test that were not sufficiently controlled. We are learning through this screening test which features will be important to control and vary in future experiments.

4.4 Variant 4

Three prototypes featured design Variant 4. ASA-2.9, ASA-2.10, and ASA-2.12 were created by applying design Variant 4 to basic design ASA-2.0. Figure 16 compares averages for the acoustic absorption in two frequency ranges to get a sense of the broadband and low frequency acoustic performance of these samples: between 500 to 3000 Hz and between 500 to 1000 Hz. Figure 17 shows acoustic absorption coefficient as a function of frequency for the prototypes with Variant 4 compared to the baselines.

One of the best performing prototypes was ASA-2.9, as shown in Figure 16 and Figure 17. Data from prototype ASA-2.9 indicates that there is potential for increasing the acoustic absorption by applying design Variant 4 modifications to the basic geometries.

4.5 Variant 5

Two prototypes featured design Variant 5. ASA-2.3 and ASA-2.5 were created by applying design Variant 5 to basic design ASA-2.1. Average acoustic absorption coefficients for these prototypes compared to baselines is shown in Figure 18 and the variation of absorption with frequency is shown in Figure 19.

Changing the designs with Variant 5 was one way that the team explored different design and manufacturing processes. Variant 5 did change the characteristics of the absorption spectra, but did not seem to improve the acoustic performance of the baseline designs. Still, valuable insight was gained by the attempt to design and then manufacture prototypes with design Variant 5, which can be used to guide future modeling research.

4.6 Variant 6

Two prototypes featured design Variant 6. ASA-2.20 was created by applying design Variant 6 to basic design ASA-2.19; ASA-2.22 was created by applying design Variant 6 to basic design ASA-2.21. ASA-2.20 was designed but was not manufactured at the time of this report, so data for ASA-2.22 is included in the plots. Figure 20 compares averages for the acoustic absorption in two frequency ranges to get a sense of the broadband and low frequency acoustic performance of these samples: between 500 and 3000 Hz and between 500 and 1000 Hz. The data in Figure 20 are arranged in order of descending values of the average absorption between 500 and 3000 Hz. Figure 21 shows acoustic absorption coefficient as a function of frequency for the prototypes with Variant 6.

The performance of these prototypes is very similar, looking at the trends in the averages, as shown in Figure 20. Taking a closer look at Figure 21, the absorption curve shifts towards the right, lowering the maximum low frequency absorption and increasing the maximum high frequency absorption. As mentioned throughout this paper, one thing we learned through this experiment was that it is important to identify and control a number of parameters during the test to help develop accurate models.

4.7 Variant 7

Two prototypes featured design Variant 7. ASA-2.2 was created by applying design Variant 7 to basic design ASA-2.21; ASA-2.13 was created by applying design Variant 7 to basic design ASA-2.14. Figure 22 compares averages for the acoustic absorption in two frequency ranges to get a sense of the broadband and low frequency acoustic performance of these samples: between 500 and 3000 Hz and between 500 and 1000 Hz. The data in Figure 22 are arranged in order of descending values of the average absorption between 500 and 3000 Hz. Figure 23 shows acoustic absorption coefficient as a function of frequency for the prototypes with Variant 7.

Variant 7 was another way that the team explored different design and manufacturing processes. These prototypes were mostly valued for the prototype design insight gained, since this design modification did not seem to enhance the acoustic performance of the basic prototype designs.

4.8 Variant 8

Three prototypes featured design Variant 8. ASA-2.0.1 was created by applying design Variant 8 to basic design ASA-2.0; ASA-2.19.1 was created by applying design Variant 8 to basic design ASA-2.1; ASA-2.13 was created by applying design Variant 8 to basic design ASA-2.14. Figure 24 compares averages for the acoustic absorption in two frequency ranges. The data in Figure 24 are arranged in pairs of basic design and the design variant, so that trends can be highlighted. Figure 25 shows acoustic absorption coefficient as a function of frequency for the prototypes with Variant 8 compared to the baselines.

As can be seen from Figure 24 and Figure 25, which shows the average acoustic absorption in two frequency ranges, ASA-2.0.1 had the high overall acoustic performance, comparing well against the baselines.

4.9 Variant 9

Most prototypes were made of ASA thermoplastic. One prototype was made of Ultem 1010 thermoplastic. Material properties are given in Reference 18. The geometric design for the Ultem 1010-2.7 and the ASA-2.7 prototypes were the same. Figure 26 shows the average absorption coefficient in the two frequency ranges for ASA-2.7 and Ultem1010-2.7. Figure 27 shows the acoustic absorption coefficients as a function of frequency for the two prototypes compared to the baselines.

We learned something from each of these comparisons that can inform modeling research and prototype design and fabrication. The average acoustic absorption coefficients for the two frequency ranges for all the tested samples is shown in Figure 28.

5.0 Conclusion

A set of 24 acoustic absorbers prototypes that mimic assemblies of natural reeds was designed, additively manufactured, and tested in normal incidence tubes at NASA. Results indicated that six basic prototype designs can be used to inform future modeling research. These prototypes exhibited substantial broadband acoustic absorption from 400 to 3000 Hz, and particularly effective absorption below 1000 Hz.

One basic prototype in particular, ASA-2.21, is recommended for modeling research, in part because the manufacturability of this design. Data from prototype ASA-2.9 indicates that there is potential for increasing the acoustic absorption by exploring the use of Variant 4.

Results of these experiments can be used to evaluate existing physics-based models of the interaction of sound waves with these structures or to develop new models. Validated physics-based models of these structures can help engineers optimize the designs for different commercial noise control applications. For more information about this technology, interested readers are encouraged to contact the NASA Glenn Technology Transfer Office.

TABLE 1.—THE CHANGE IN THE NUMBER OF VEHICLES IN THE UNITED STATES FROM 1960 TO 2017 FROM REFERENCE

Year	1960	2017
Commercial Aircraft	2,135	7,141
General Aviation	76,549	211,757
Transit	65,292	135,805
Rail	1,994,517	1,296,440
Water	2,476,730	12,004,283
Highway	74,431,800	272,480,899

TABLE 2.—NAMES OF BASIC PROTOTYPE DESIGNS AND DESIGN VARIANTS

		Basic Designs					
		Basic design 1 ASA-2.0	Basic design 2 ASA-2.19	Basic design 3 ASA-2.1	Basic design 4 ASA-2.7	Basic design 5 ASA-2.14	Basic design 6 ASA-2.21
Design variants	Variant 1	ASA-2.11		ASA-2.4 ASA-2.5		ASA-2.17	
	Variant 2	ASA-2.18		ASA-2.8		ASA-2.15	
	Variant 3			ASA-2.6		ASA-2.16	
	Variant 4	ASA-2.9 ASA-2.10 ASA-2.12					
	Variant 5			ASA-2.3 ASA-2.5			
	Variant 6		ASA-2.20				ASA-2.22
	Variant 7			ASA-2.2		ASA-2.13	
	Variant 8	ASA-2.0.1	ASA-2.19.1			ASA-2.13	
	Variant 9				Ultem-2.7		

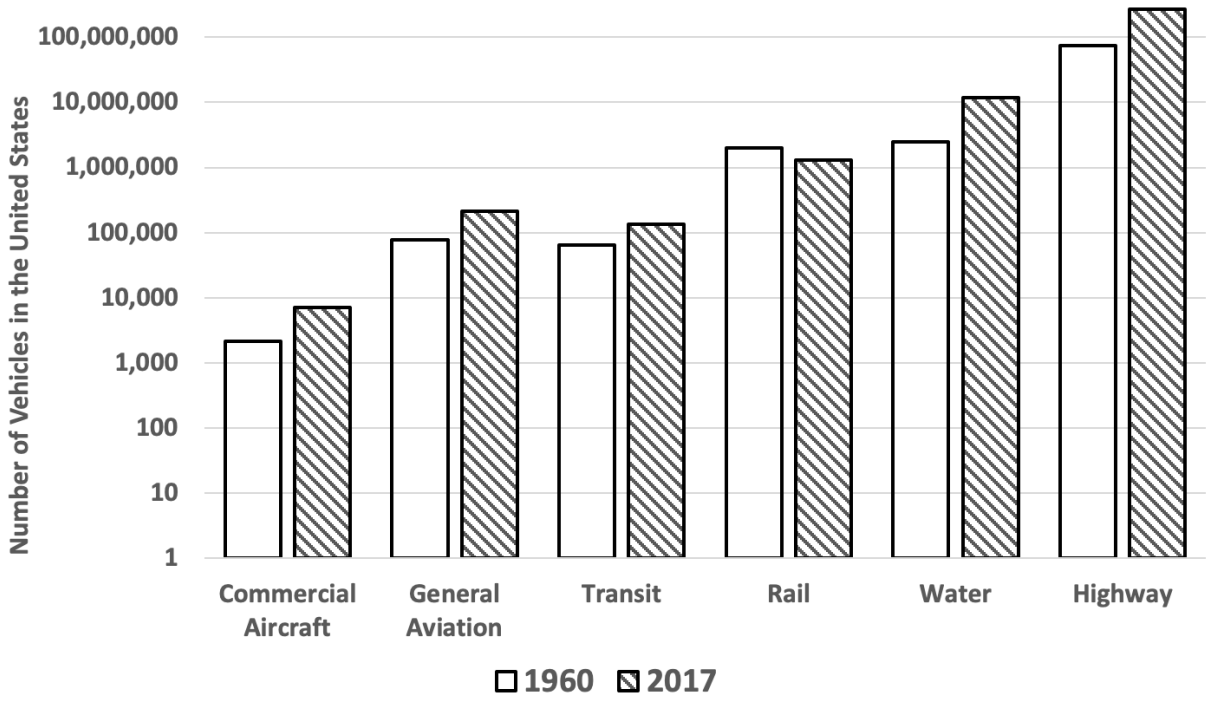

Figure 1.—The change in the number of vehicles in the United States from 1960 to 2017 from Reference 1.

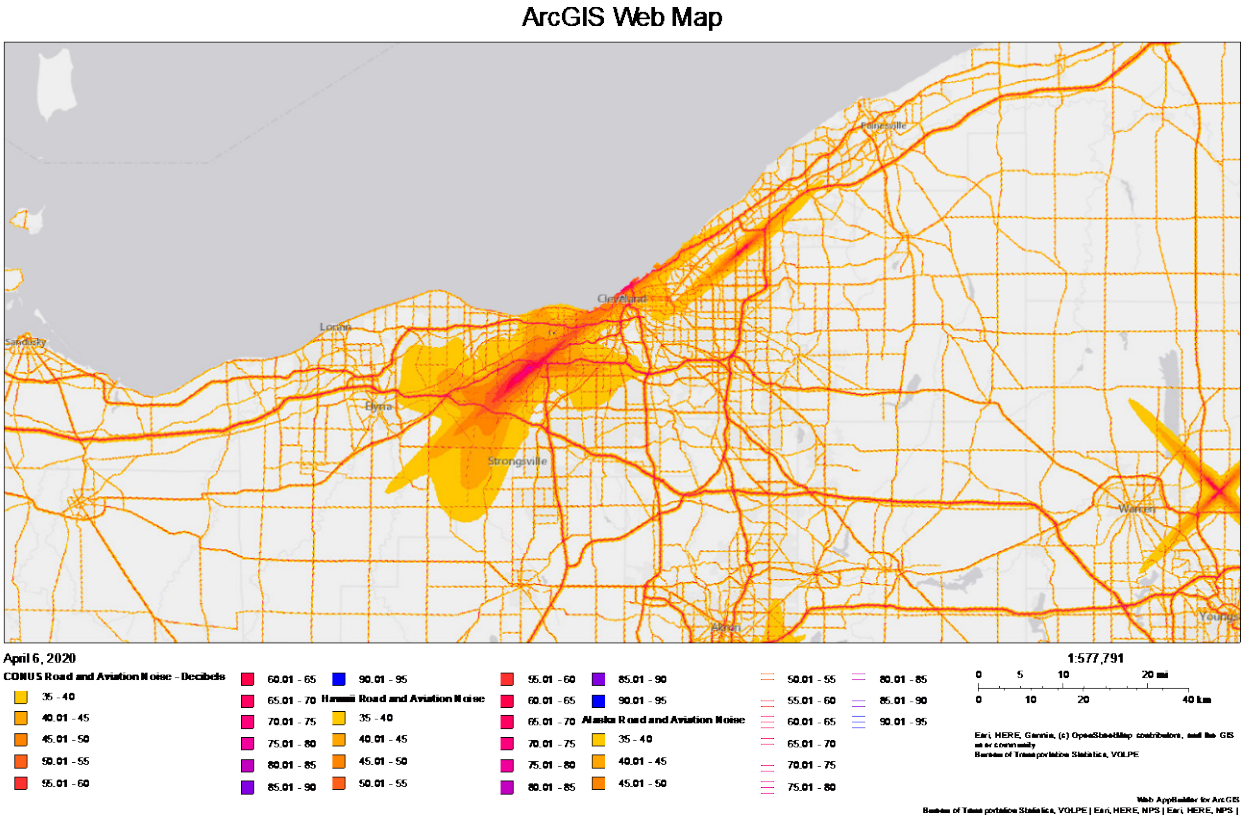

Figure 2.—Estimate of transportation noise in the vicinity of Cleveland, Ohio, from Reference 4.

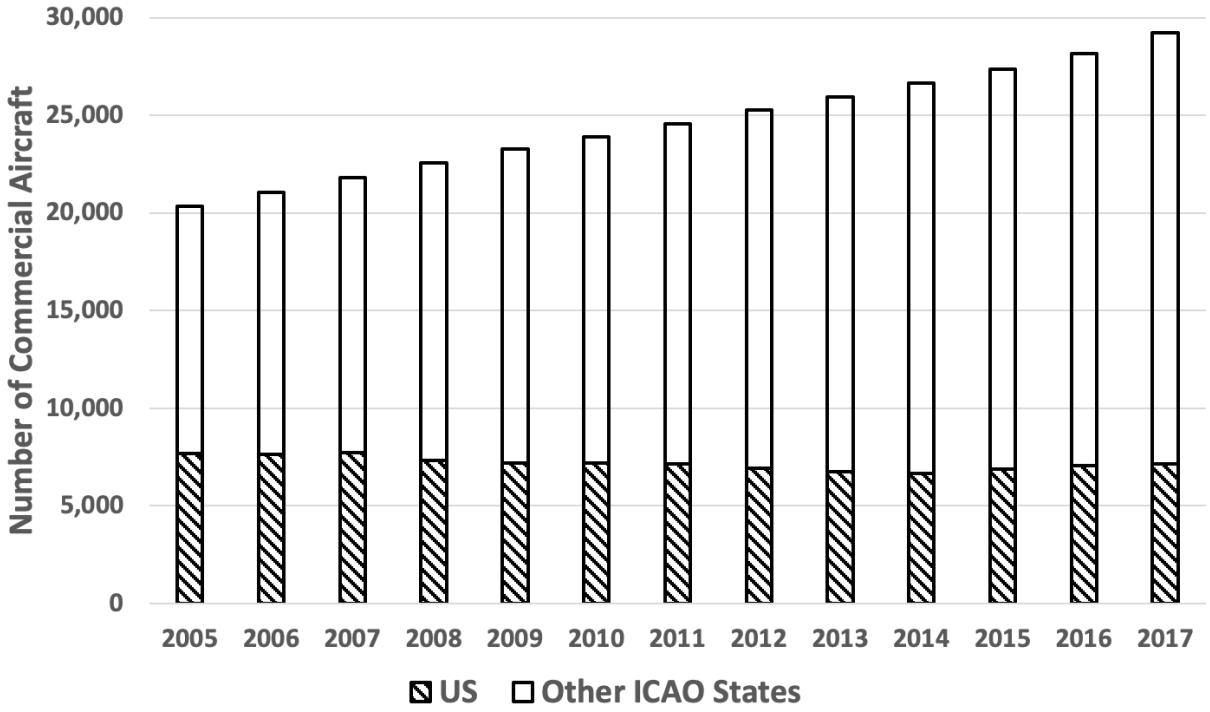

Figure 3.—The change in the number of commercial aircraft from 2005 to 2017.

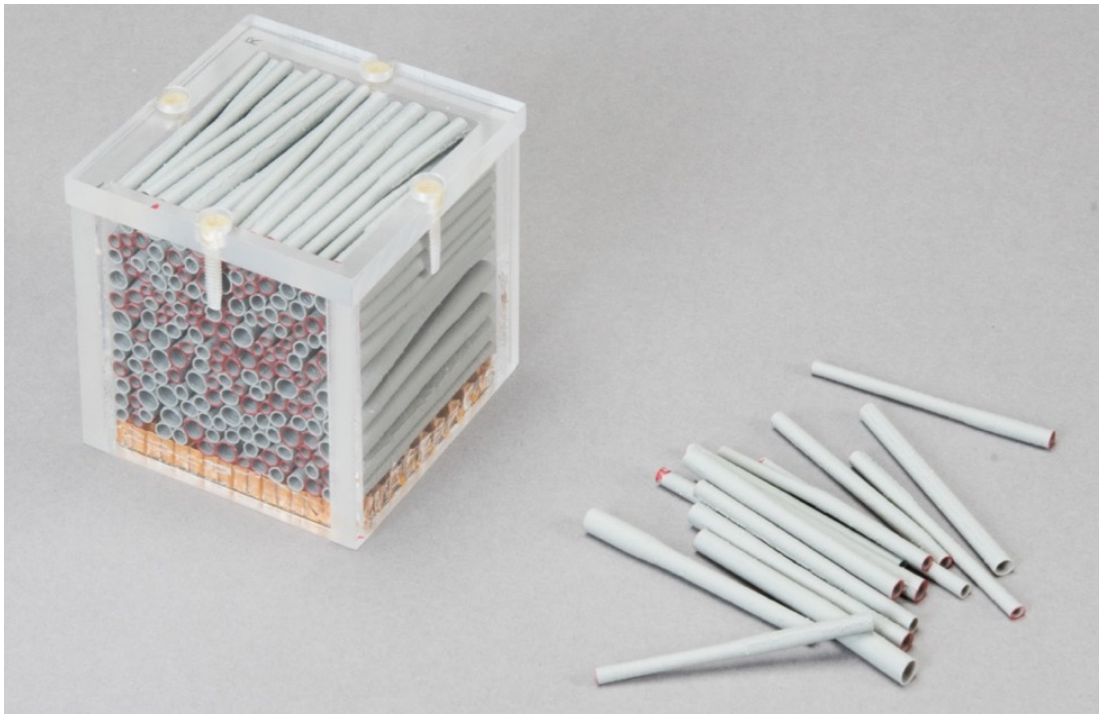

Figure 4.—“Loose” style prototype that requires a retainer to hold its shape.

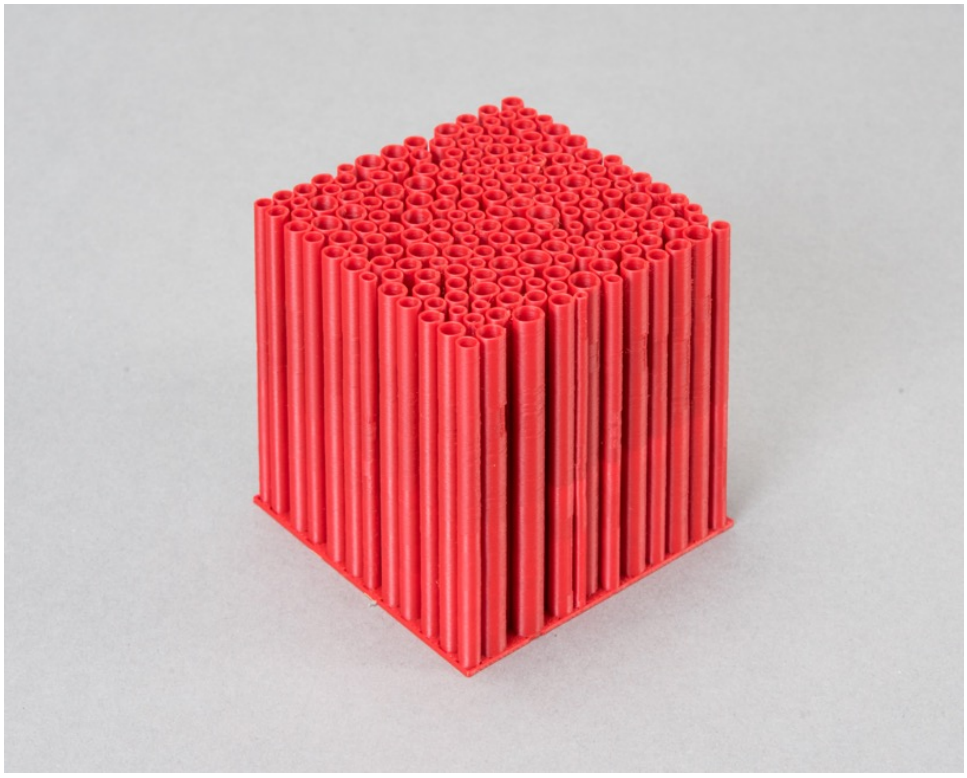

Figure 5.—“Fixed” style prototype that does not need a retainer to hold its shape.

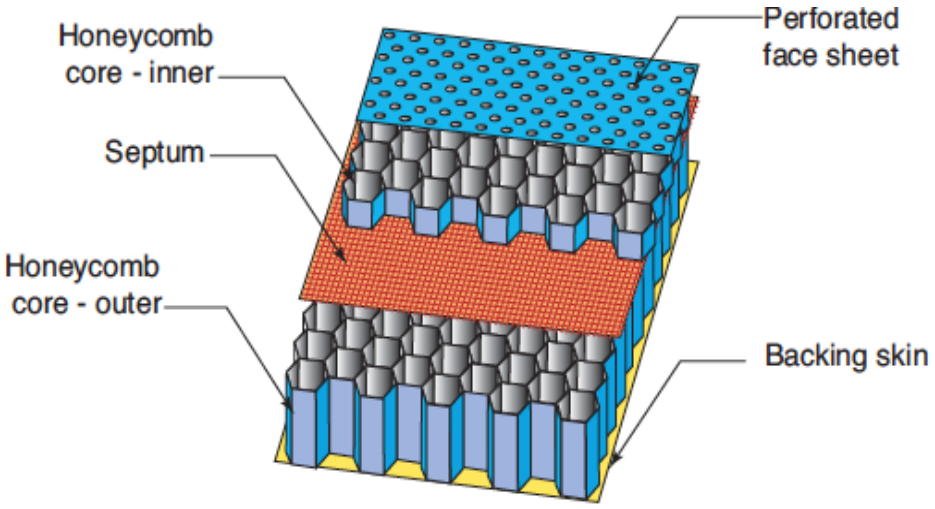

Figure 6.—Illustration of a double degree of freedom perforate over honeycomb acoustic liner.

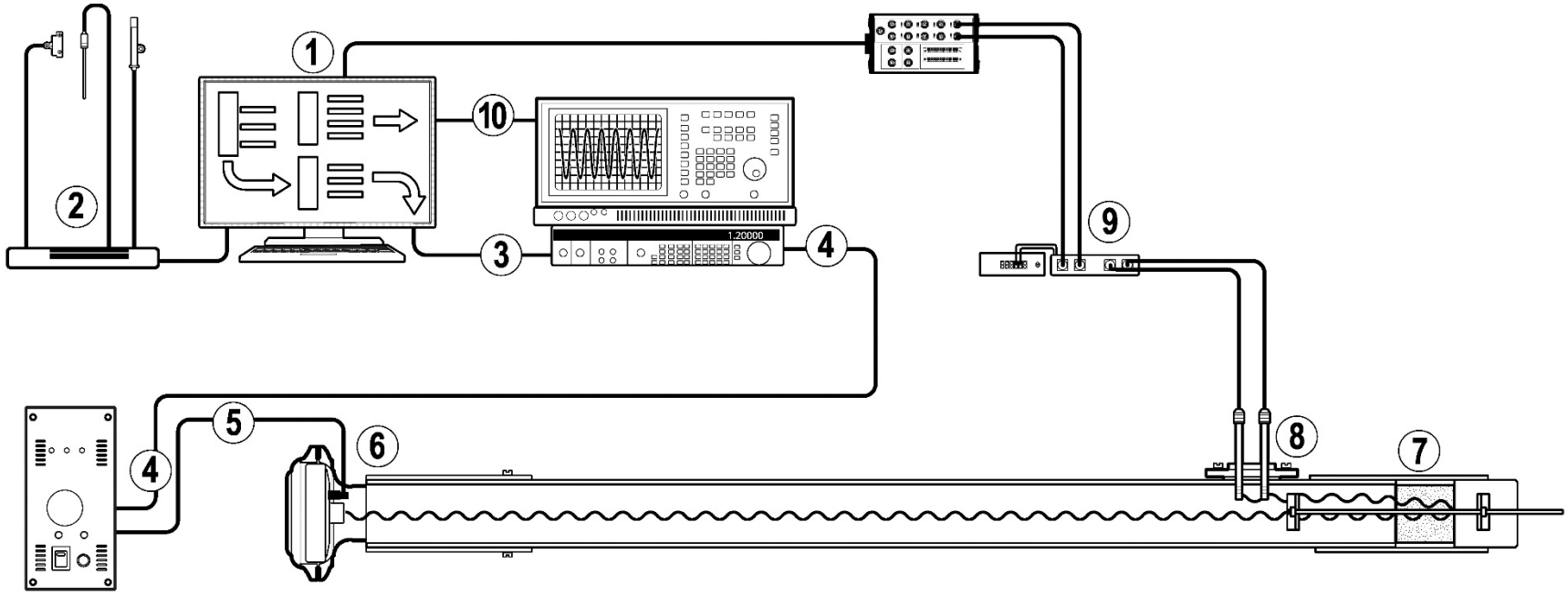

Figure 7.—Procedure and apparatus for acquiring data using the NASA Glenn Normal Incidence Tube: (1) Experimental parameters defined in the data acquisition and control computer; (2) Environmental data (temperature, barometric pressure, humidity) measured; (3) Excitation frequency and amplitude sent to audio signal generator; (4) Audio signal generated and sent to power amplifier; (5) Amplified signal sent to sound driver, (6) Sound driver converts electrical signal to sound; (7) Sound interacts with sample, reflecting off of terminator, (8) Sound is sensed by the microphones and converted to an electrical signal; (9) Microphone signals are conditioned, filtered, and amplified in the preamplifier; 1(0) Amplified microphone signals are sampled by the data acquisition system and displayed on the monitor oscilloscope. Sampled data is processed to yield a reflection ratio. Steps 3 through 10 are repeated for each frequency in the test range.

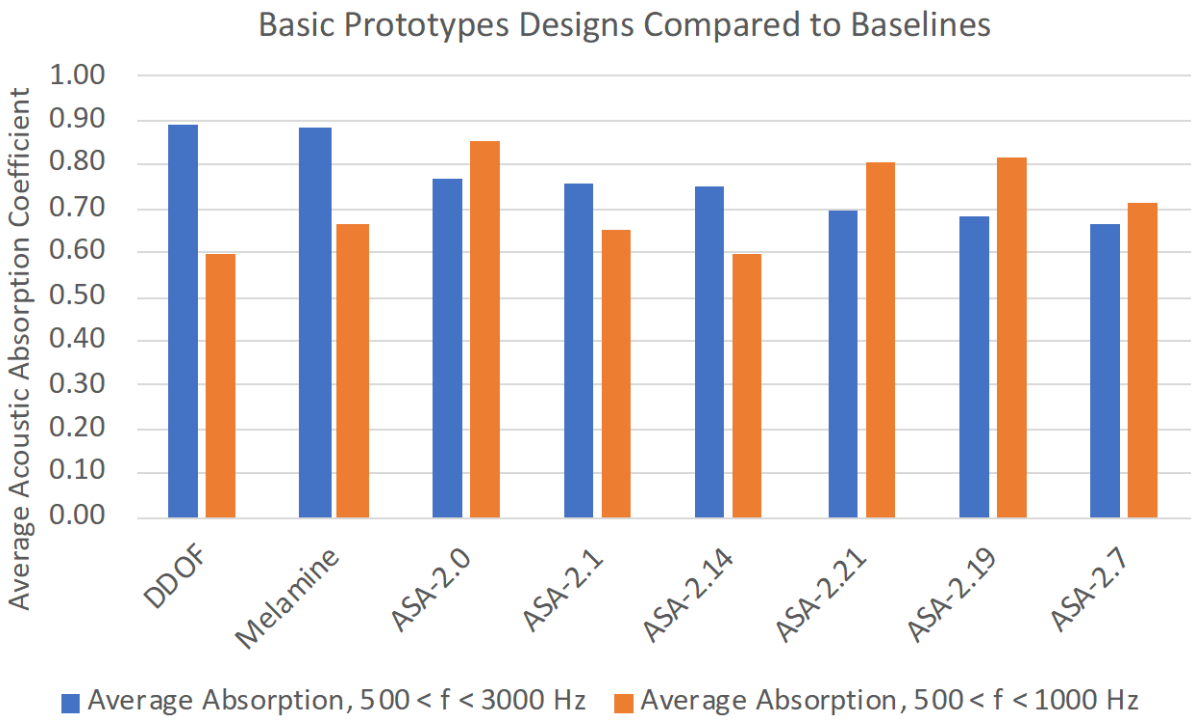

Figure 8.—Average acoustic absorption coefficient for baselines and six basic prototype designs sorted by decreasing values of average absorption in the 500 to 3000 Hz frequency range.

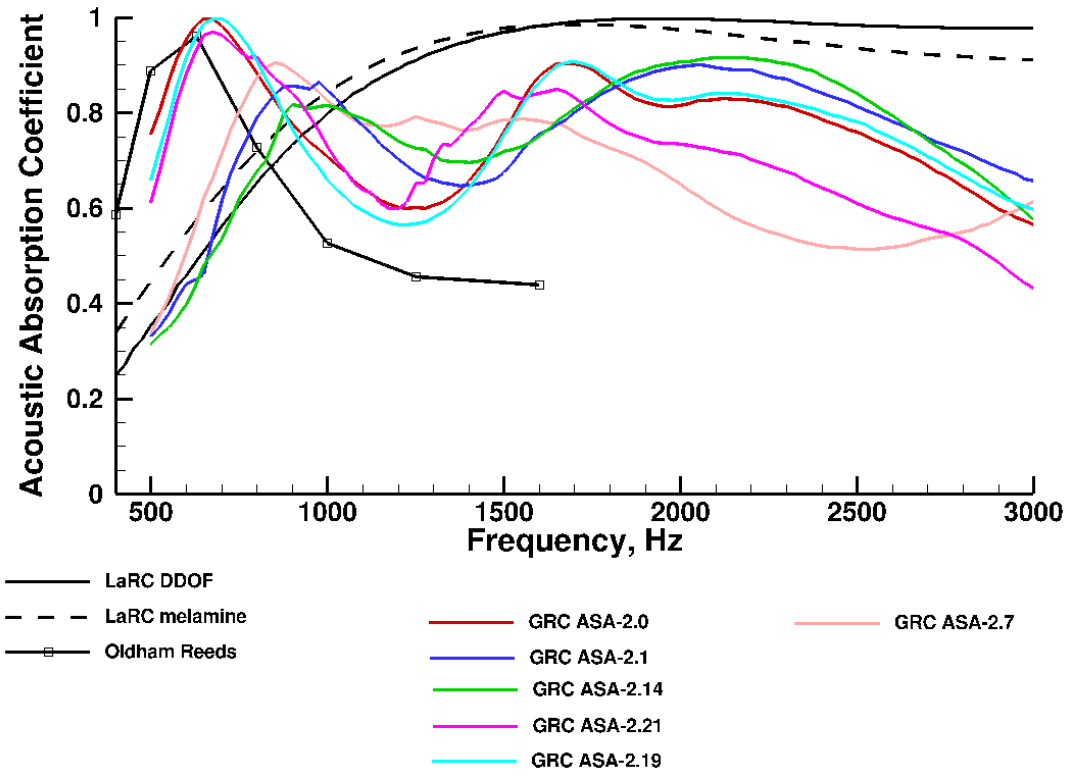

Figure 9.—Acoustic absorption coefficient versus frequency for baselines and basic designs.

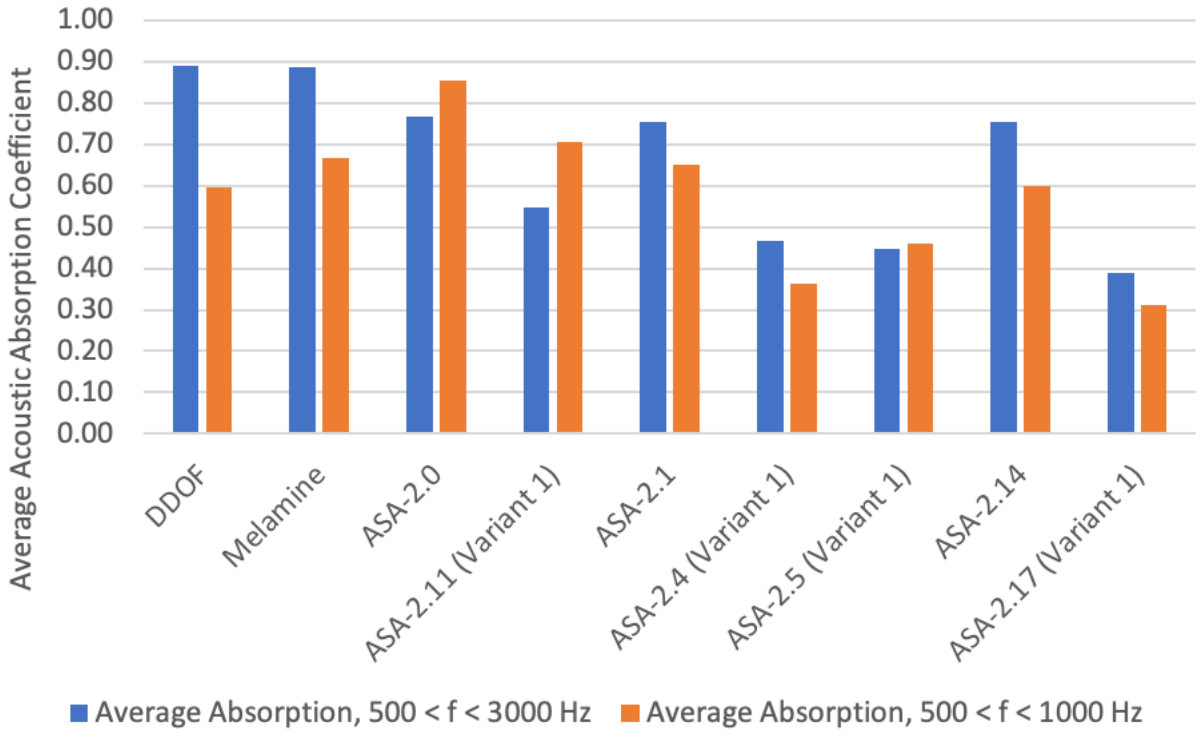

Figure 10.—Average acoustic absorption coefficient for baselines, basic designs, and Variant 1.

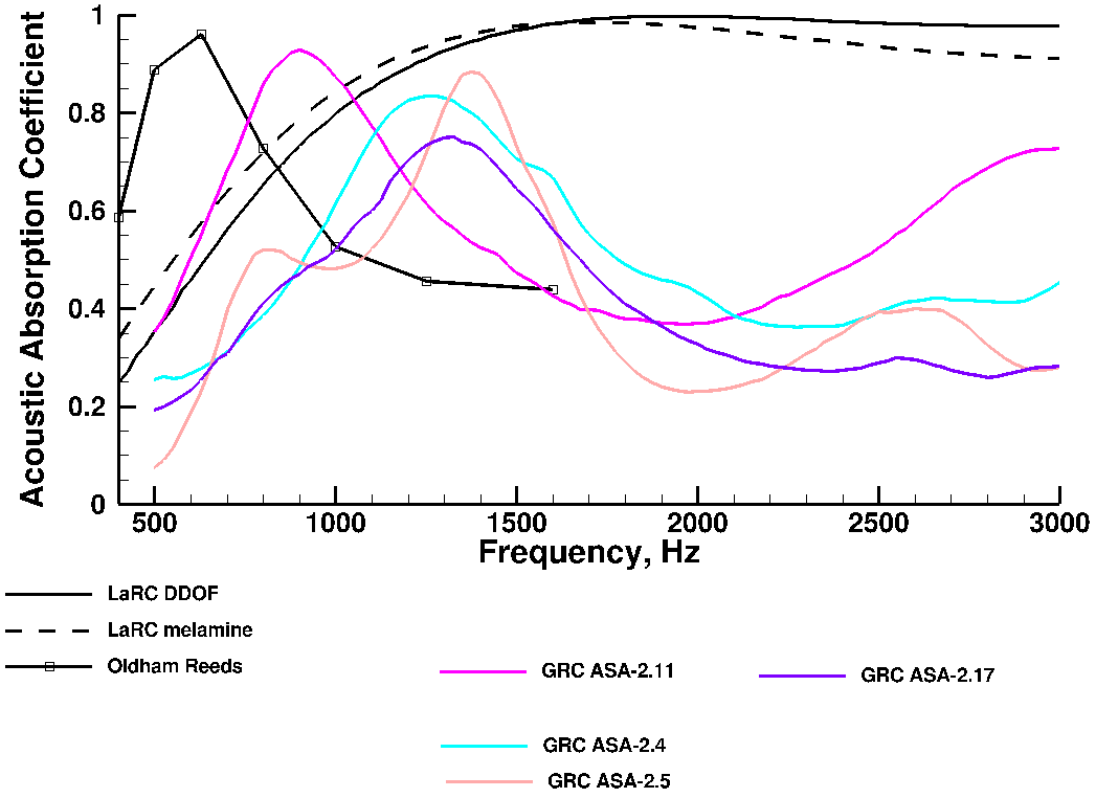

Figure 11.—Acoustic absorption coefficient versus frequency for baselines, basic designs, and Variant 1.

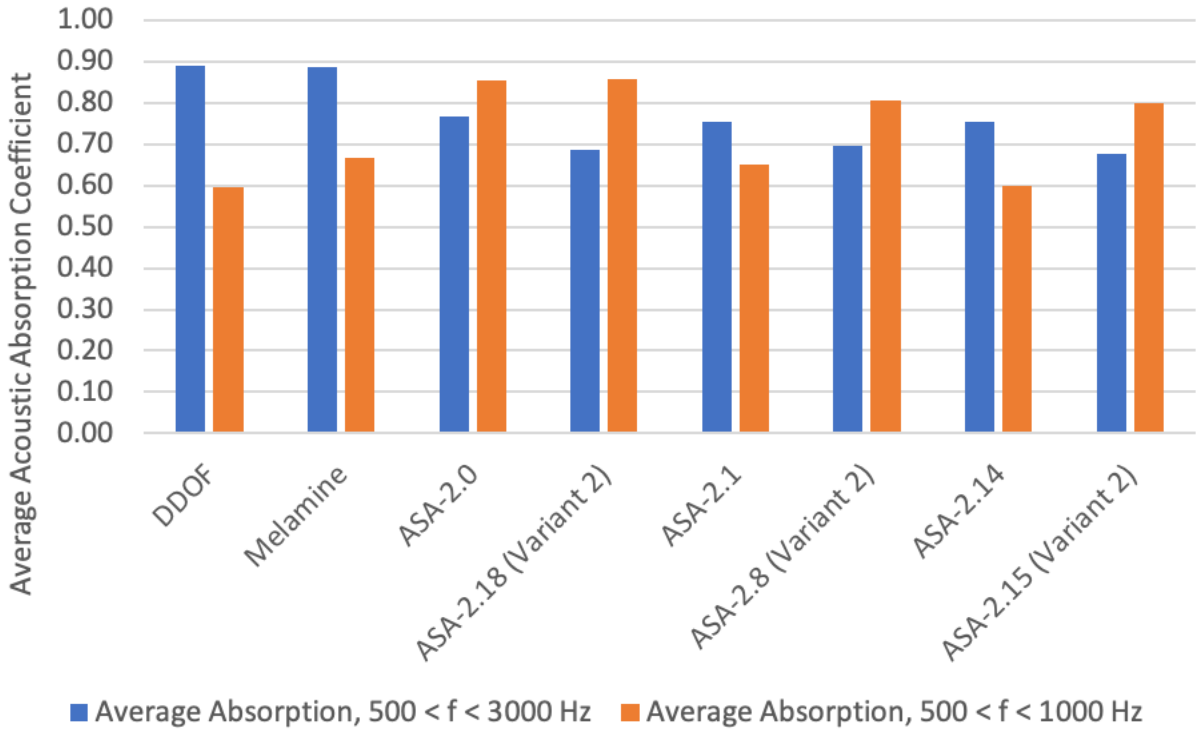

Figure 12.—Average acoustic absorption coefficient for baselines, basic designs, and Variant 2.

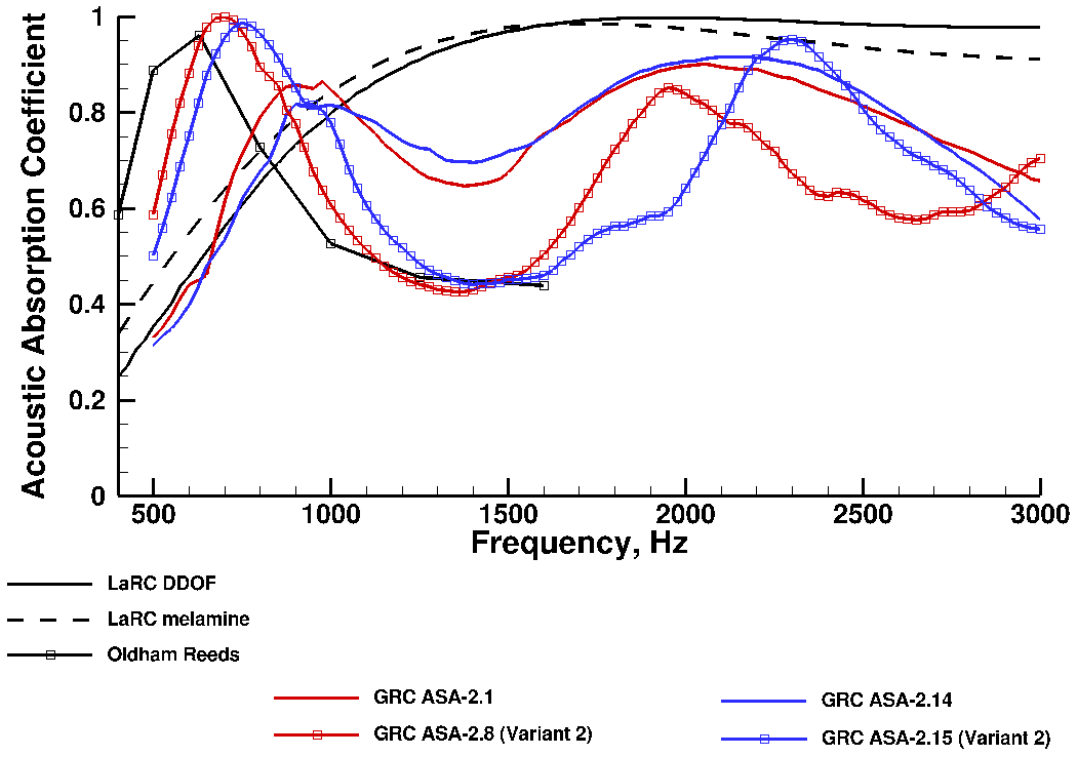

Figure 13.—Acoustic absorption coefficient versus frequency for baselines, basic designs, and Variant 2.

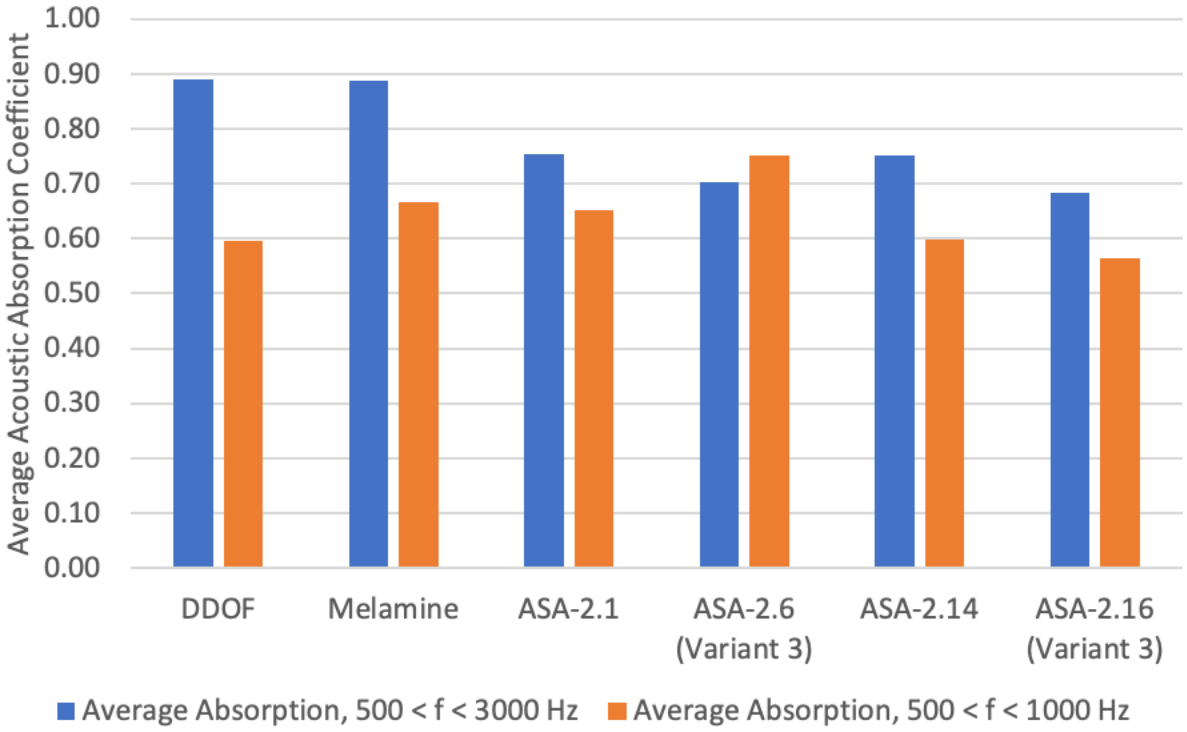

Figure 14.—Average acoustic absorption coefficient for baselines, basic designs, and Variant 3.

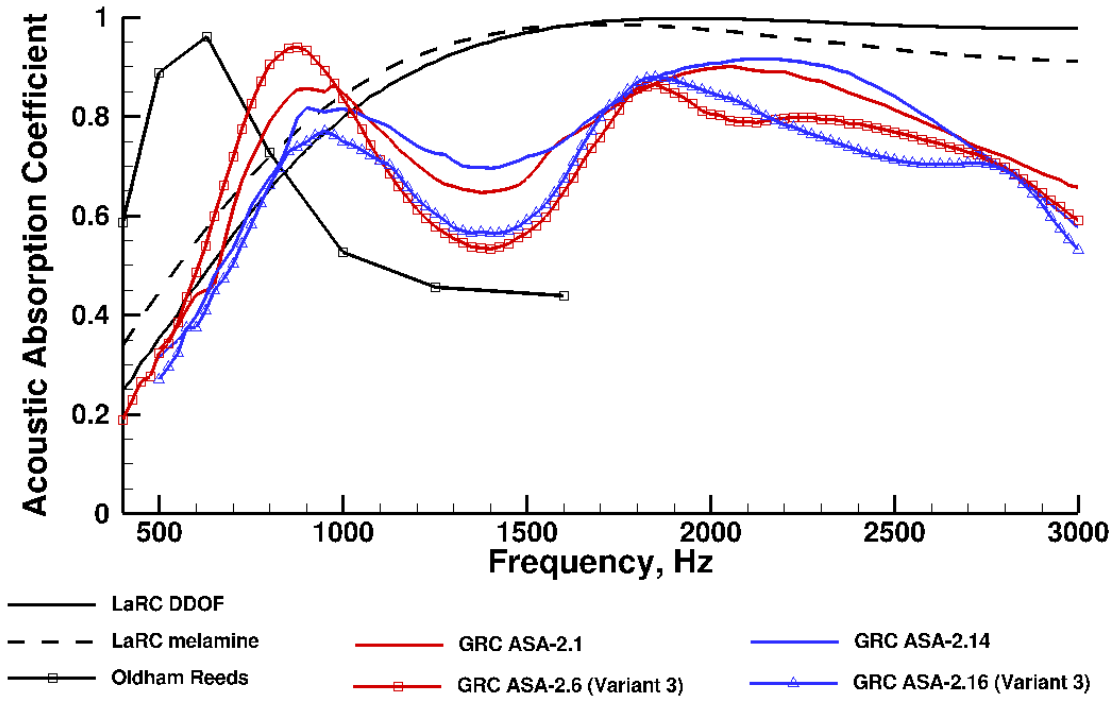

Figure 15.—Acoustic absorption coefficient versus frequency for baselines, basic designs, and Variant 3.

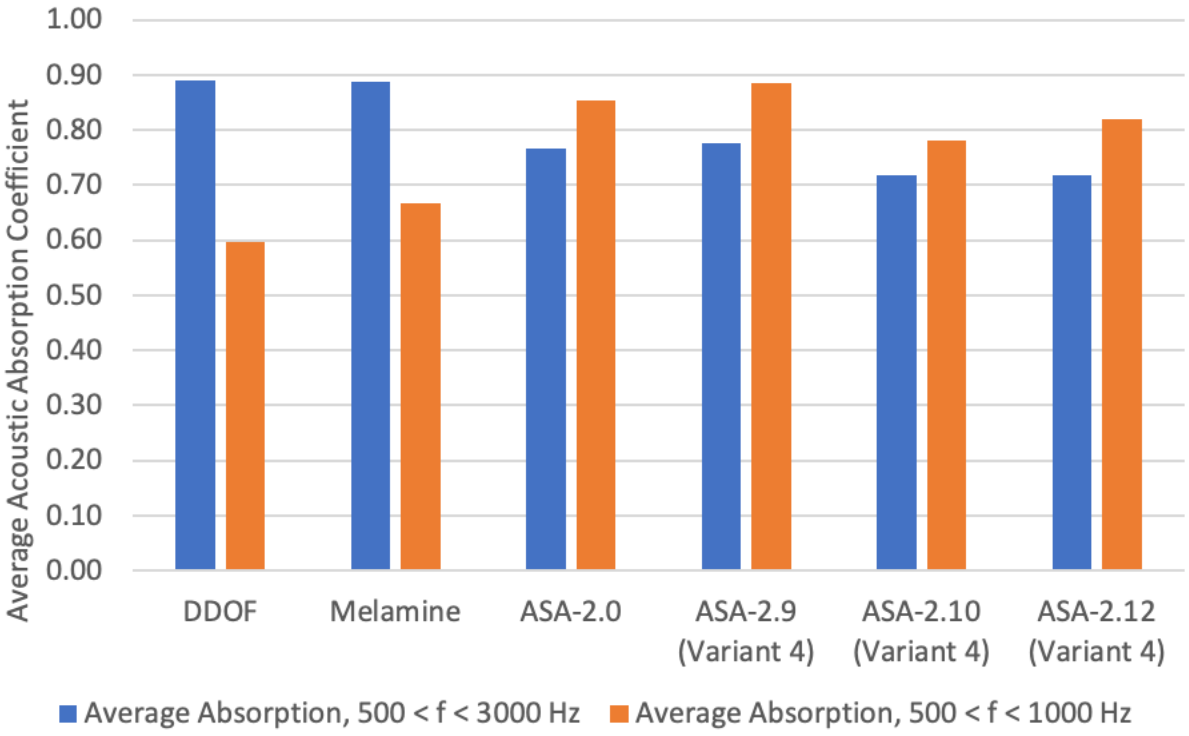

Figure 16.—Average acoustic absorption coefficient for baselines, basic designs, and Variant 4.

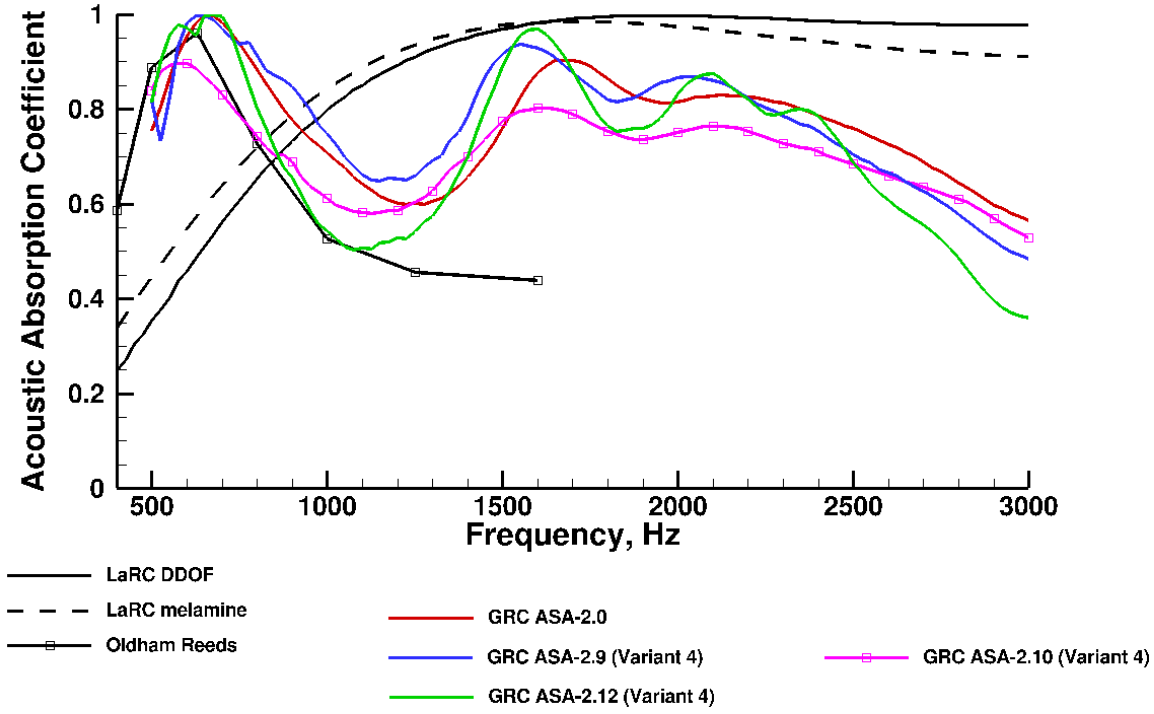

Figure 17.—Acoustic absorption coefficient versus frequency for baselines, basic designs, and Variant 4.

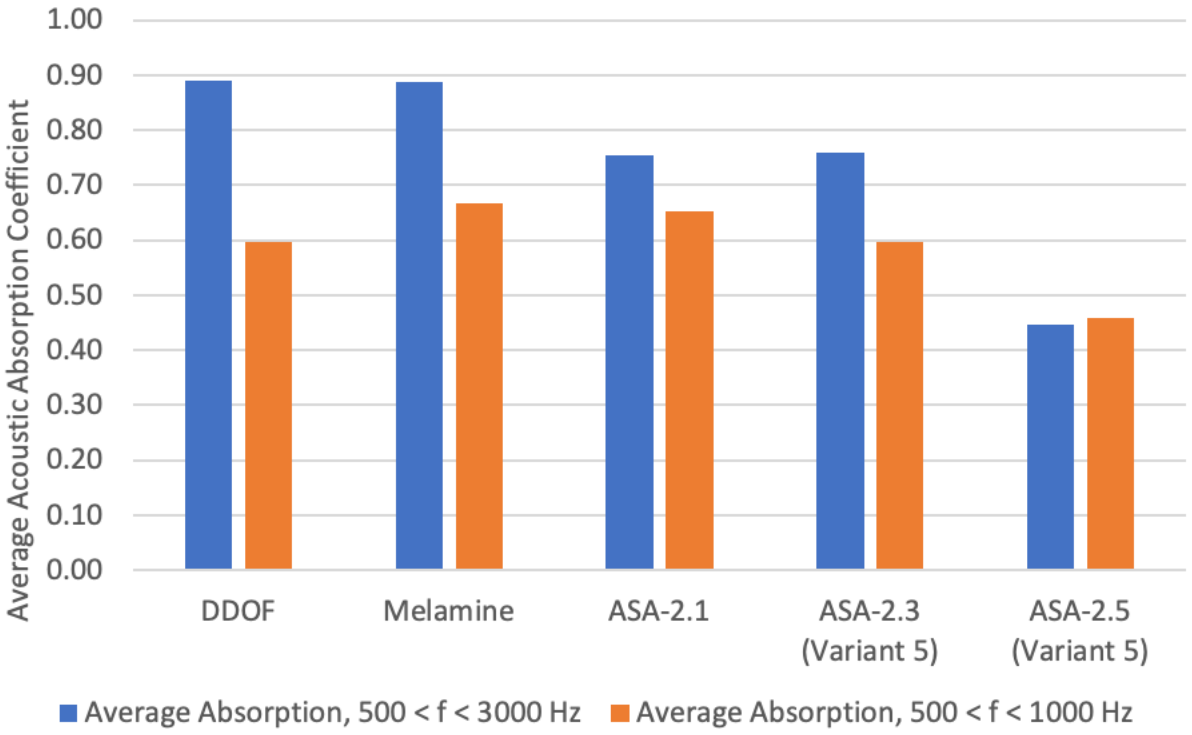

Figure 18.—Average acoustic absorption coefficient for baselines, basic designs, and Variant 5.

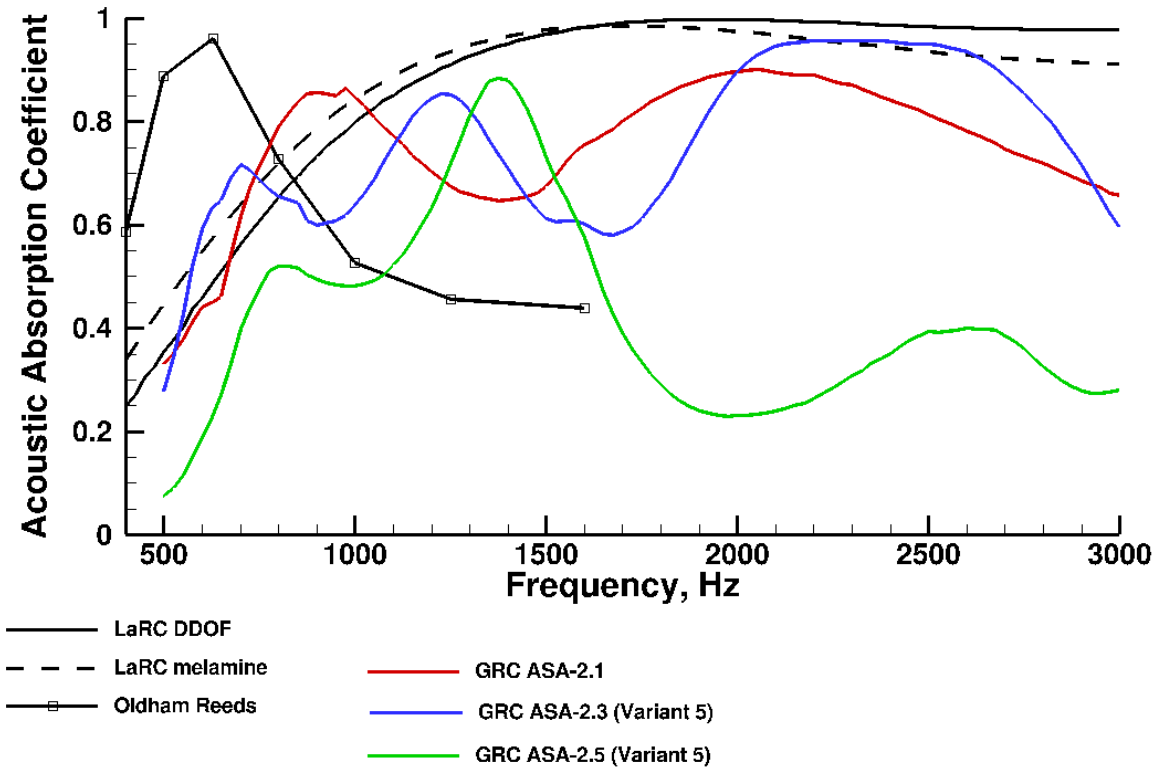

Figure 19.—Acoustic absorption coefficient versus frequency for baselines, basic designs, and Variant 5.

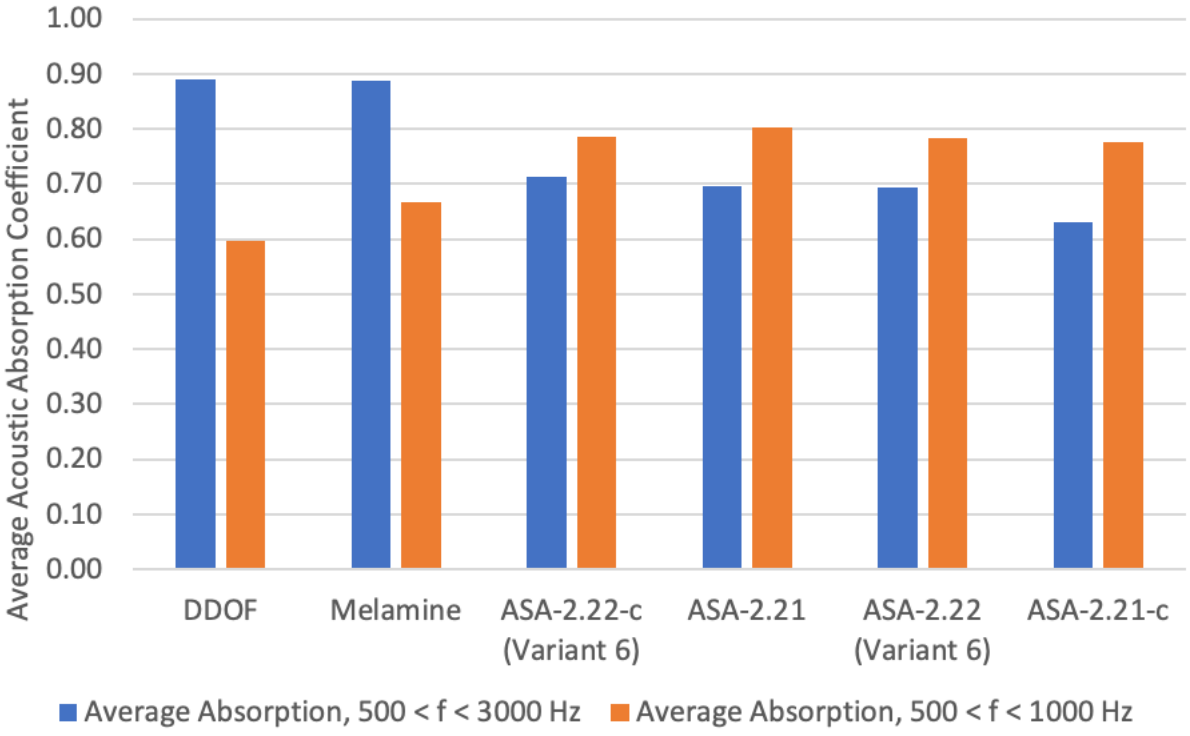

Figure 20.—Average acoustic absorption coefficient for baselines, basic designs, and Variant 6.

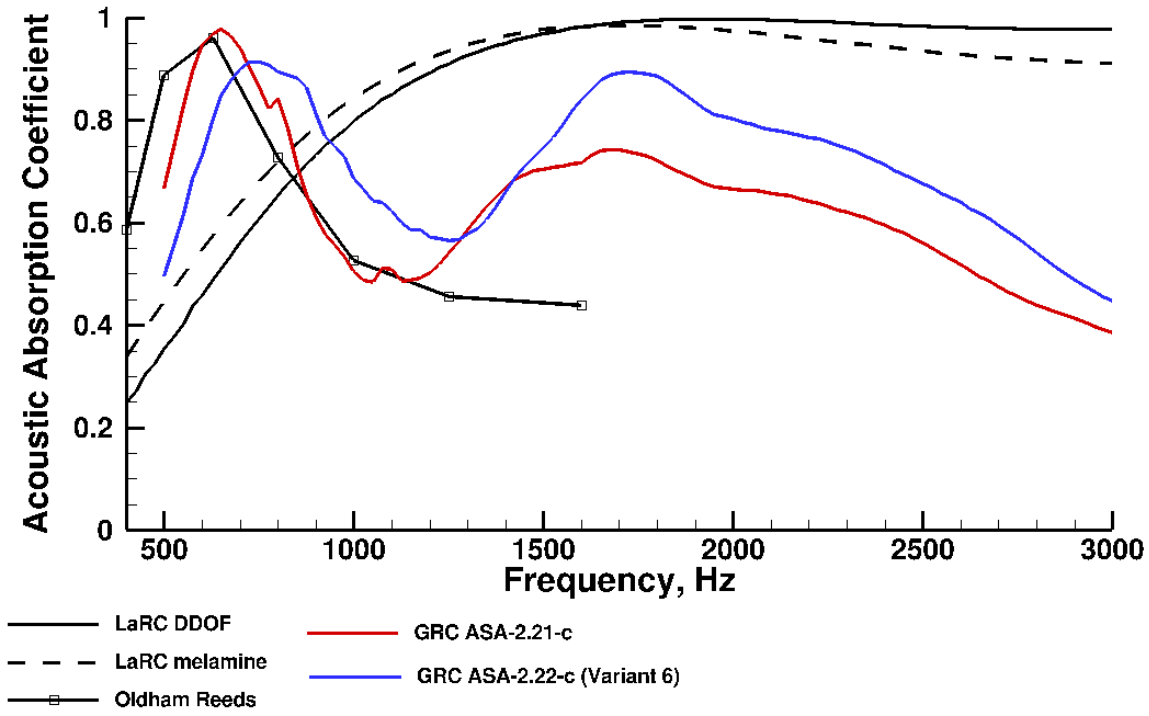

Figure 21.—Acoustic absorption coefficient versus frequency for baselines, basic designs, and Variant 6.

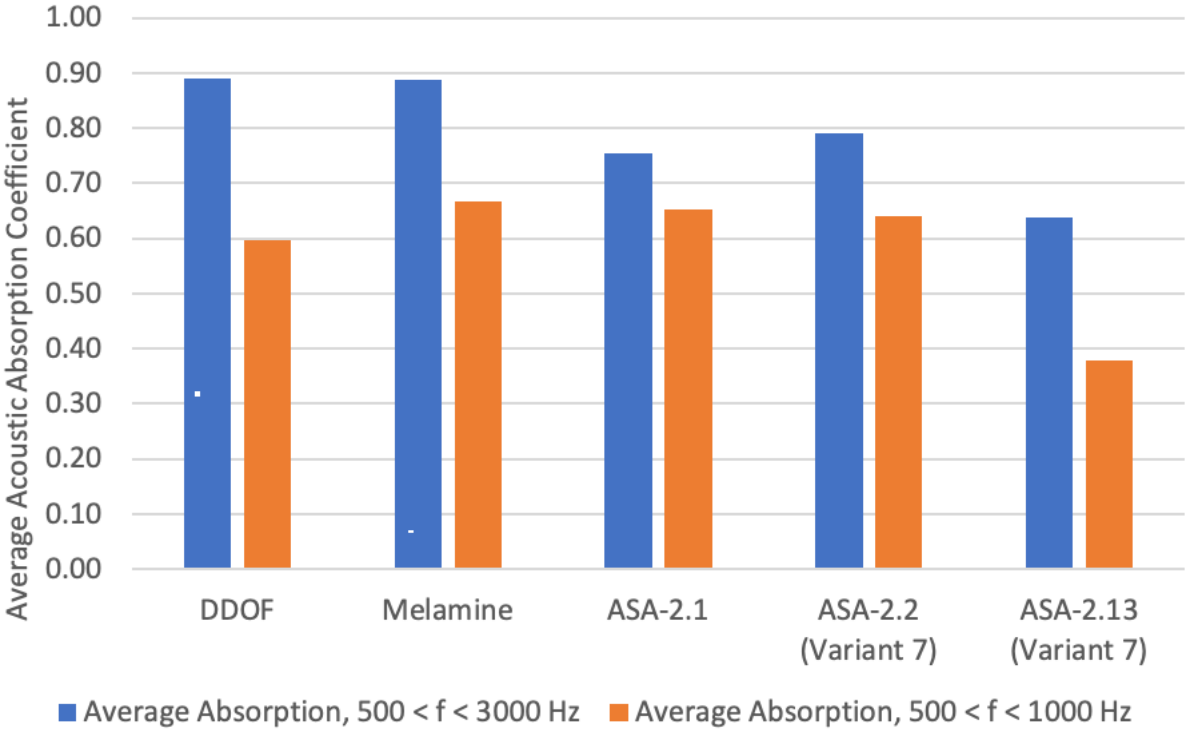

Figure 22.—Average acoustic absorption coefficient for baselines, basic designs, and Variant 7.

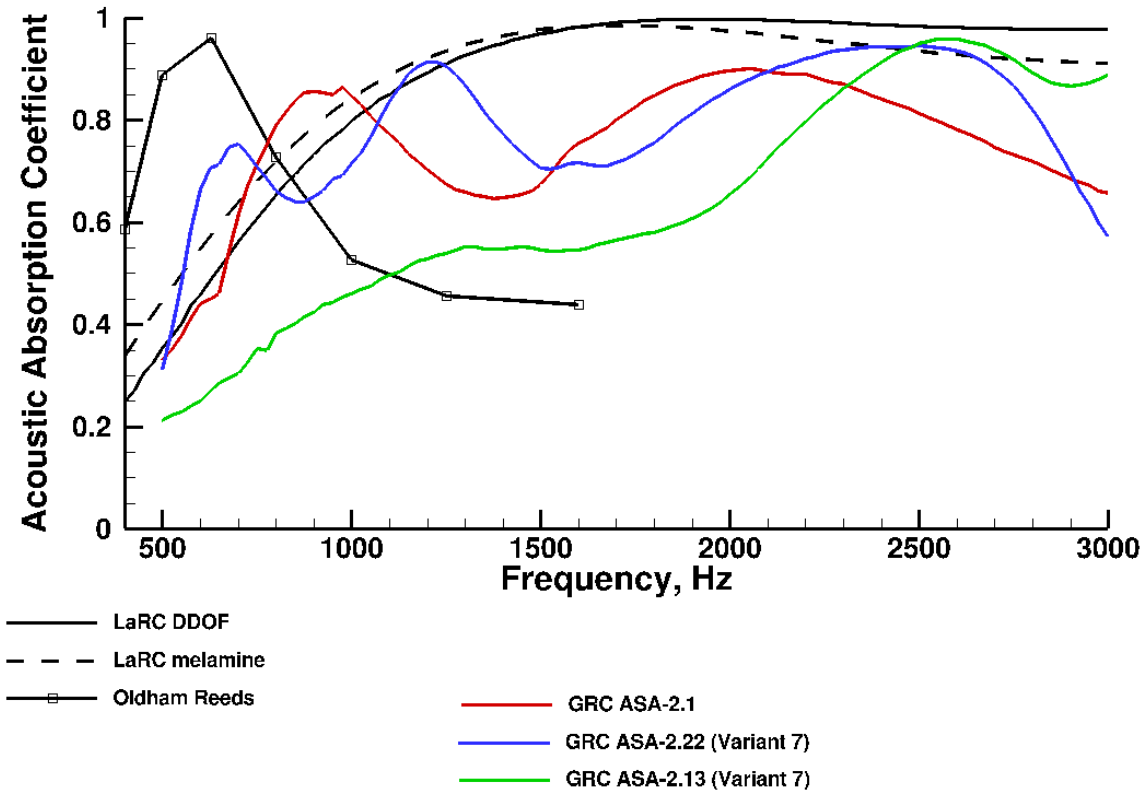

Figure 23.—Acoustic absorption coefficient versus frequency for baselines, basic designs, and Variant 7.

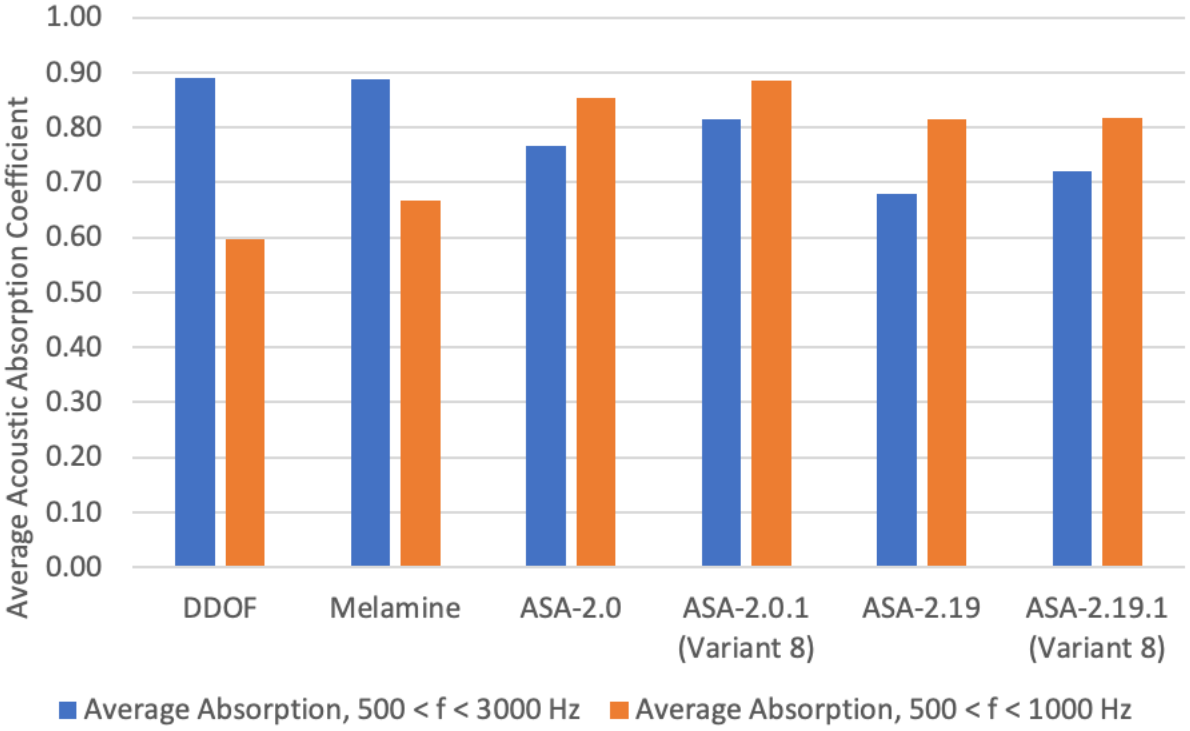

Figure 24.—Average acoustic absorption coefficient for baselines, basic designs, and Variant 8.

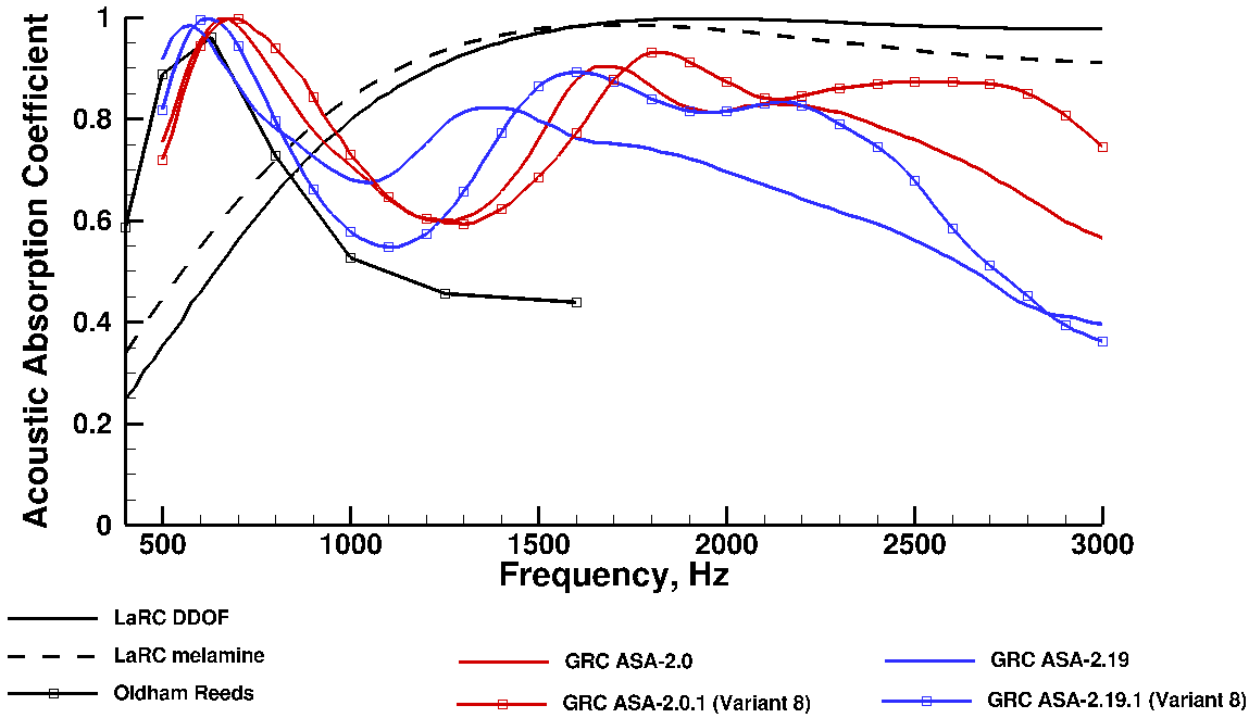

Figure 25.—Acoustic absorption coefficient versus frequency of prototypes with crossed layers.

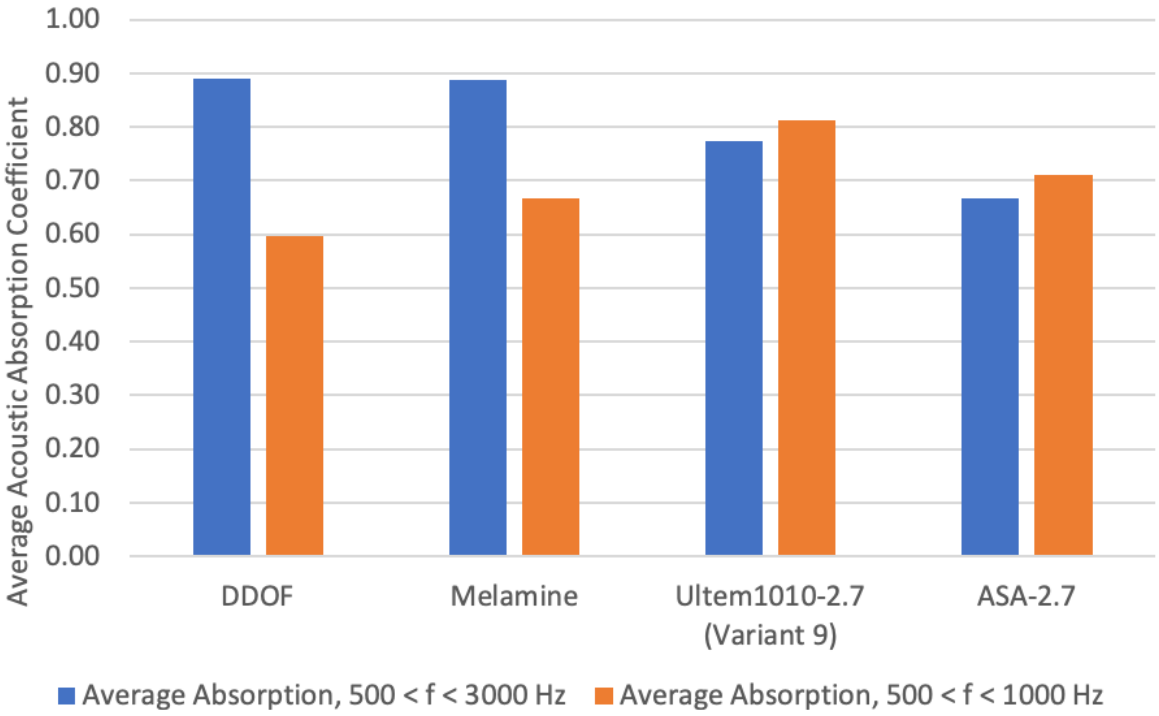

Figure 26.—Average acoustic absorption coefficient of baselines compared to bioliner prototypes of two different materials Ultem 1010 (Variant 9) and ASA thermoplastic. The geometric design for the Ultem 1010-2.7 and the ASA-2.7 prototypes were the same.

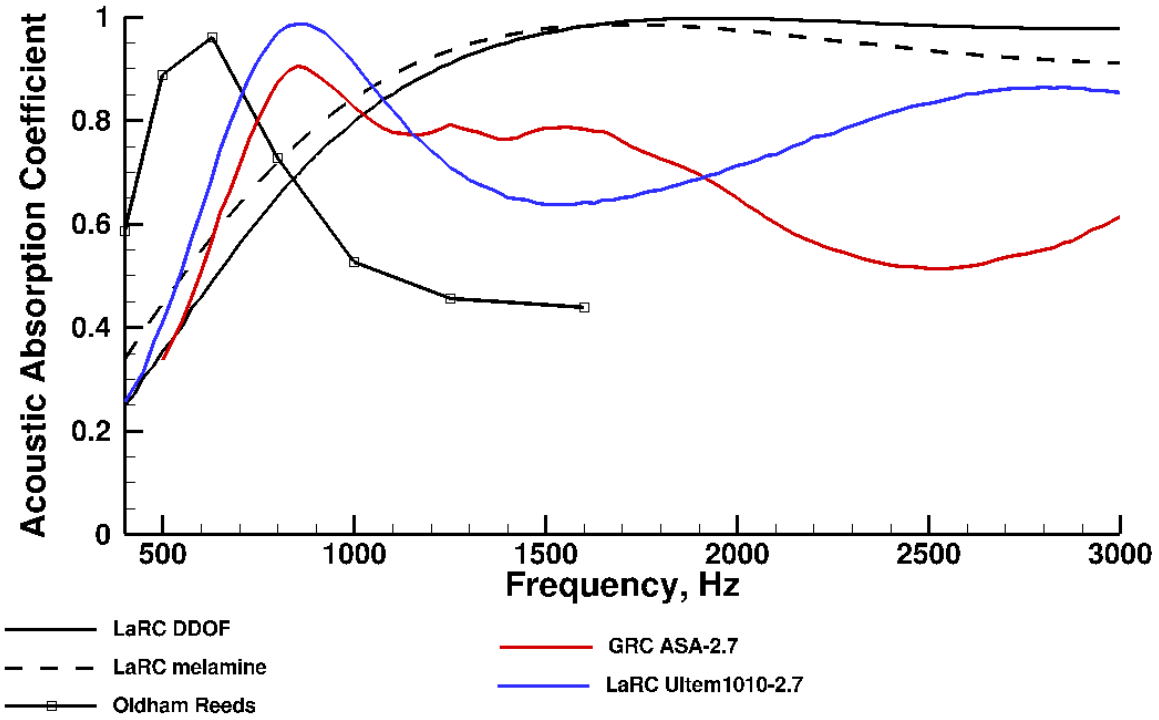

Figure 27.—Acoustic absorption coefficient versus frequency of baselines compared to bioliner prototypes of two different materials Ultem 1010 and ASA thermoplastic. The geometric design for the Ultem 1010-2.7 and the ASA-2.7 prototypes were the same.

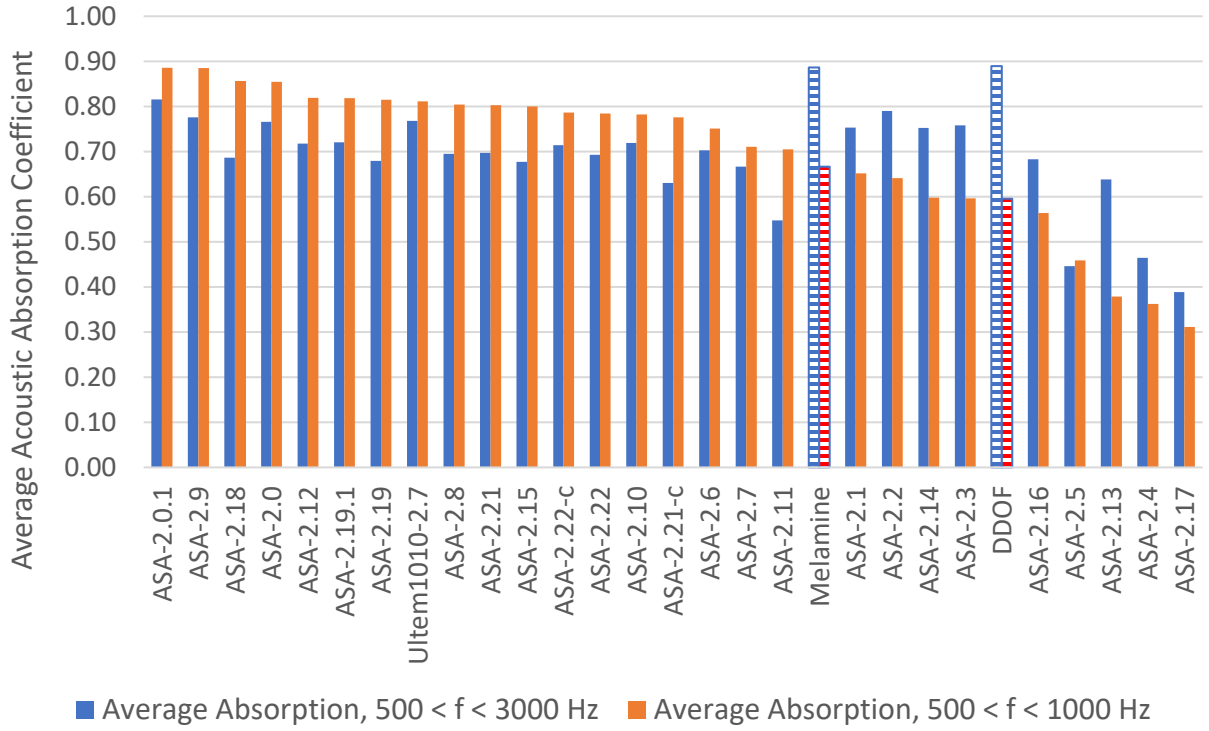

Figure 28.—Acoustic absorption coefficient versus frequency, sorted by low frequency performance, of all prototypes and the baselines. Baselines are shown with pattern-filled bars.

Appendix A

Figure A.1 to Figure A.77 in the Appendix contain groupings of plots for each prototype, and images for some of the prototypes. For example, Figure A.1 is a plot of acoustic absorption coefficient versus frequency for prototype ASA-2.0. Figure A.2 is a plot of normalized resistance and normalized reactance versus frequency for prototype ASA-2.0. Figure A.3 is a plot of acoustic absorption coefficient versus normalized resistance and normalized reactance.

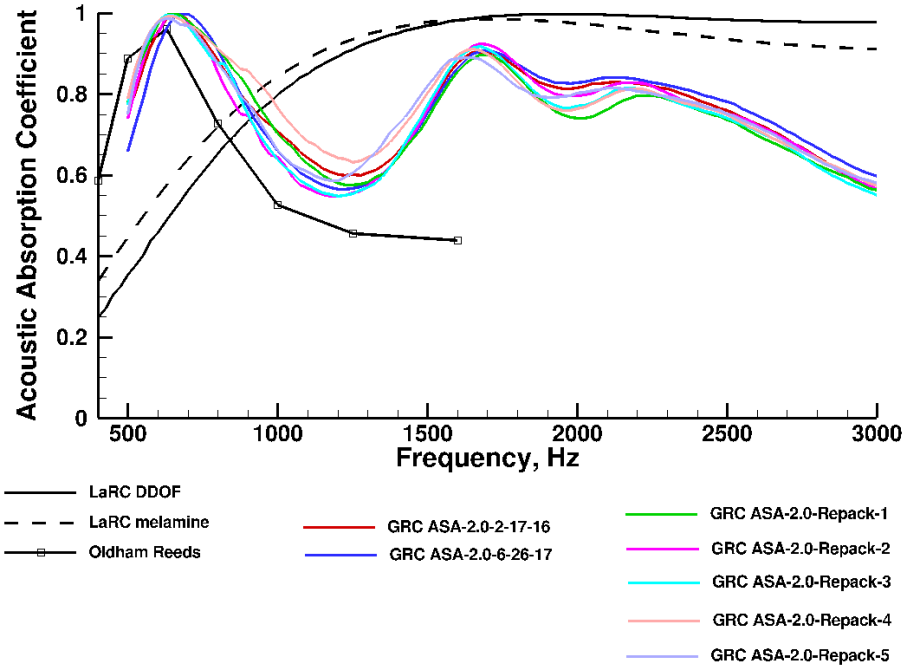

Figure A.1.—The variation of acoustic absorption coefficient with frequency for prototype ASA-2.0.

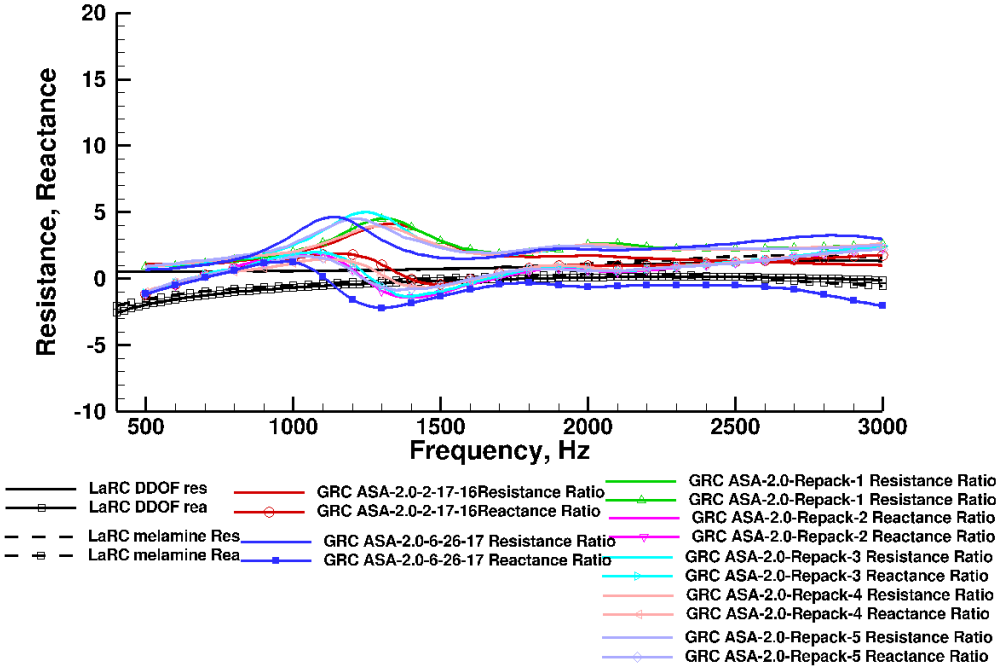

Figure A.2.—The variation of resistance and reactance with frequency for prototype ASA-2.0.

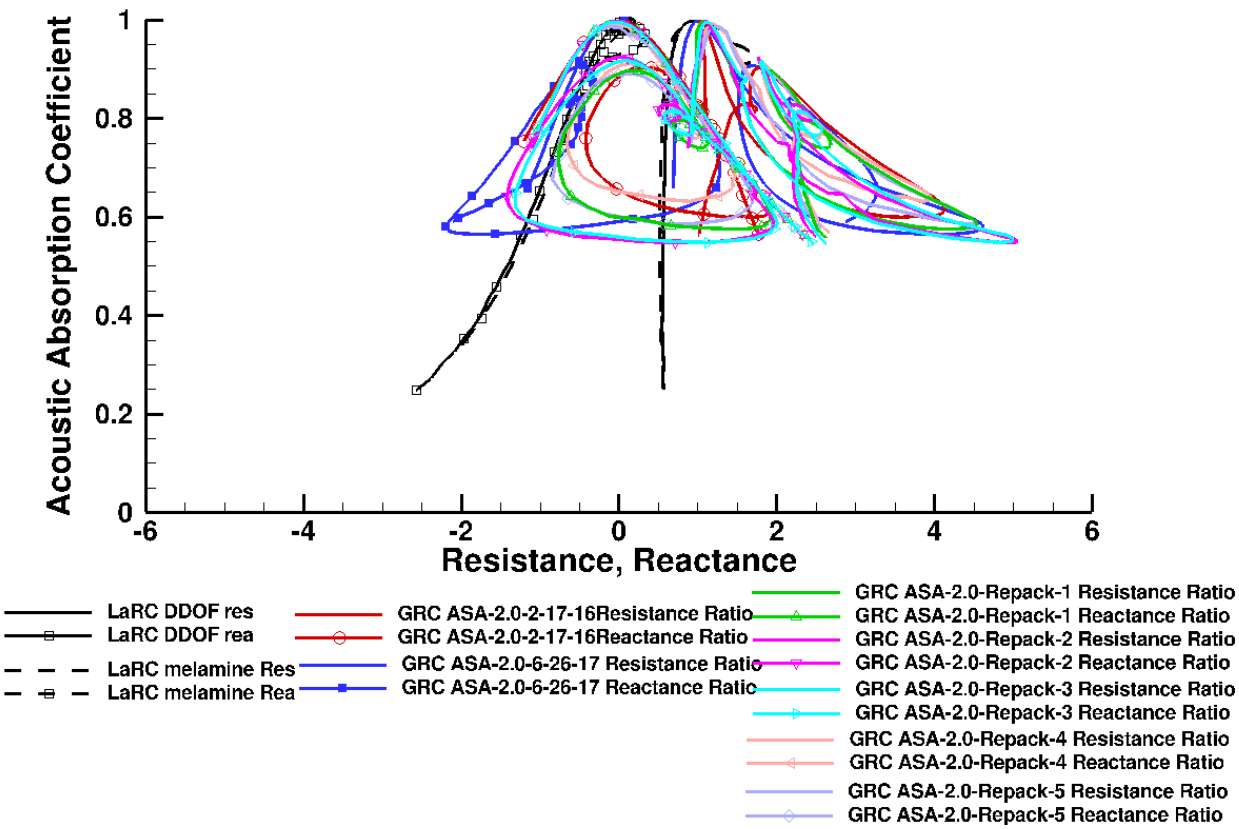

Figure A.3.—The variation of acoustic absorption coefficient with resistance and reactance for prototypes ASA-2.0.

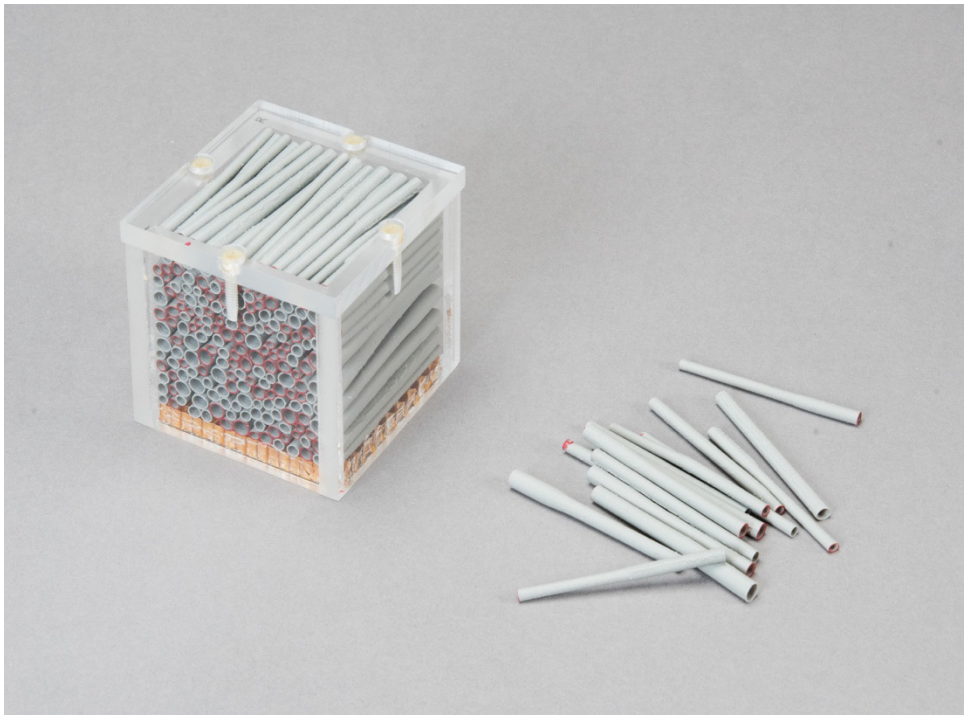

Figure A.4.—Prototype ASA-2.0.

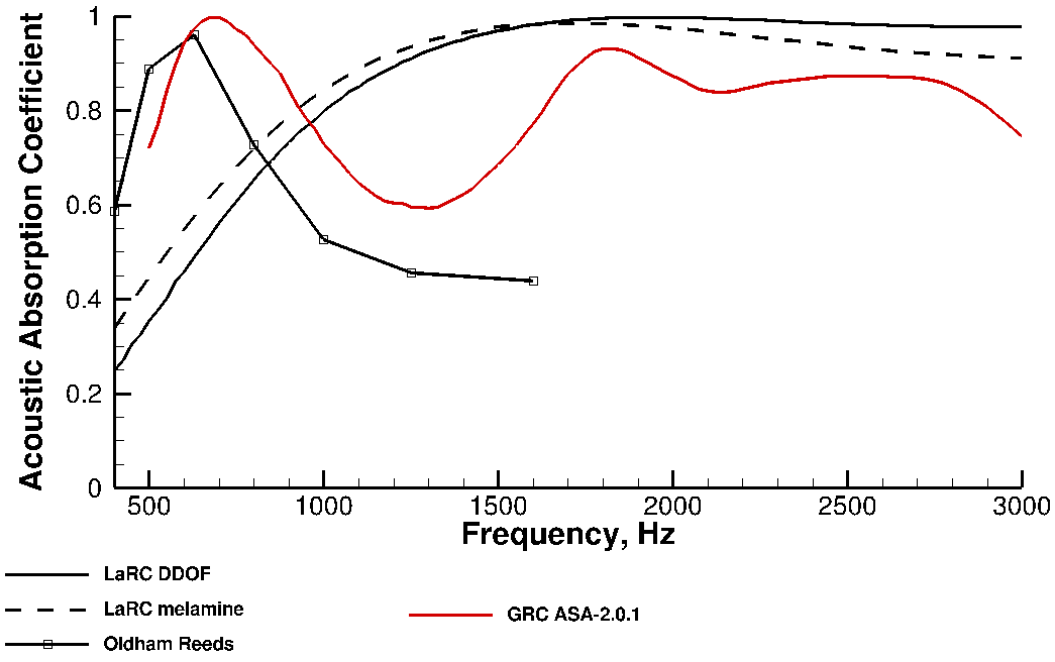

Figure A.5.—The variation of acoustic absorption coefficient with frequency for prototype ASA-2.0.1.

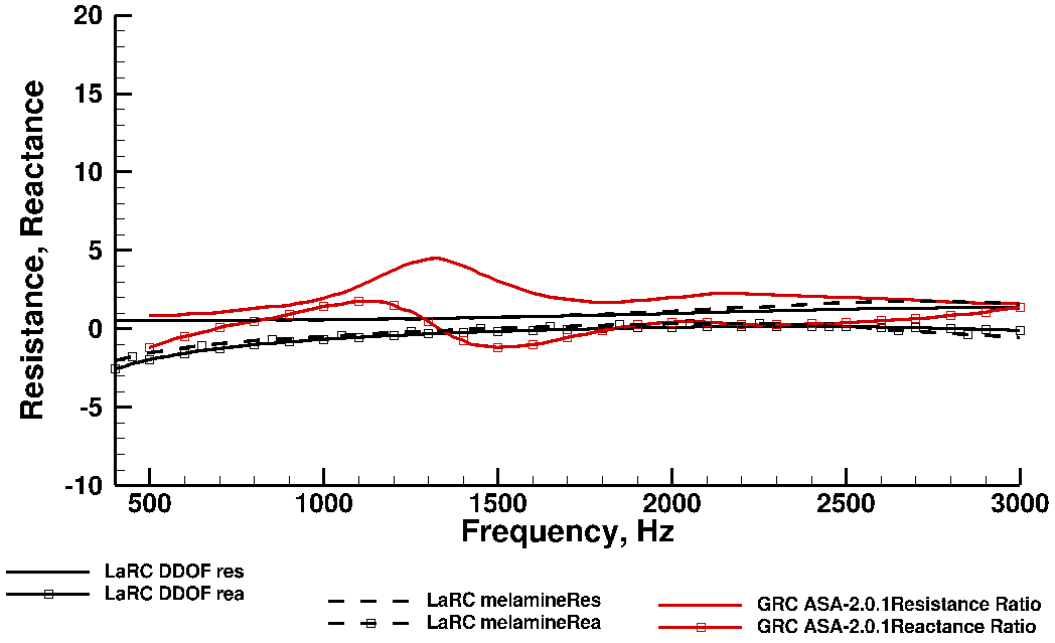

Figure A.6.—The variation of resistance and reactance with frequency for prototype ASA-2.0.1.

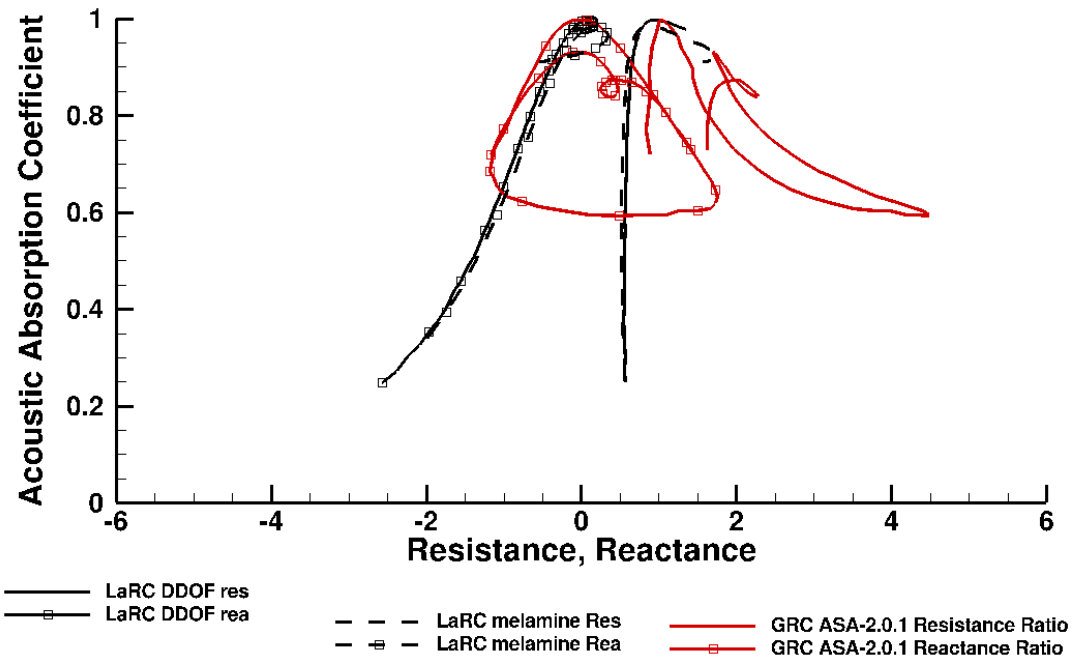

Figure A.7.—The variation of acoustic absorption coefficient with resistance and reactance for prototypes ASA-2.0.1.

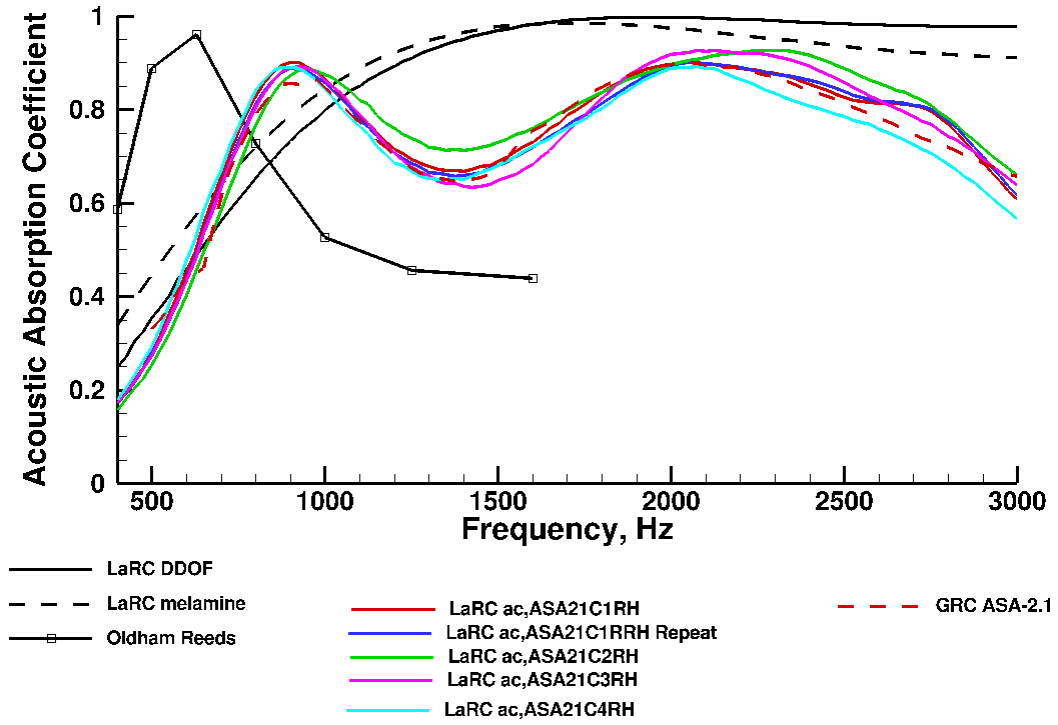

Figure A.8.—The variation of acoustic absorption coefficient with frequency for prototype ASA-2.1.

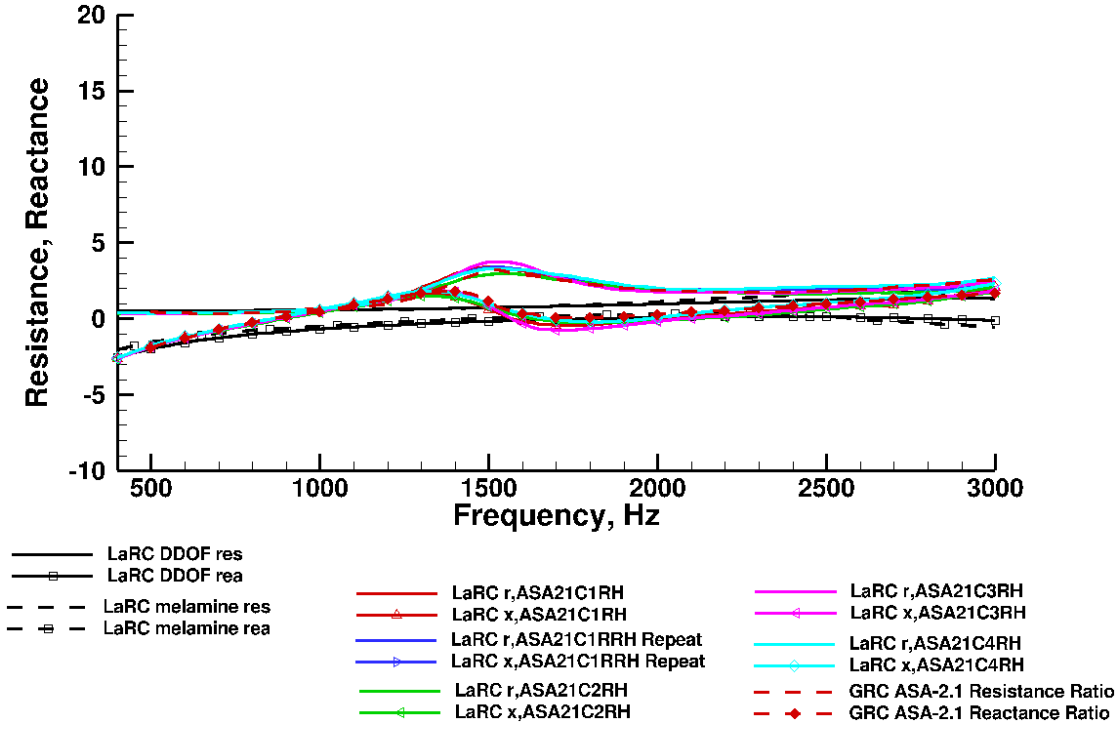

Figure A.9.—The variation of resistance and reactance with frequency for prototype ASA-2.1.

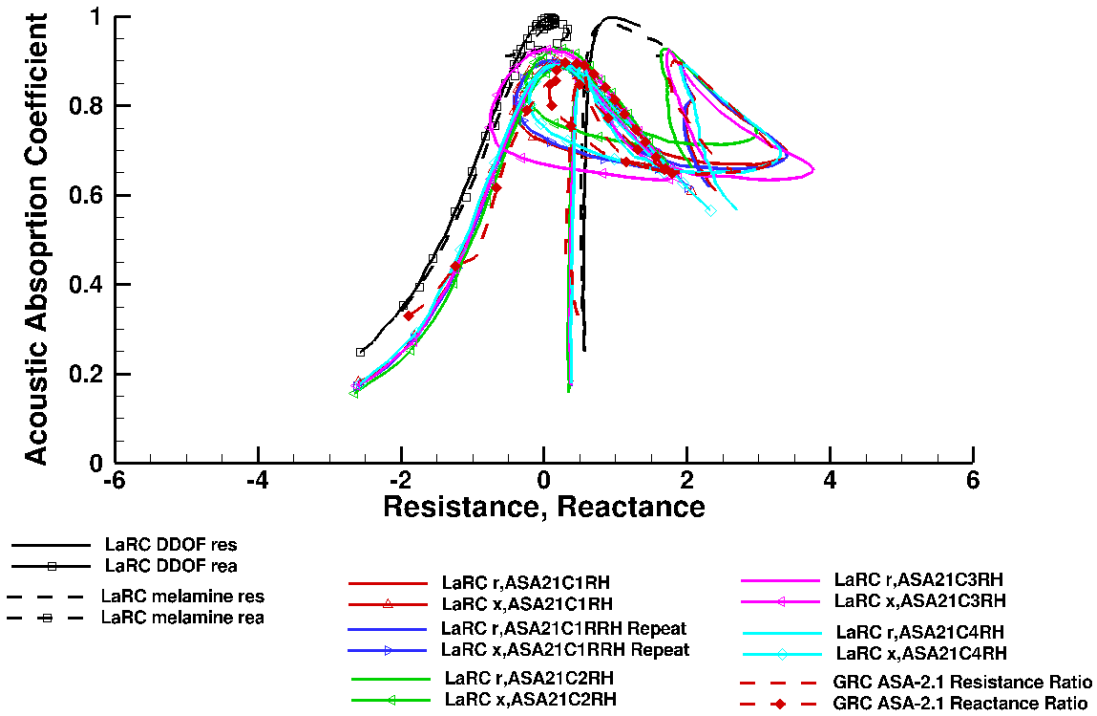

Figure A.10.—The variation of acoustic absorption coefficient with resistance and reactance for prototypes ASA-2.1.

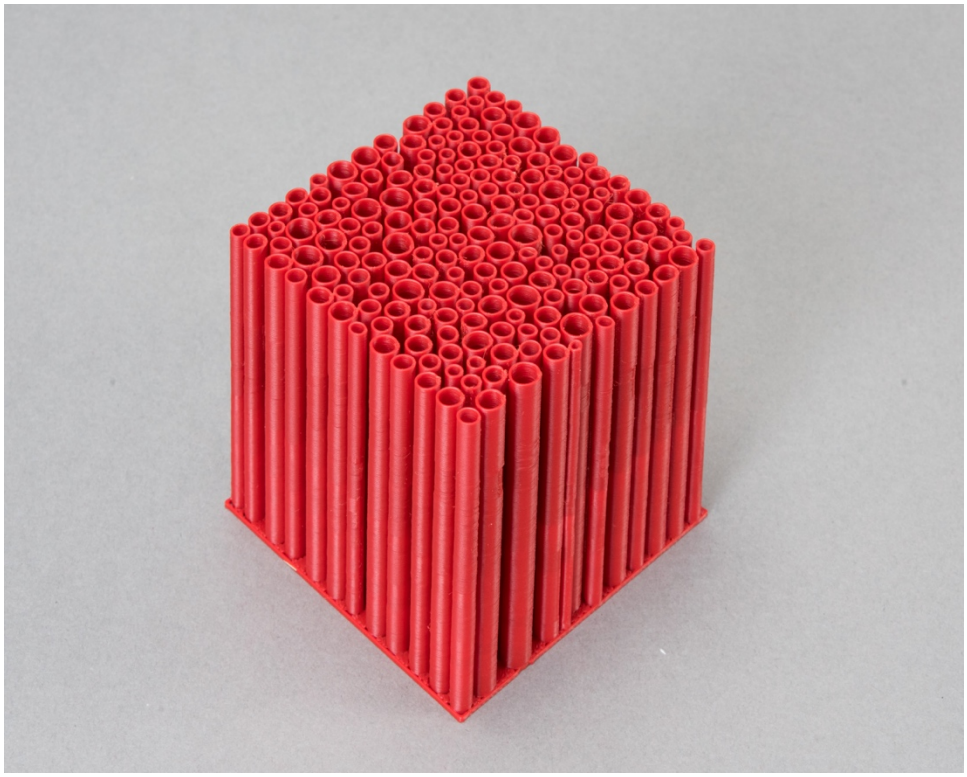

Figure A.11.—Prototype ASA-2.1 printed irregular reeds held fixed with a baseplate.

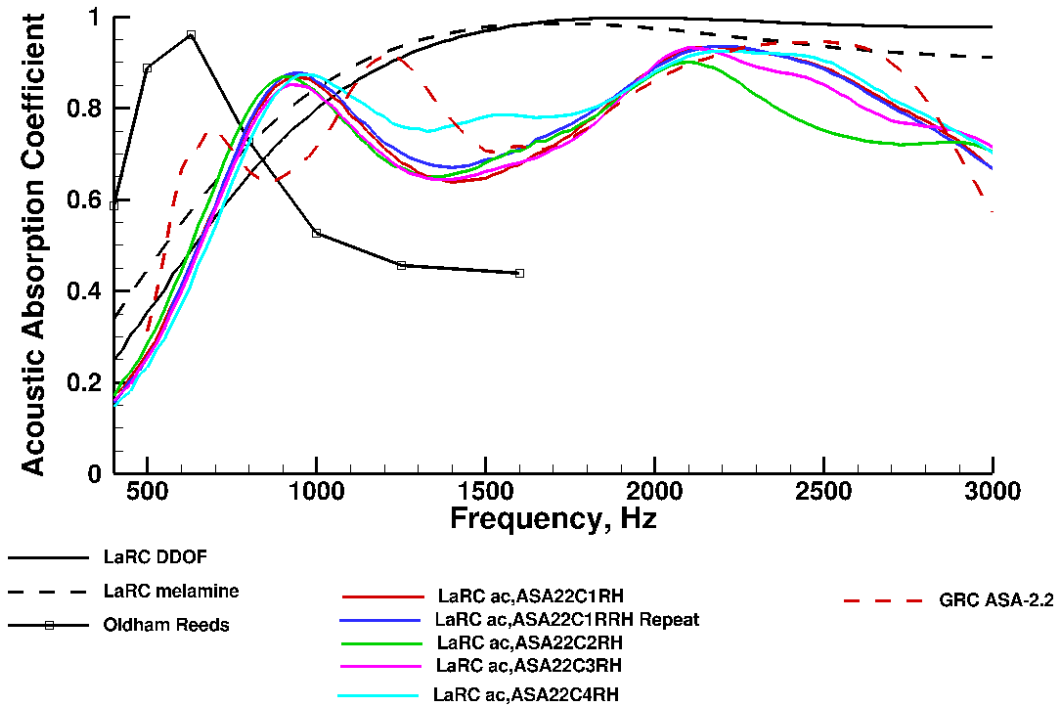

Figure A.12.—The variation of acoustic absorption coefficient with frequency for prototype ASA-2.2.

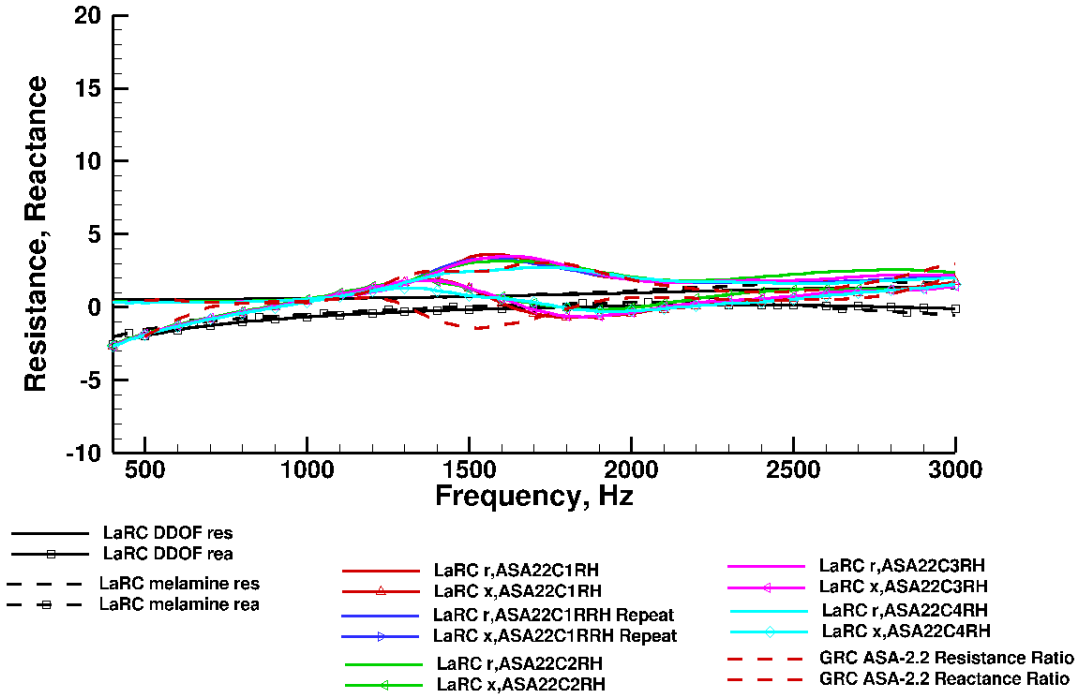

Figure A.13.—The variation of resistance and reactance with frequency for prototype ASA-2.2.

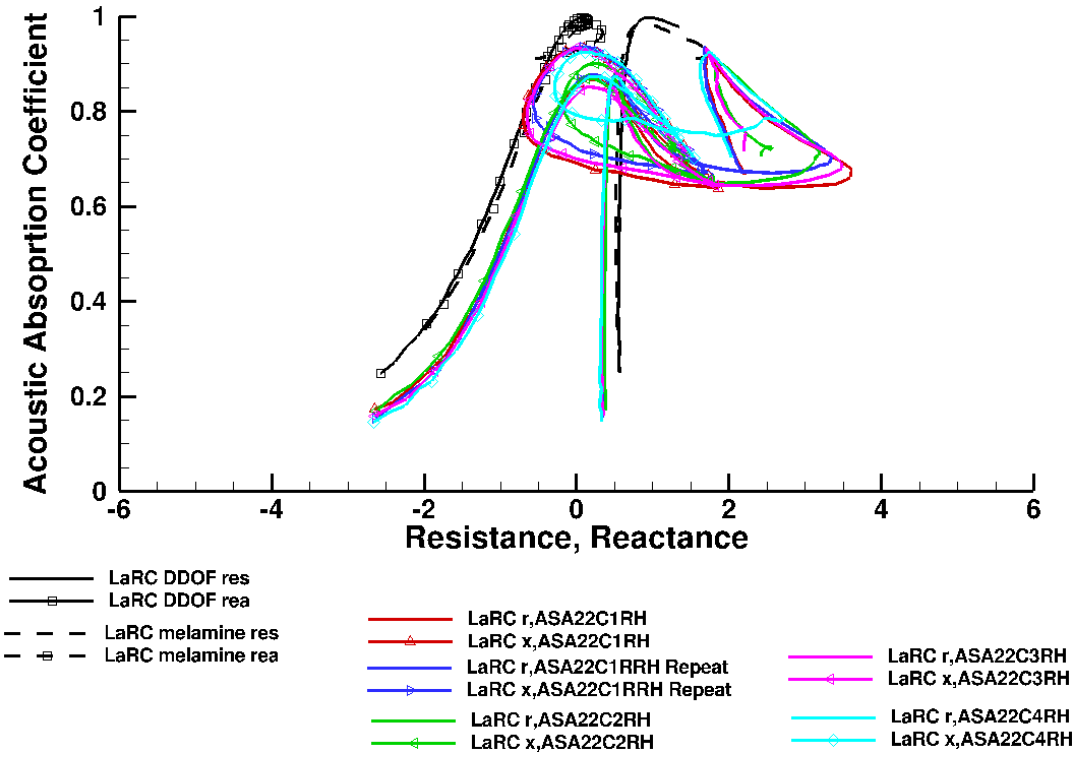

Figure A.14.—Variation of acoustic absorption coefficient with resistance and reactance for prototype ASA-2.2.

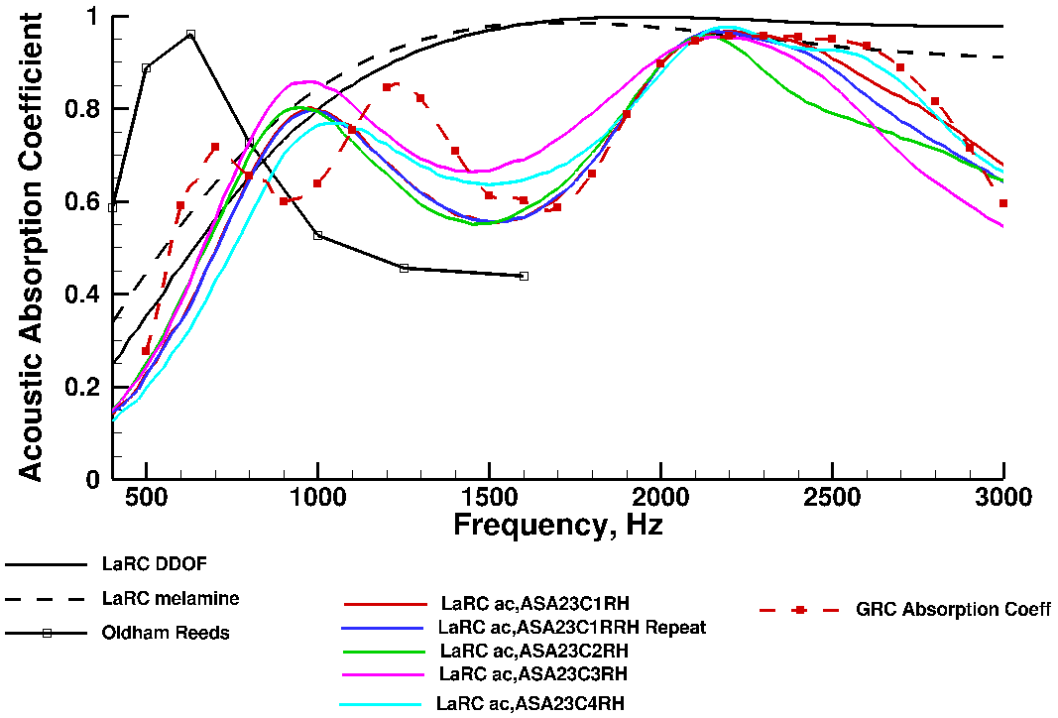

Figure A.15.—The variation of acoustic absorption coefficient with frequency for prototype ASA-2.3.

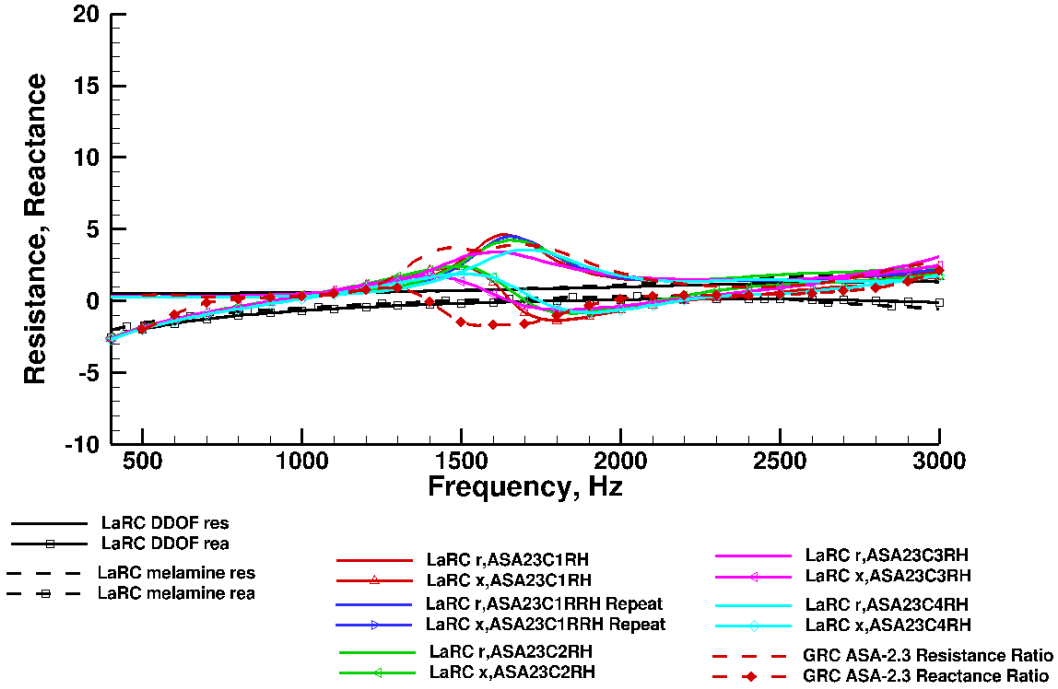

Figure A.16.—The variation of resistance and reactance with frequency for prototype ASA-2.3.

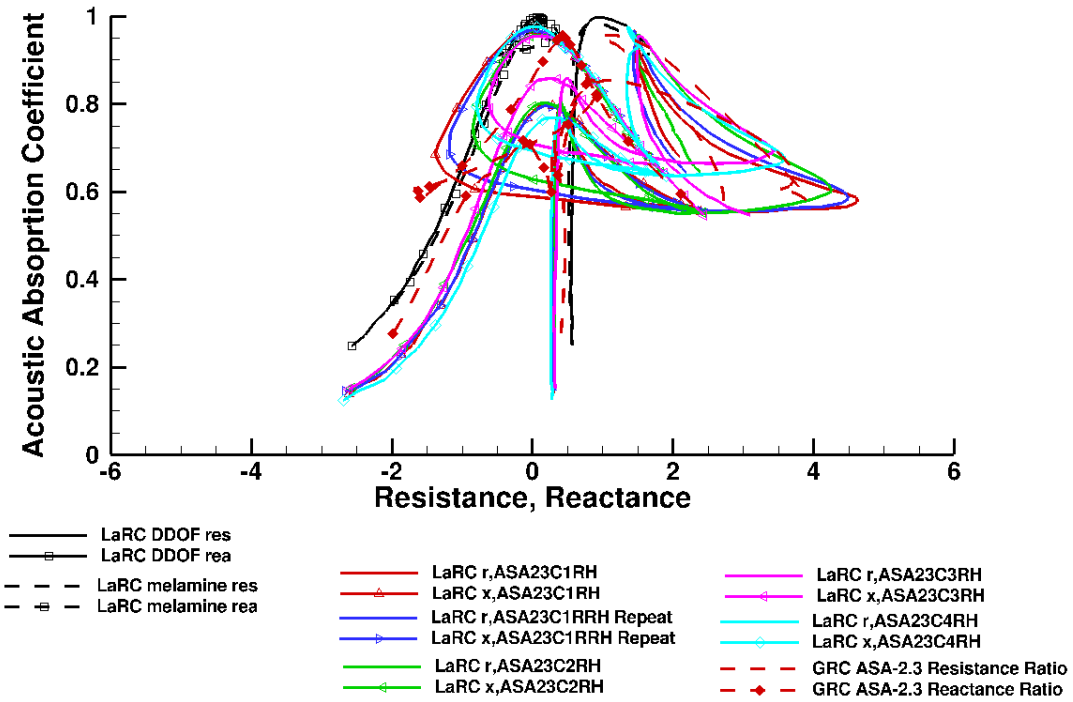

Figure A.17.—The variation of acoustic absorption coefficient with resistance and reactance for prototypes ASA-2.3.

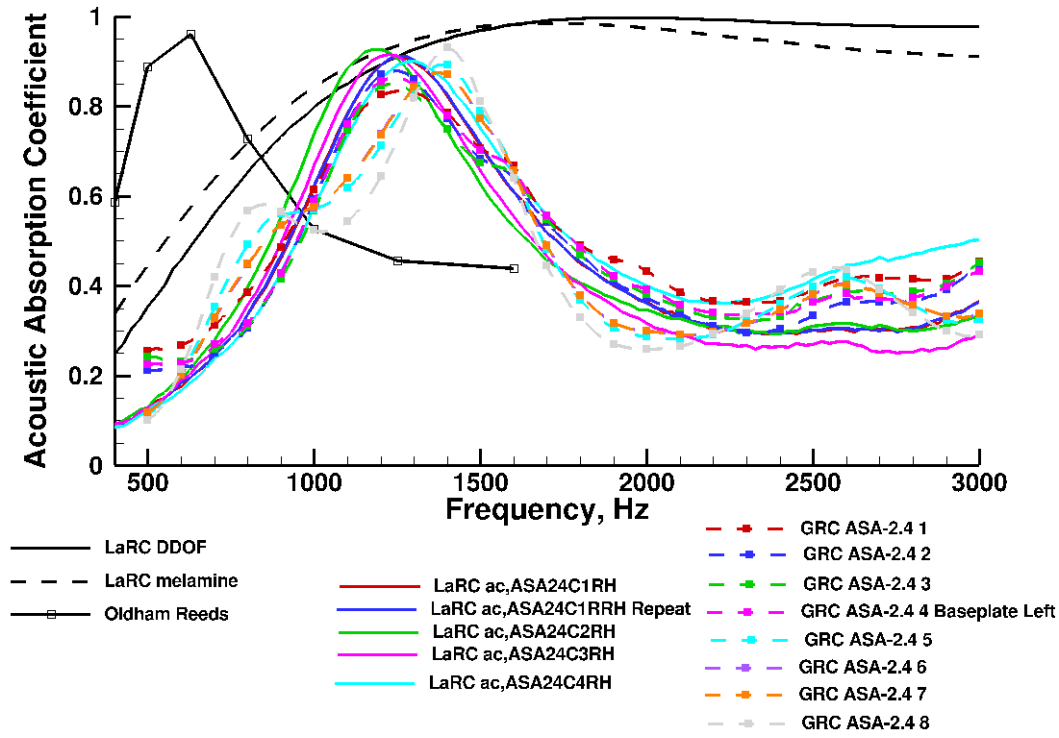

Figure A.18.—The variation of acoustic absorption coefficient with frequency for prototype ASA-2.4.

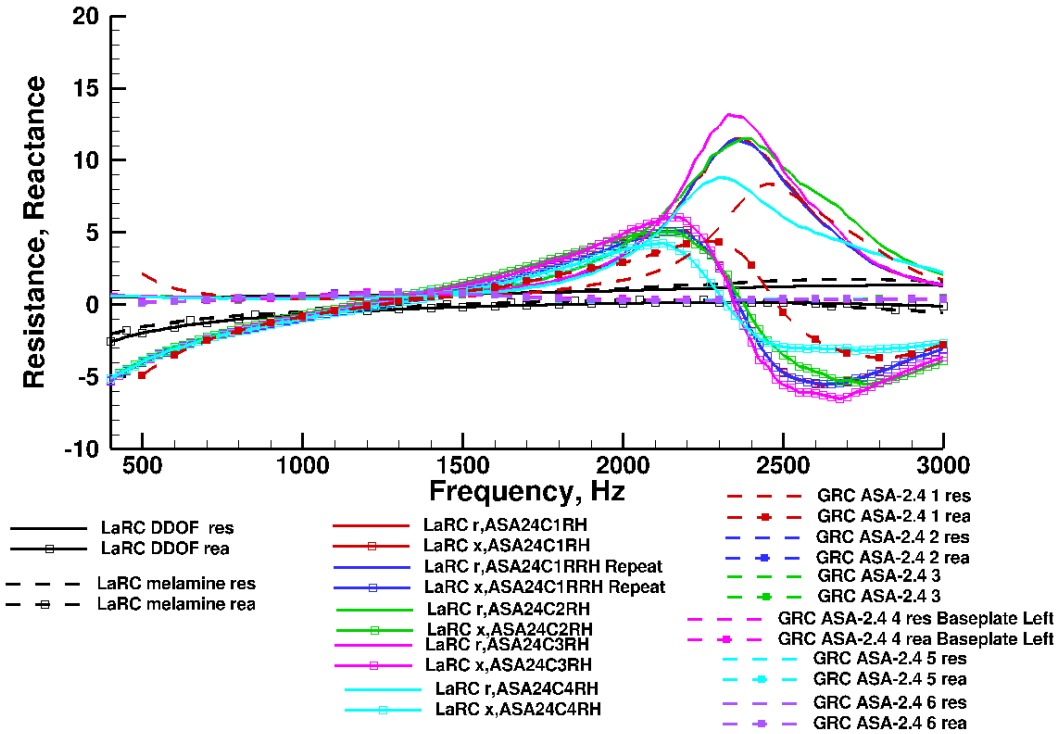

Figure A.19.—The variation of resistance and reactance with frequency for prototype ASA-2.4.

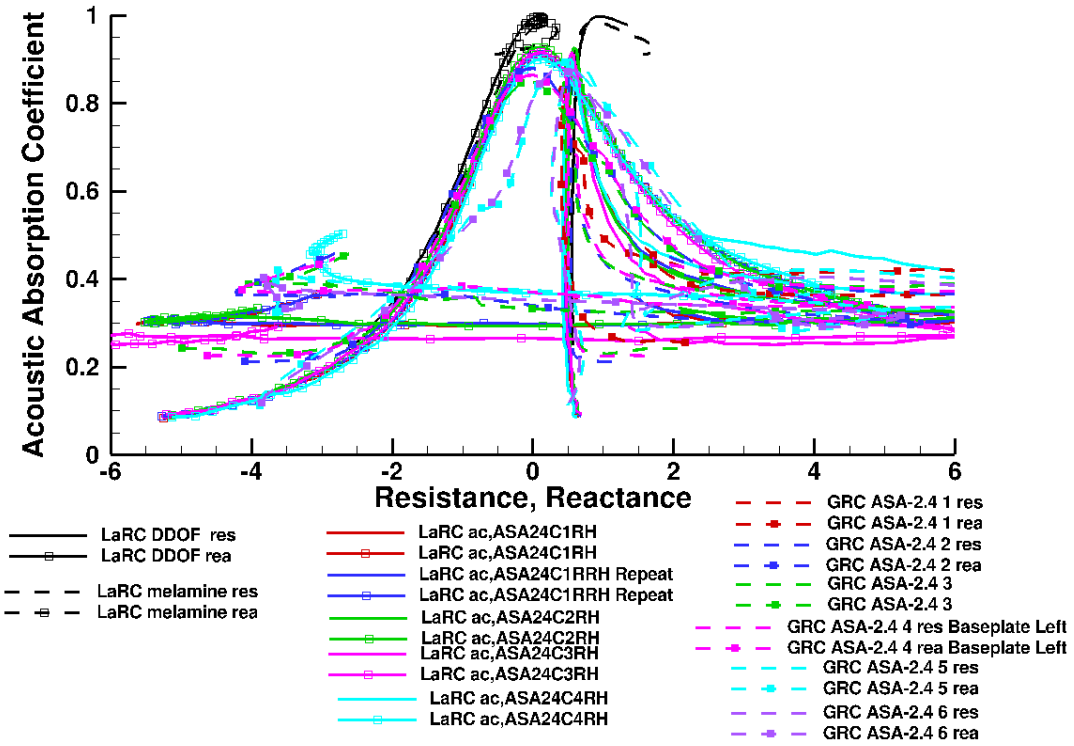

Figure A.20.—The variation of acoustic absorption coefficient with resistance and reactance for prototypes ASA-2.4.

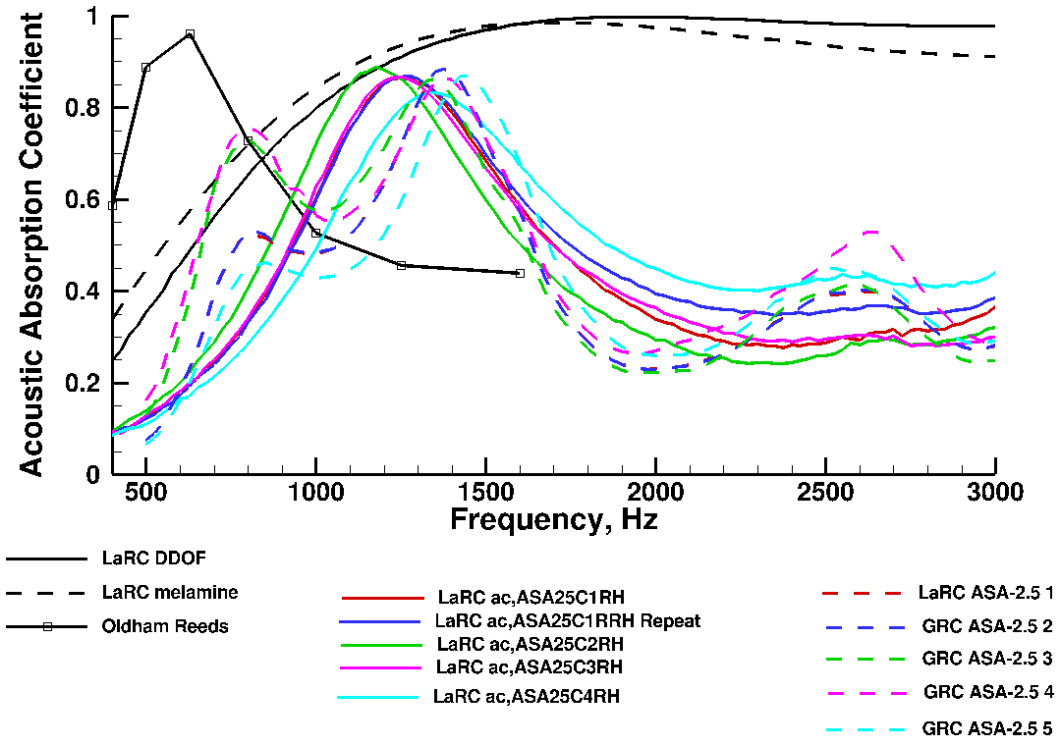

Figure A.21.—The variation of acoustic absorption coefficient with frequency for prototype ASA-2.5.

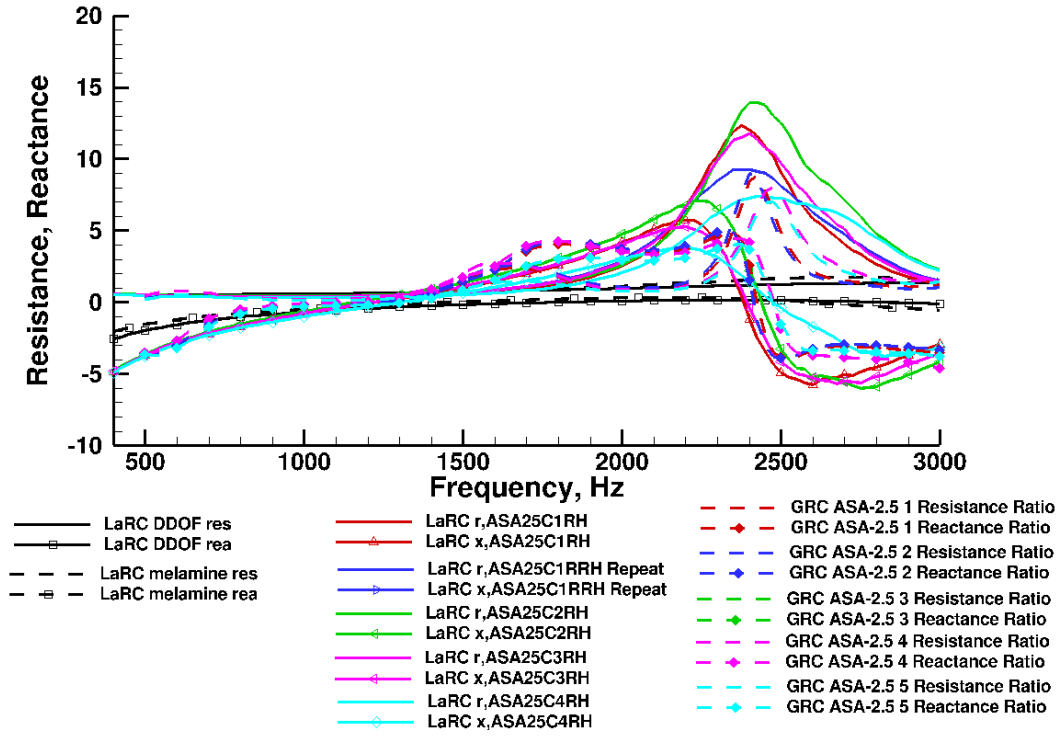

Figure A.22.—The variation of resistance and reactance with frequency for prototype ASA-2.5.

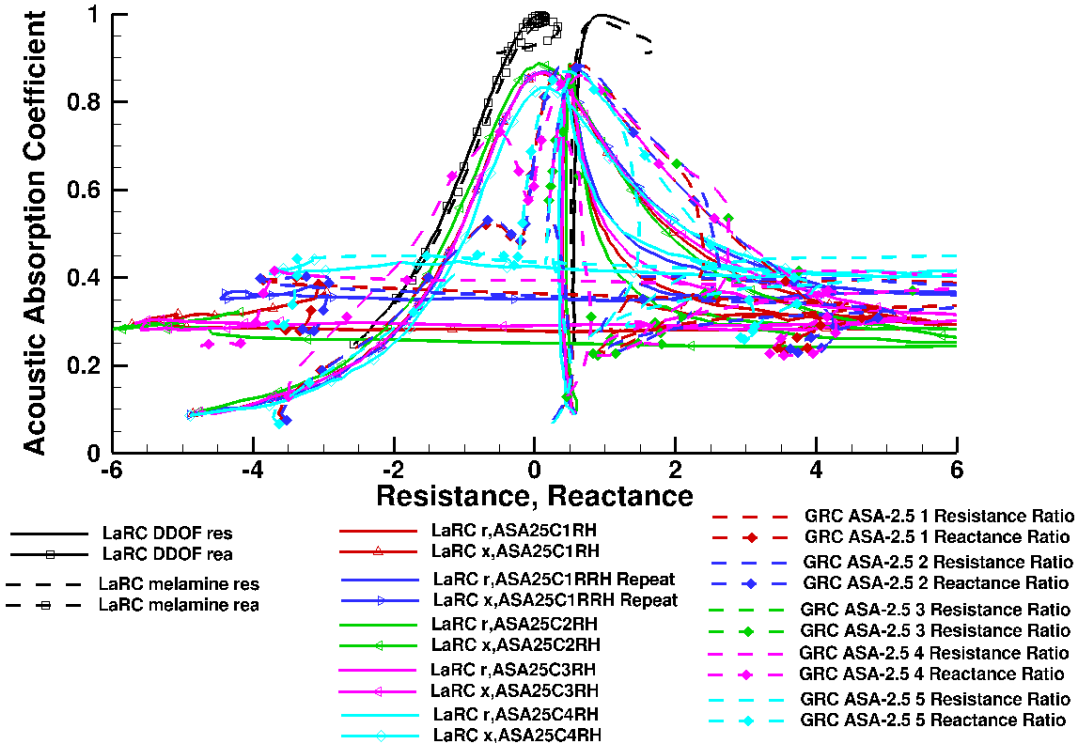

Figure A.23.—Variation of acoustic absorption coefficient with resistance and reactance for prototypes ASA-2.5.

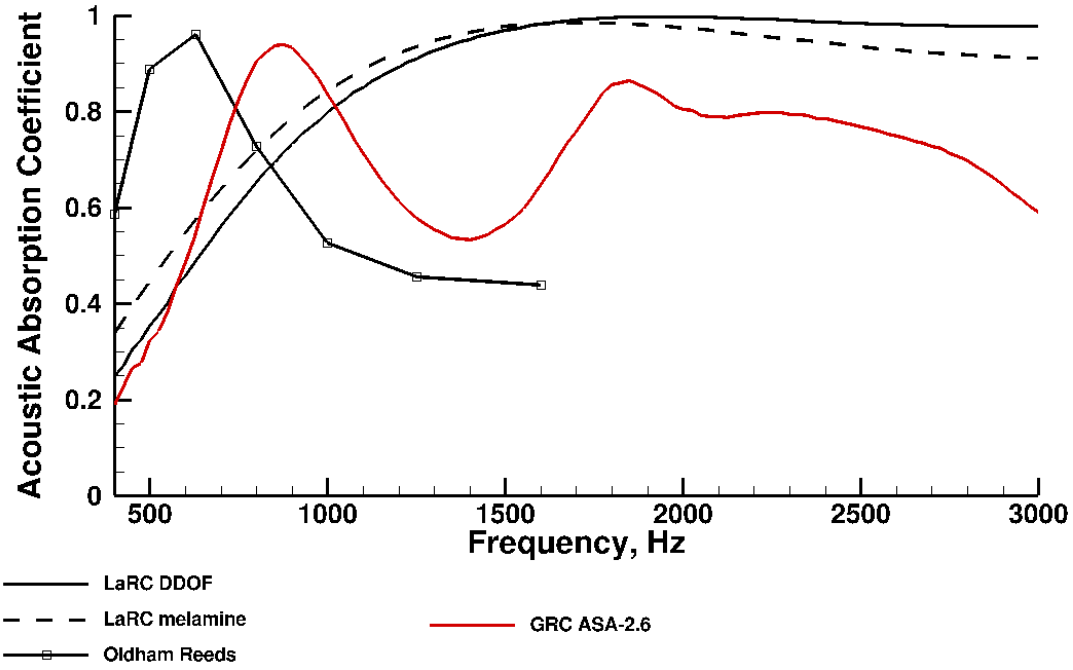

Figure A.24.—The variation of acoustic absorption coefficient with frequency for prototype ASA-2.6.

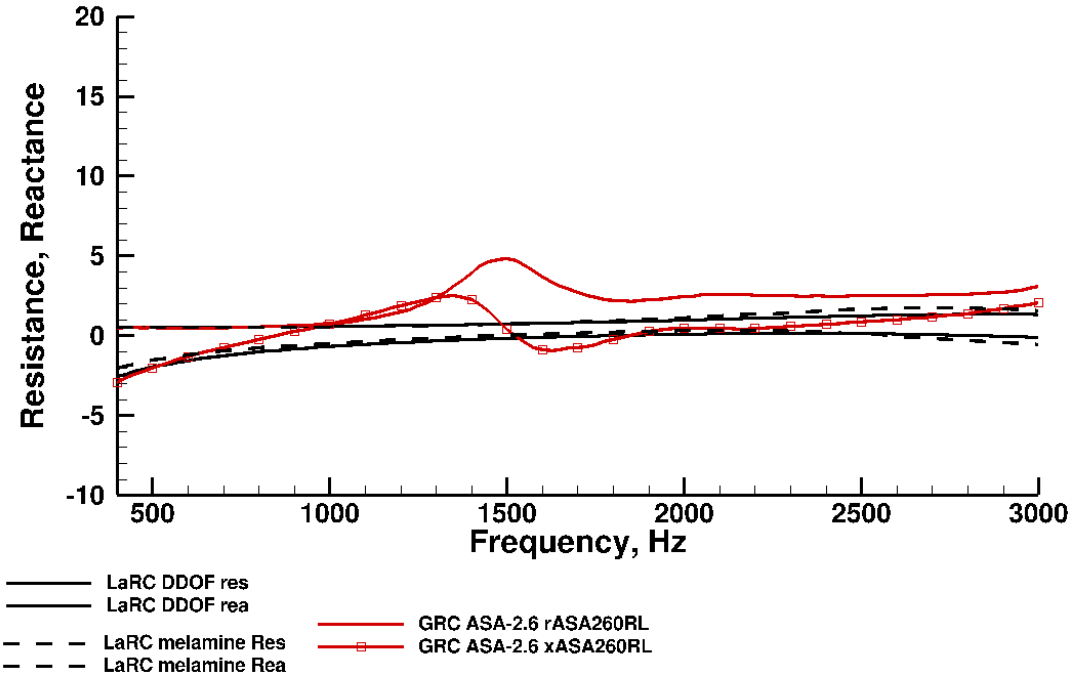

Figure A.25.—The variation of resistance and reactance with frequency for prototype ASA-2.6.

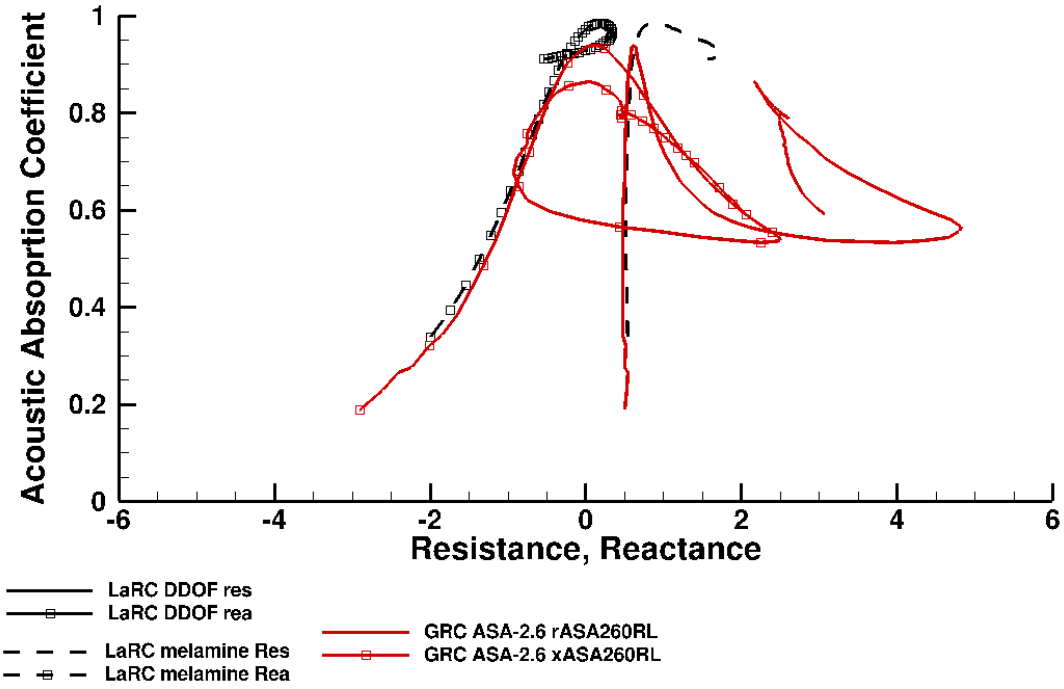

Figure A.26.—The variation of resistance and reactance with frequency for prototype ASA-2.6.

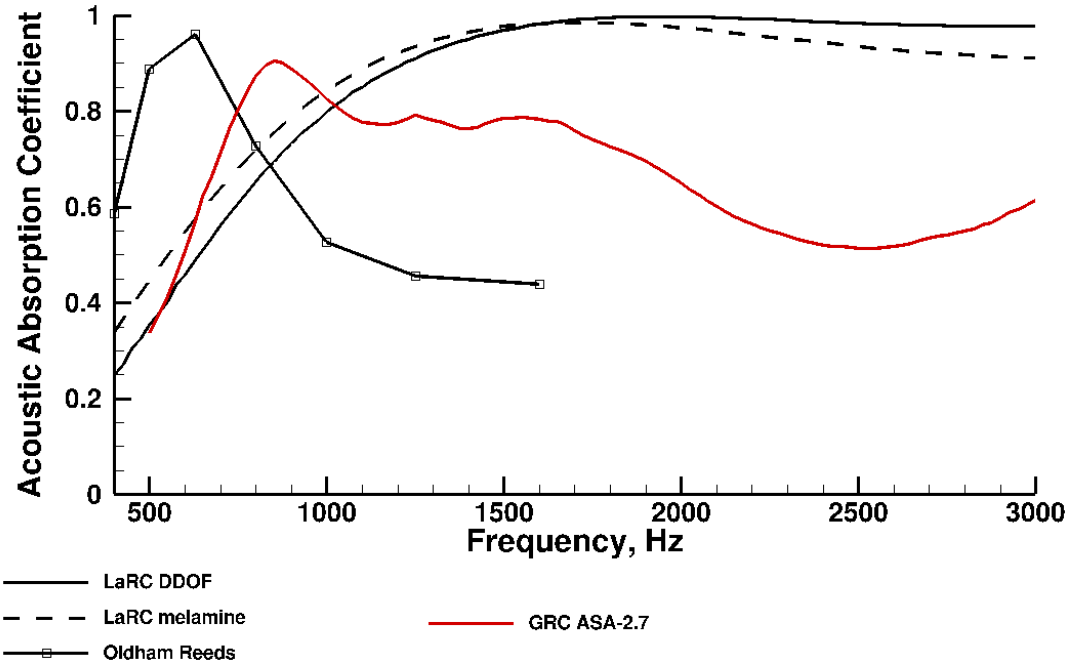

Figure A.27.—The variation of acoustic absorption coefficient with frequency for prototype ASA-2.7.

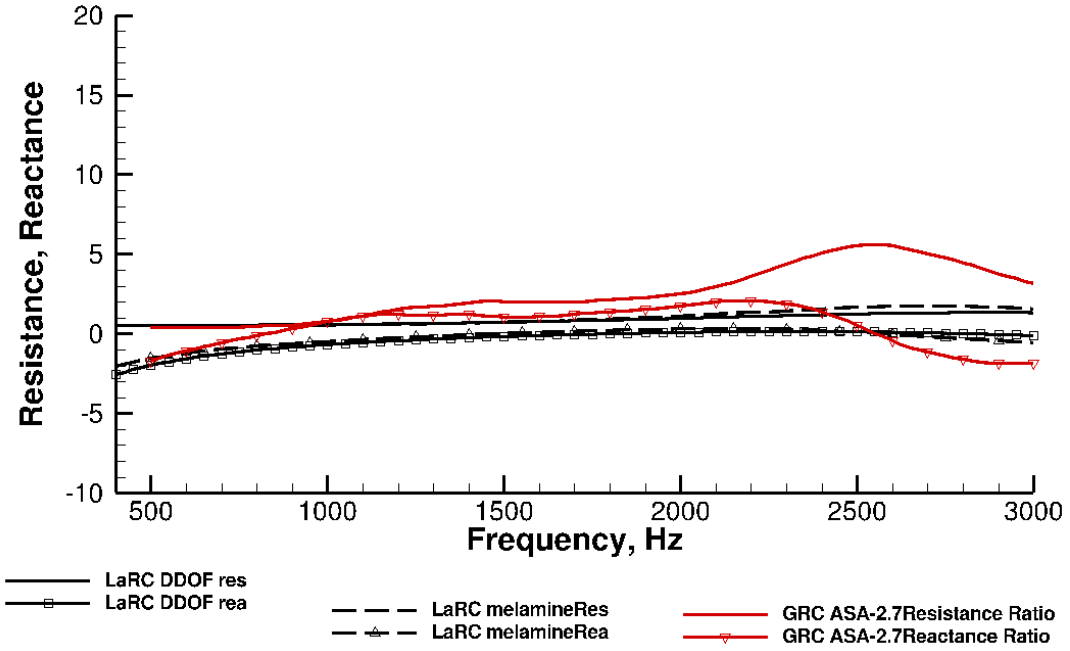

Figure A.28.—The variation of resistance and reactance with frequency for prototype ASA-2.7.

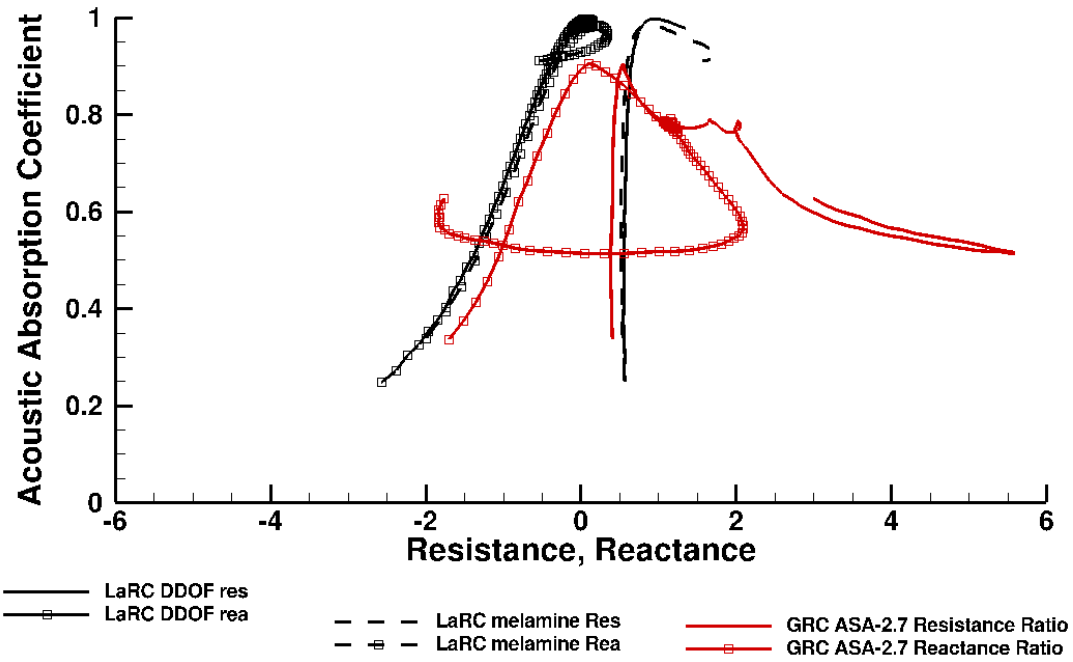

Figure A.29.—The variation of acoustic absorption coefficient with resistance and reactance for prototypes ASA-2.7.

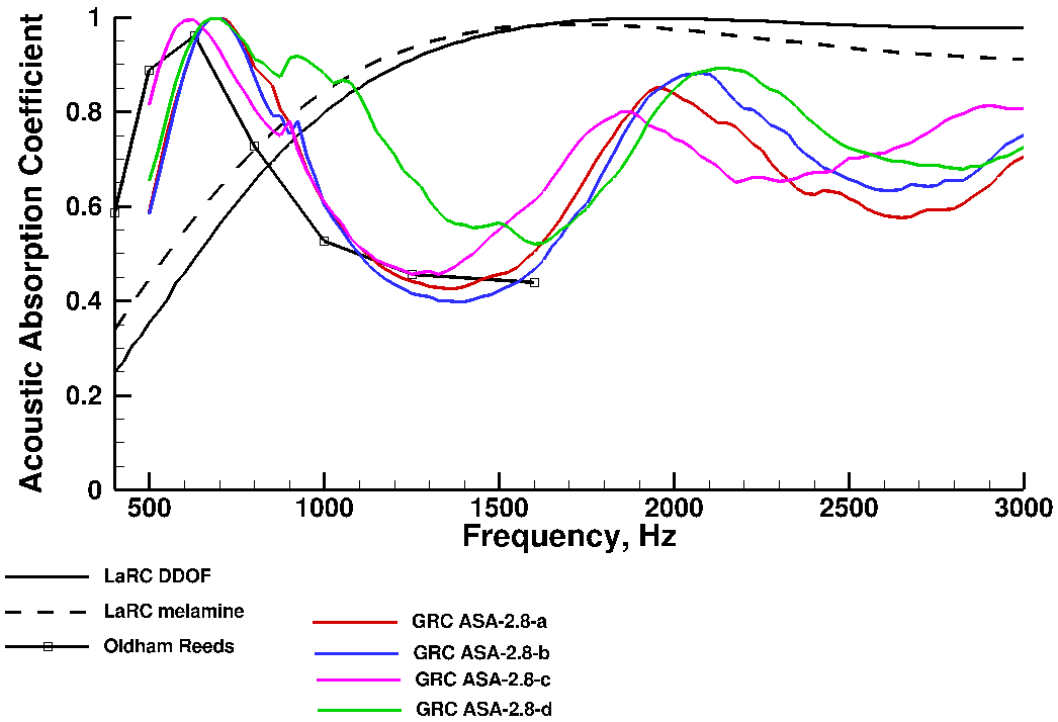

Figure A.30.—The variation of acoustic absorption coefficient with frequency for prototype ASA-2.8.

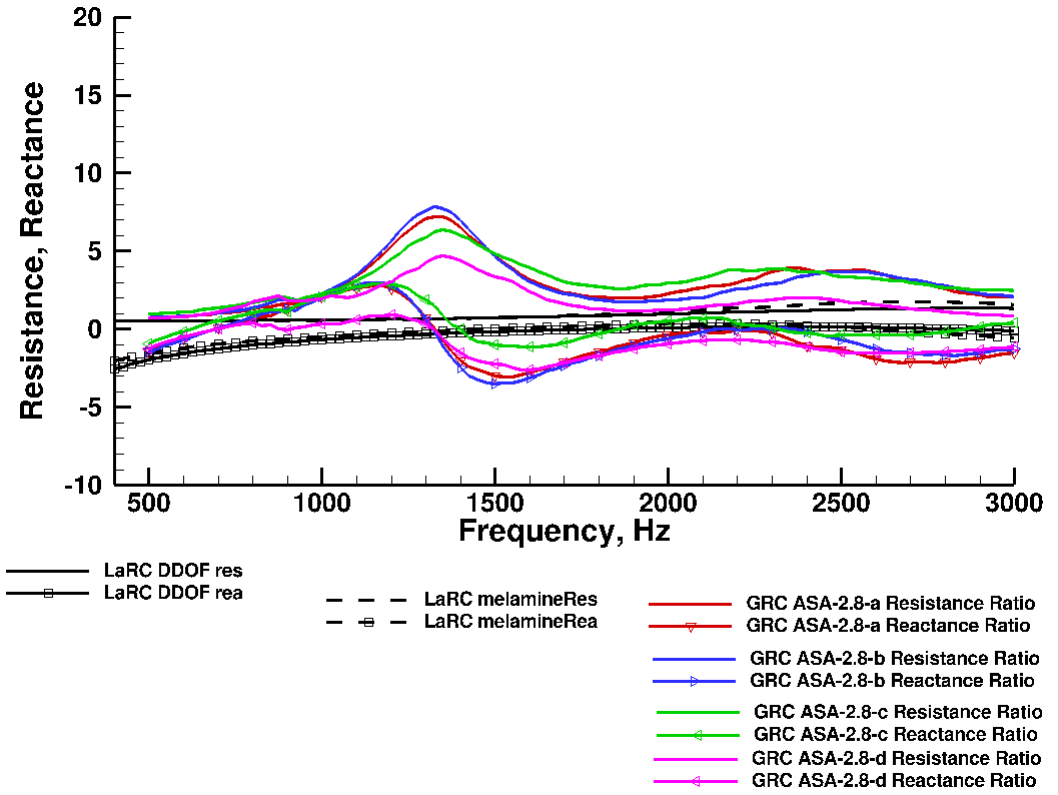

Figure A.31.—The variation of resistance and reactance with frequency for prototype ASA-2.8.

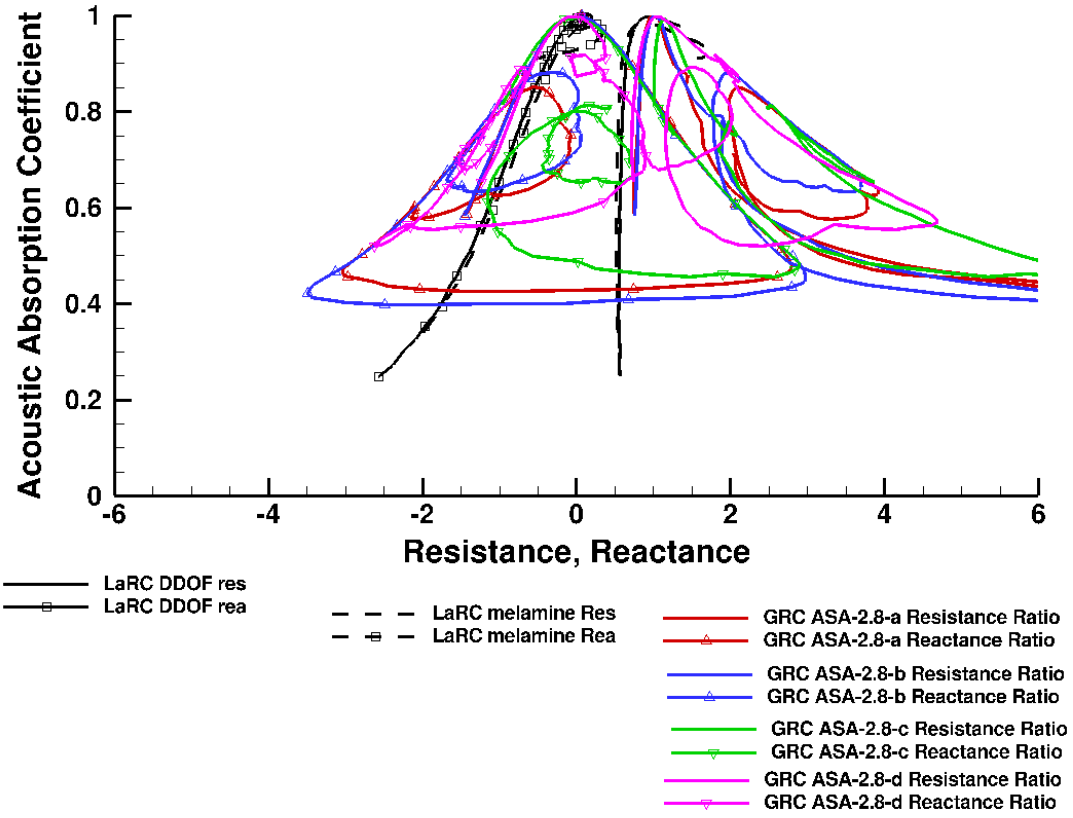

Figure A.32.—The variation of acoustic absorption coefficient with resistance and reactance for prototypes ASA-2.8.

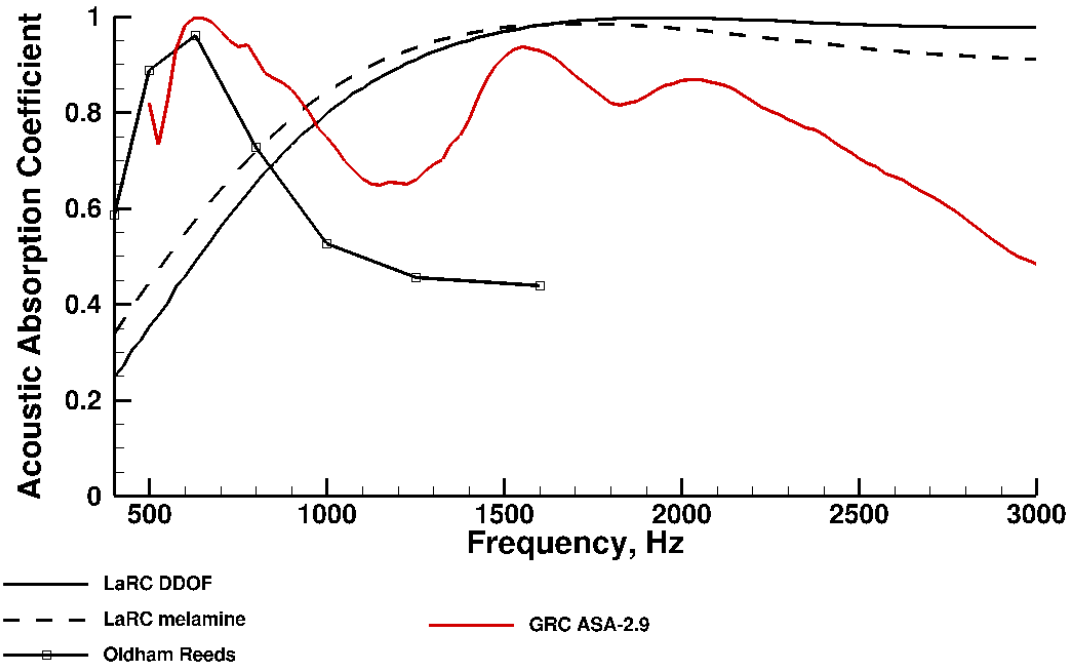

Figure A.33.—The variation of acoustic absorption coefficient with frequency for prototype ASA-2.9.

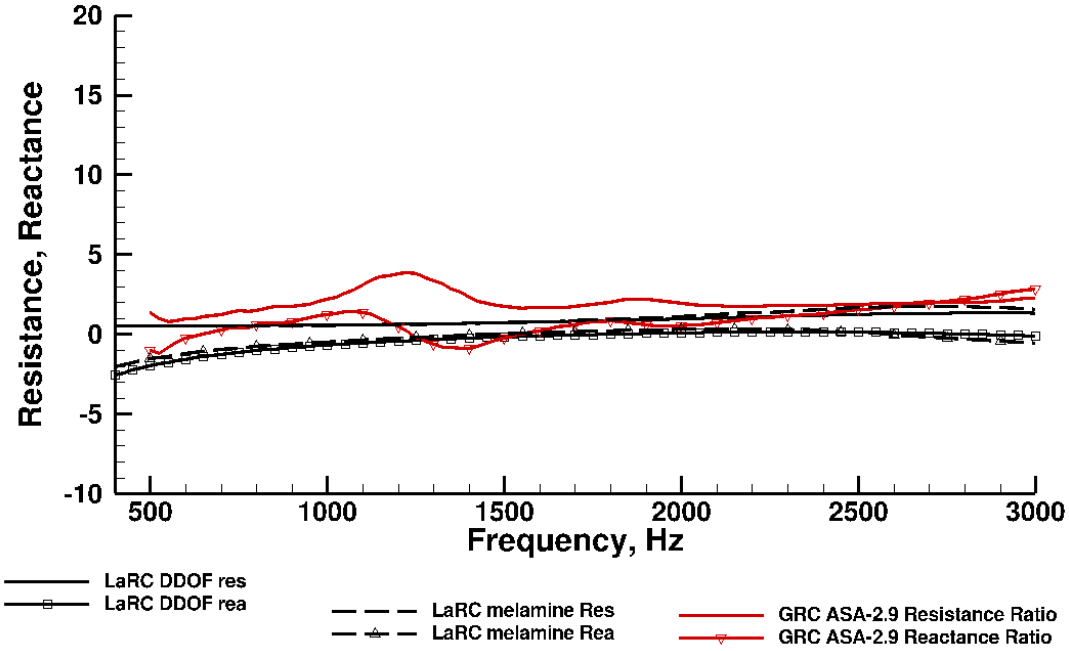

Figure A.34.—The variation of resistance and reactance with frequency for prototype ASA-2.9.

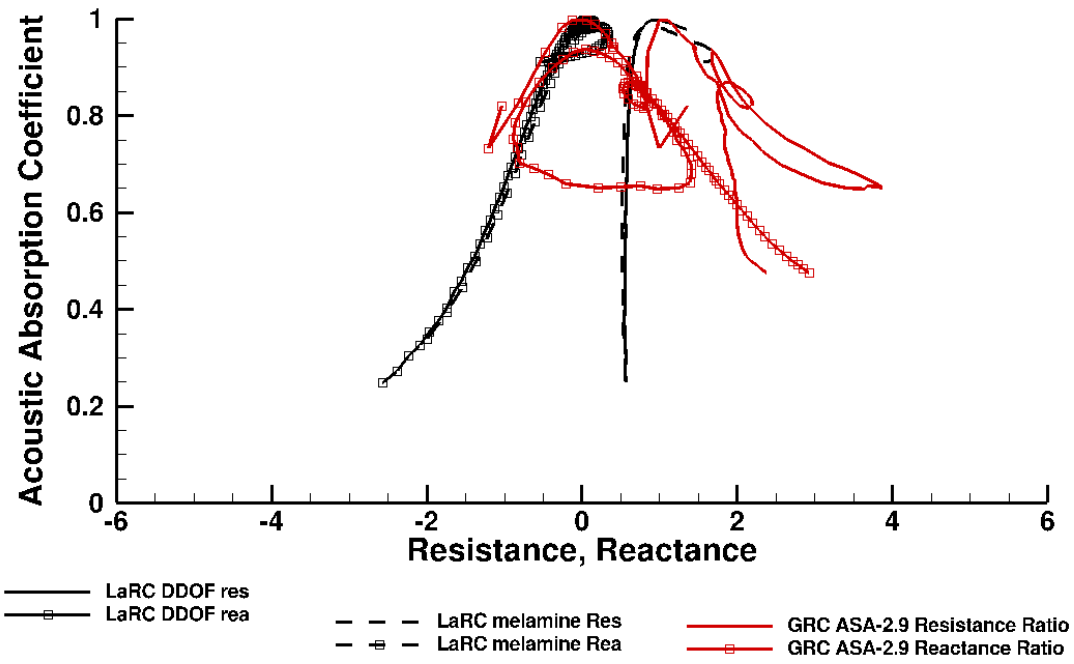

Figure A.35.—The variation of acoustic absorption coefficient with resistance and reactance for prototypes ASA-2.9.

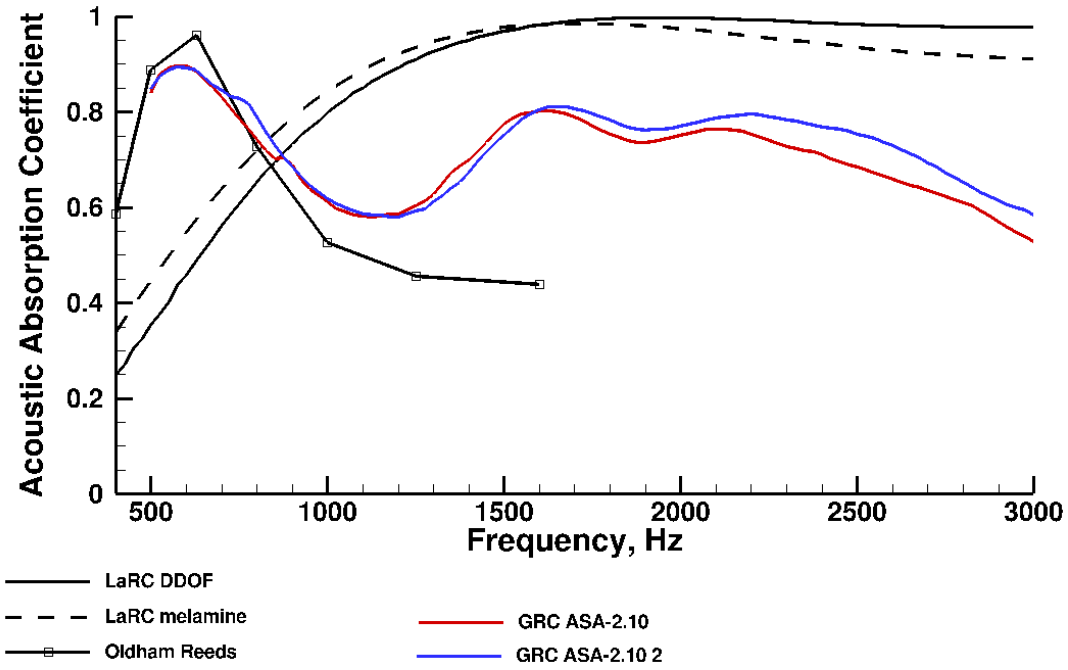

Figure A.36.—The variation of acoustic absorption coefficient with frequency for prototype ASA-2.10.

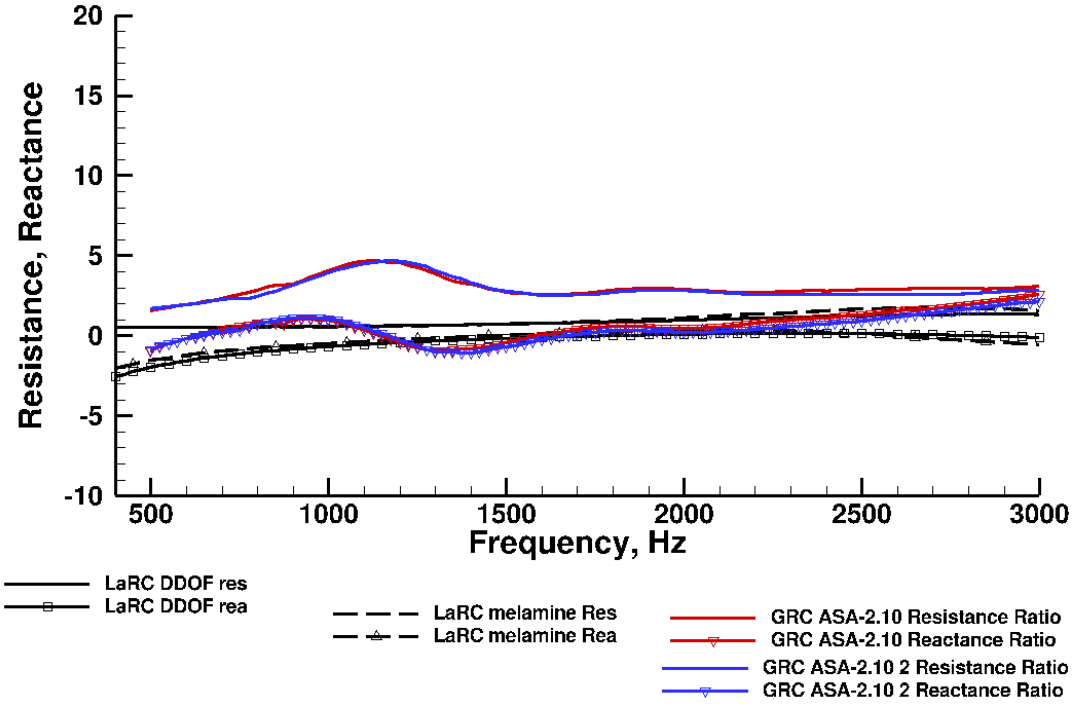

Figure A.37.—The variation of resistance and reactance with frequency for prototype ASA-2.10.

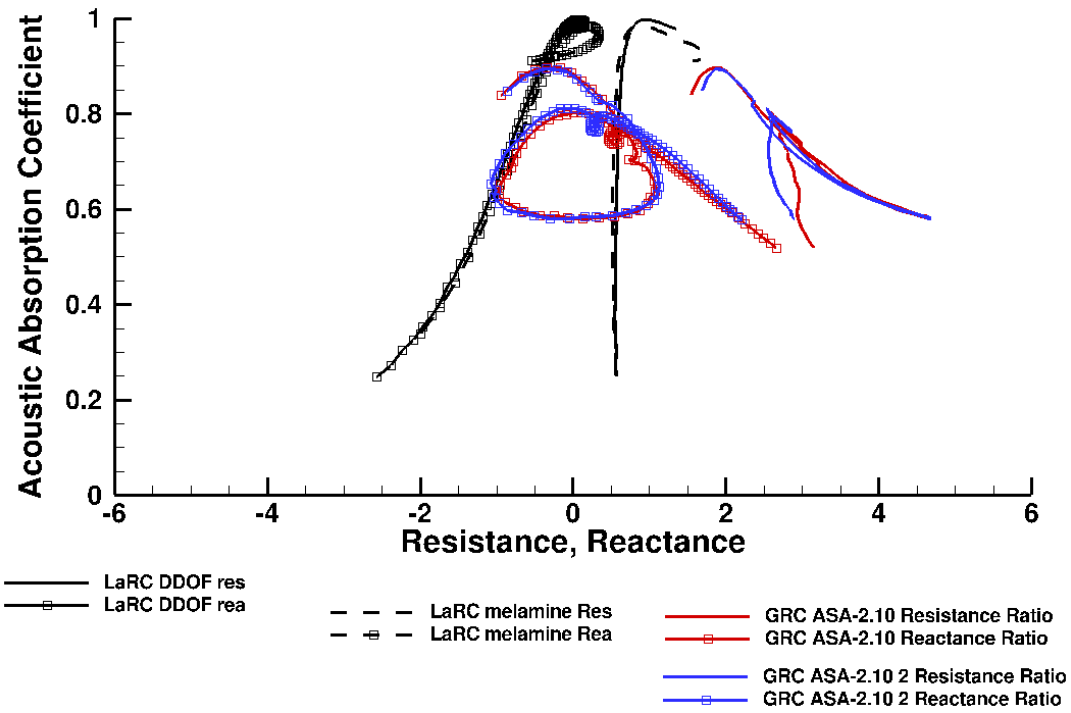

Figure A.38.—The variation of acoustic absorption coefficient with resistance and reactance for prototypes ASA-2.10.

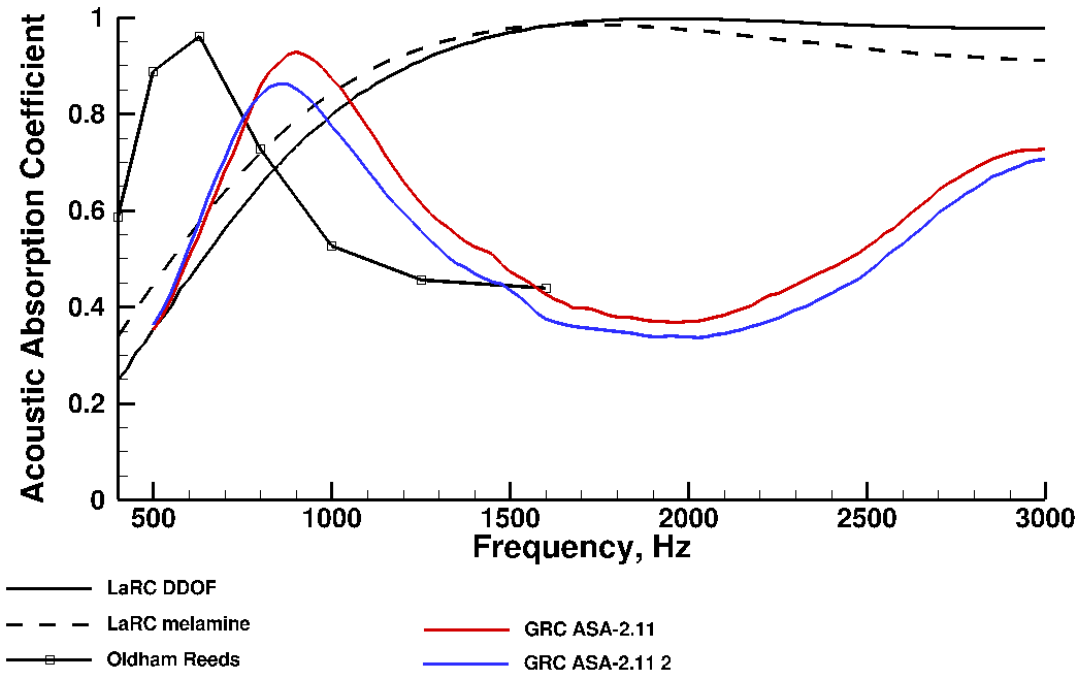

Figure A.39.—The variation of acoustic absorption coefficient with frequency for prototype ASA-2.11.

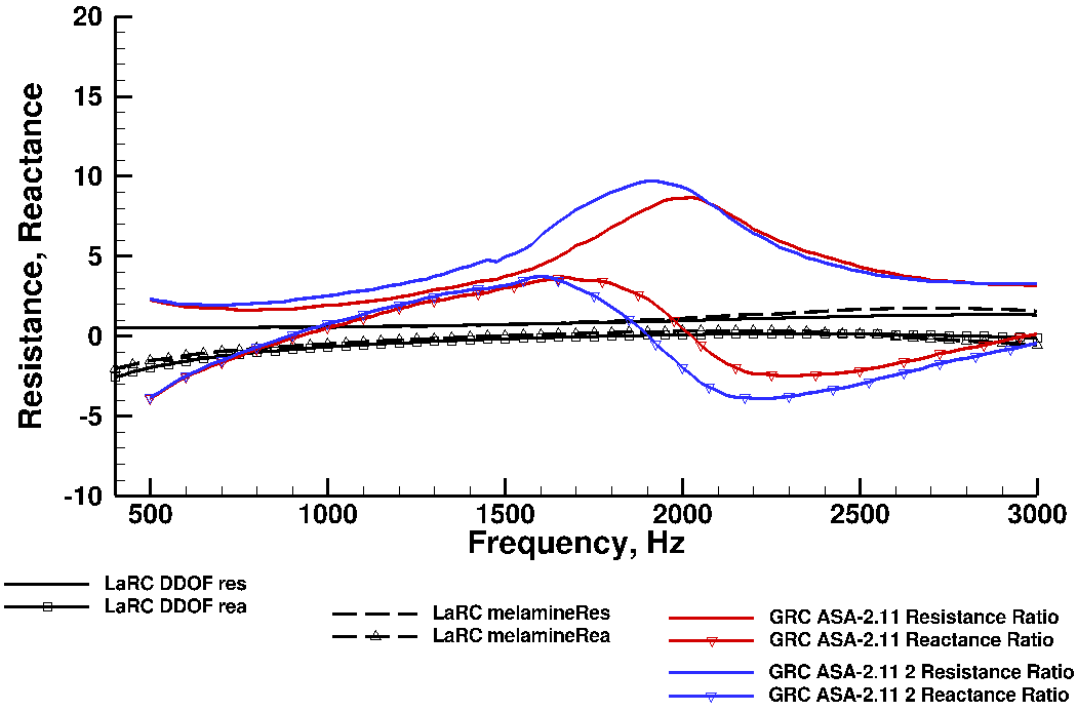

Figure A.40.—The variation of resistance and reactance with frequency for prototype ASA-2.11.

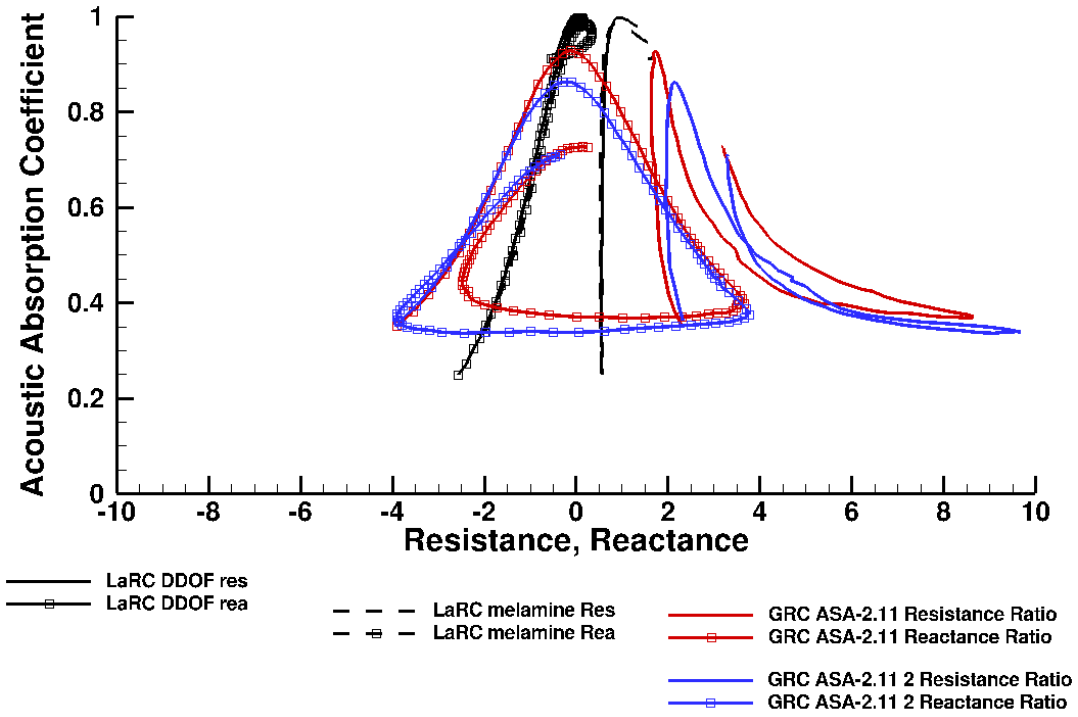

Figure A.41.—The variation of acoustic absorption coefficient with resistance and reactance for prototypes ASA-2.11.

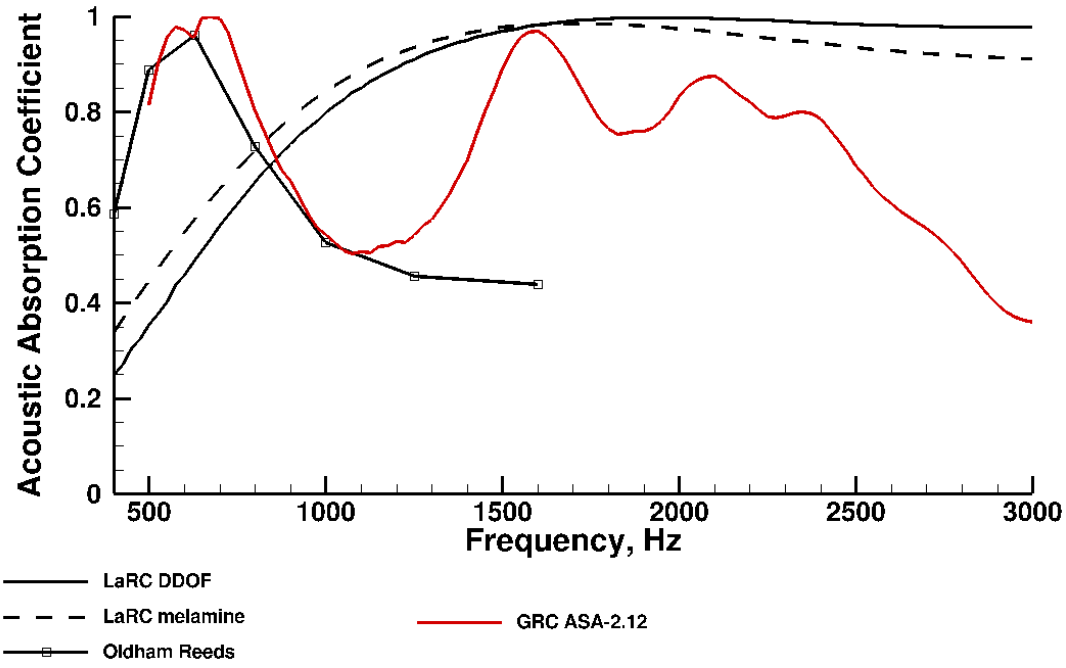

Figure A.42.—The variation of acoustic absorption coefficient with frequency for prototype ASA2.12.

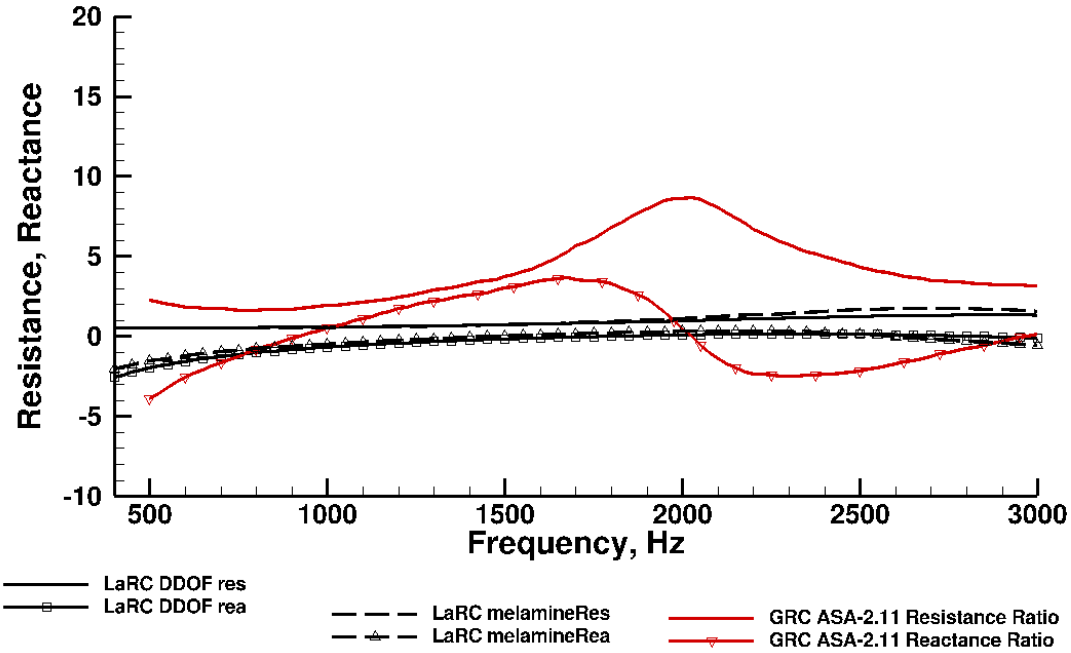

Figure A.43.—The variation of resistance and reactance with frequency for prototype ASA-2.12.

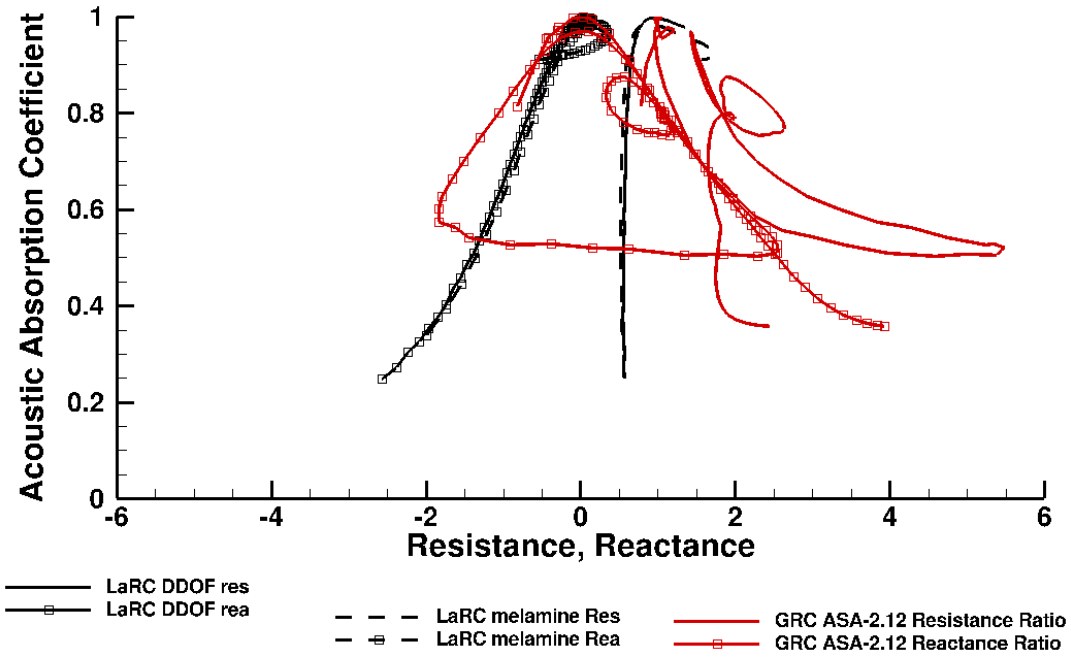

Figure A.44.—The variation of acoustic absorption coefficient with resistance and reactance for prototypes ASA-2.12.

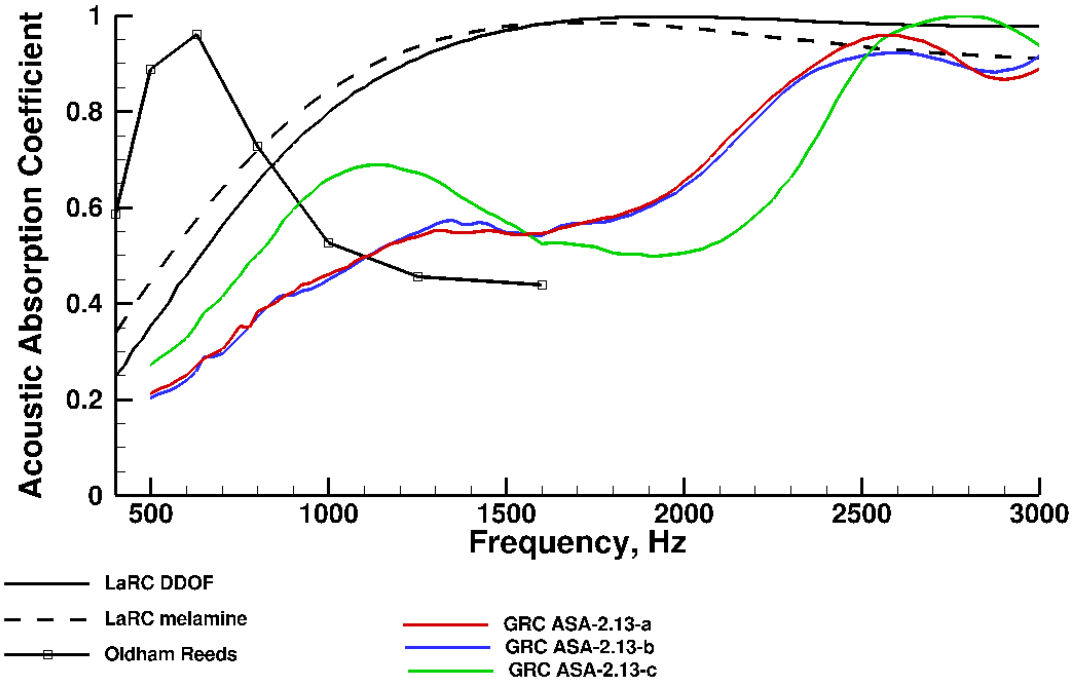

Figure A.45.—The variation of acoustic absorption coefficient with frequency for prototype ASA-2.13.

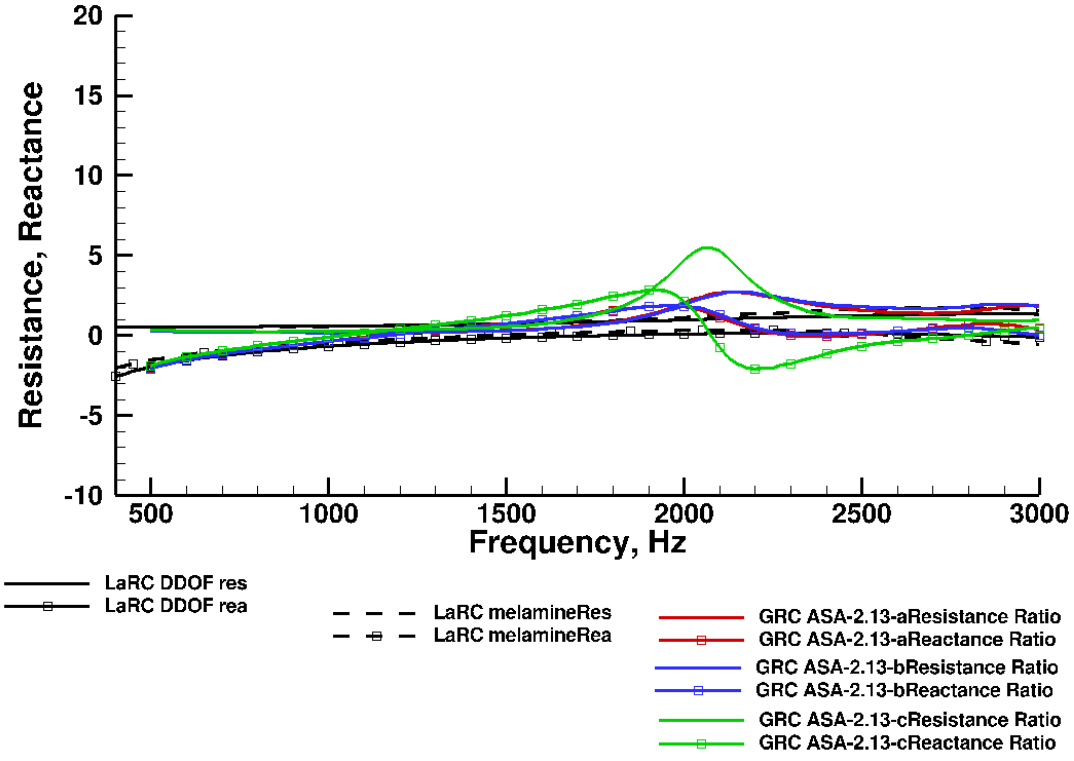

Figure A.46.—The variation of resistance and reactance with frequency for prototype ASA-2.13.

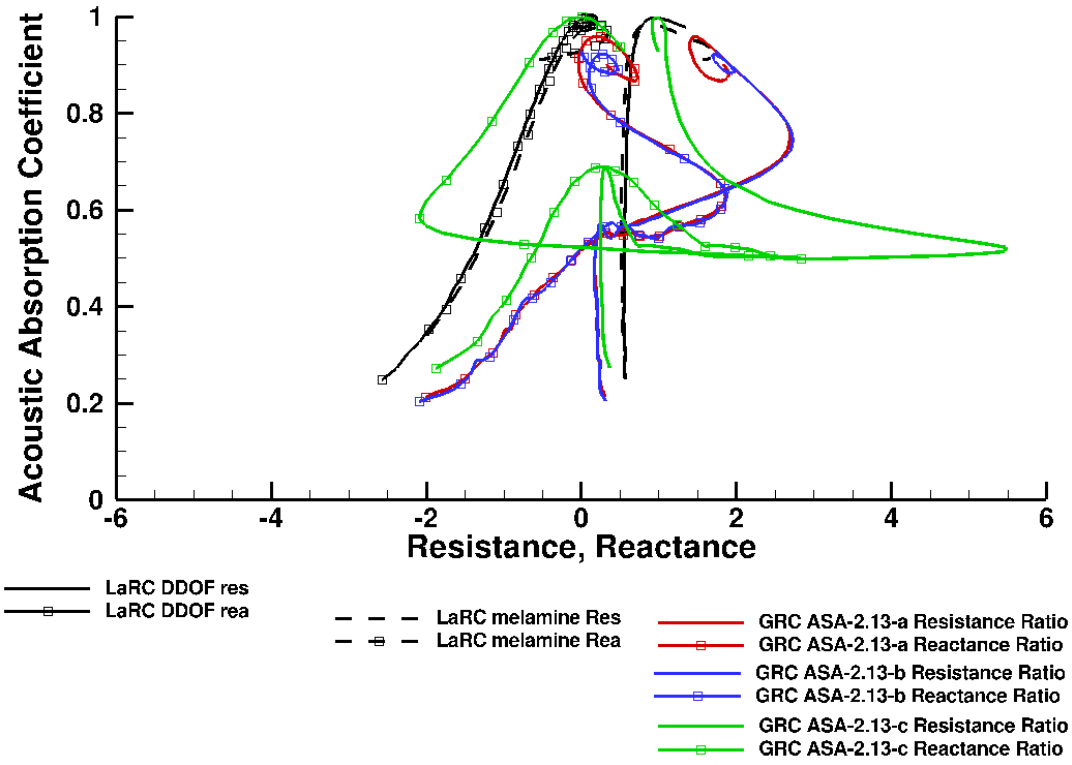

Figure A.47.—The variation of acoustic absorption coefficient with resistance and reactance for prototypes ASA-2.13.

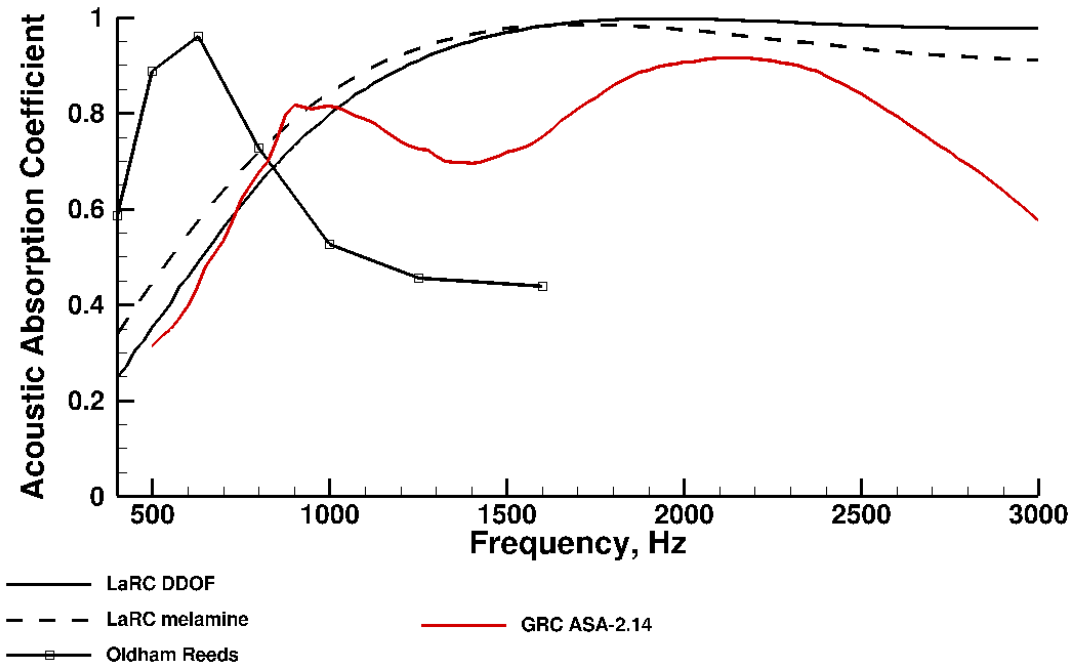

Figure A.48.—The variation of acoustic absorption coefficient with frequency for prototype ASA-2.14.

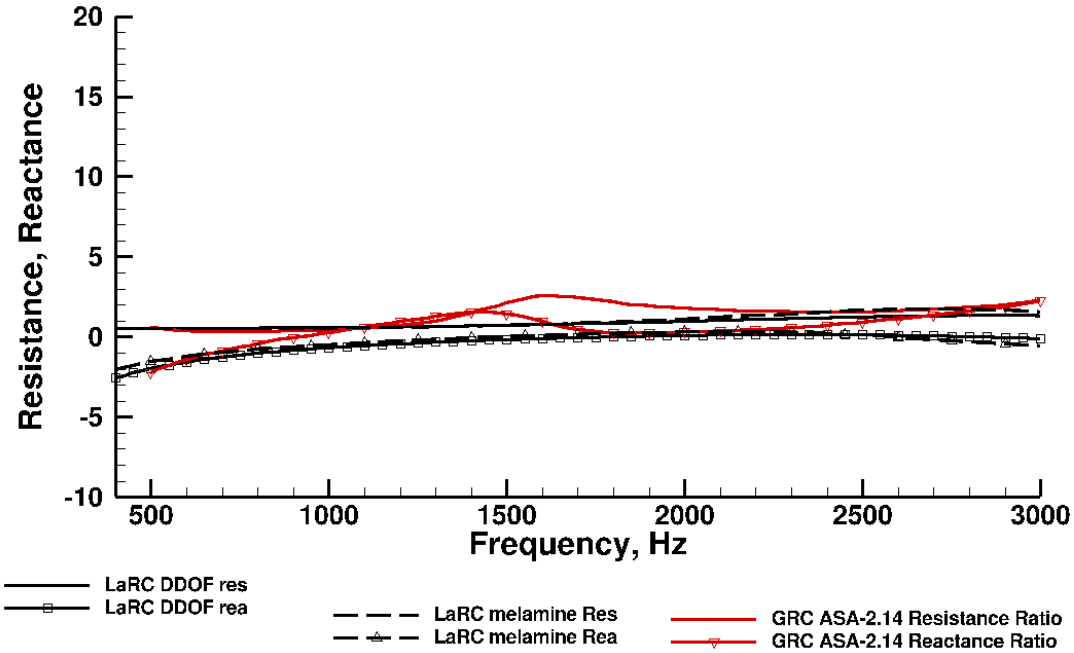

Figure A.49.—The variation of resistance and reactance with frequency for prototype ASA-2.14.

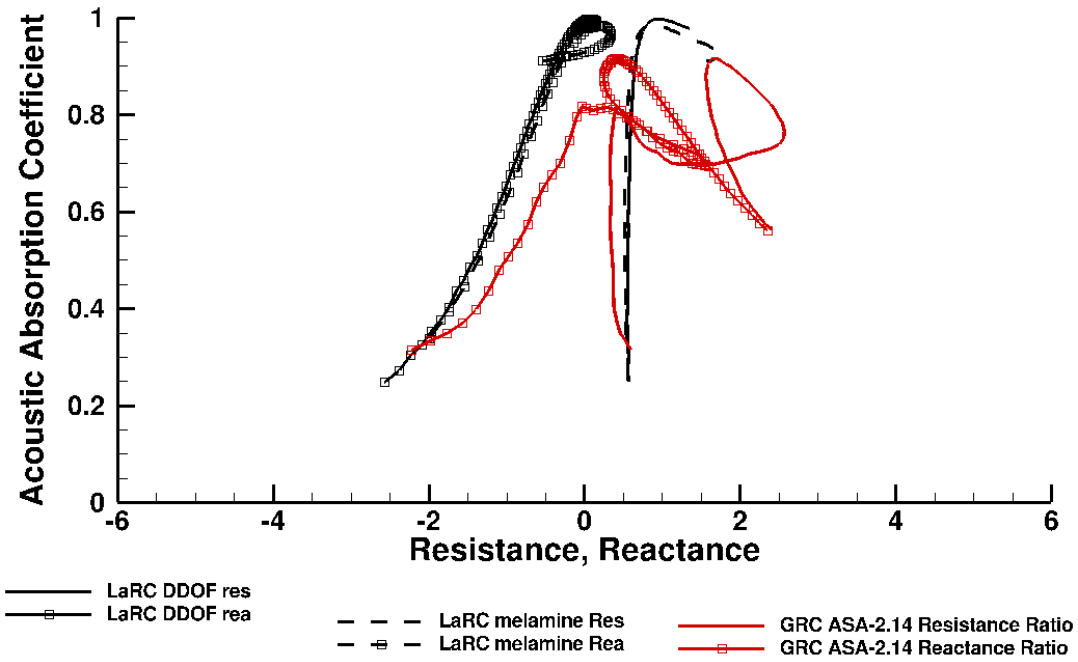

Figure A.50.—The variation of acoustic absorption coefficient with resistance and reactance for prototype ASA-2.14.

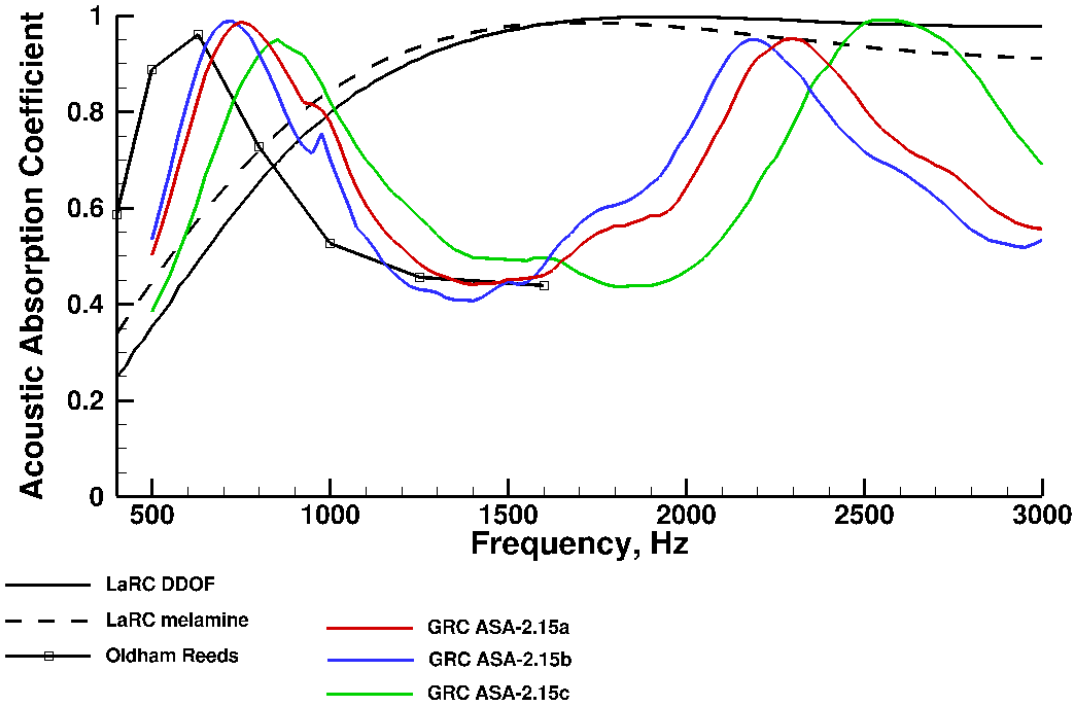

Figure A.51.—The variation of acoustic absorption coefficient with frequency for prototype ASA-2.15.

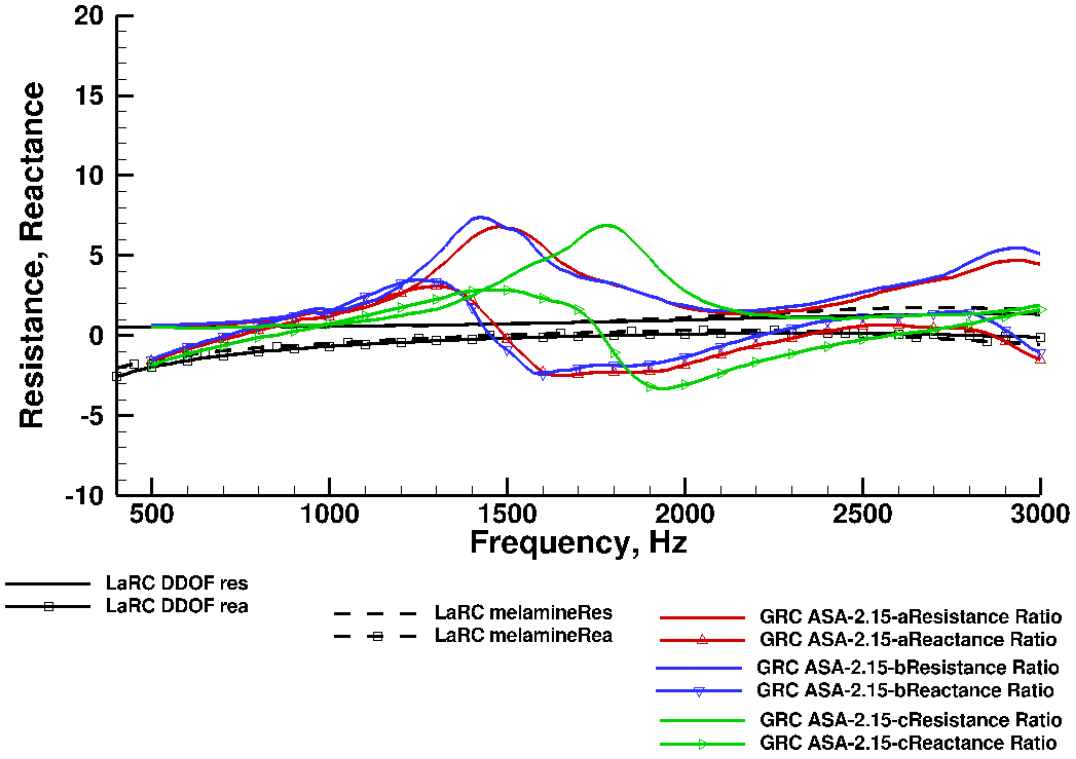

Figure A.52.—The variation of resistance and reactance with frequency for prototype ASA-2.15.

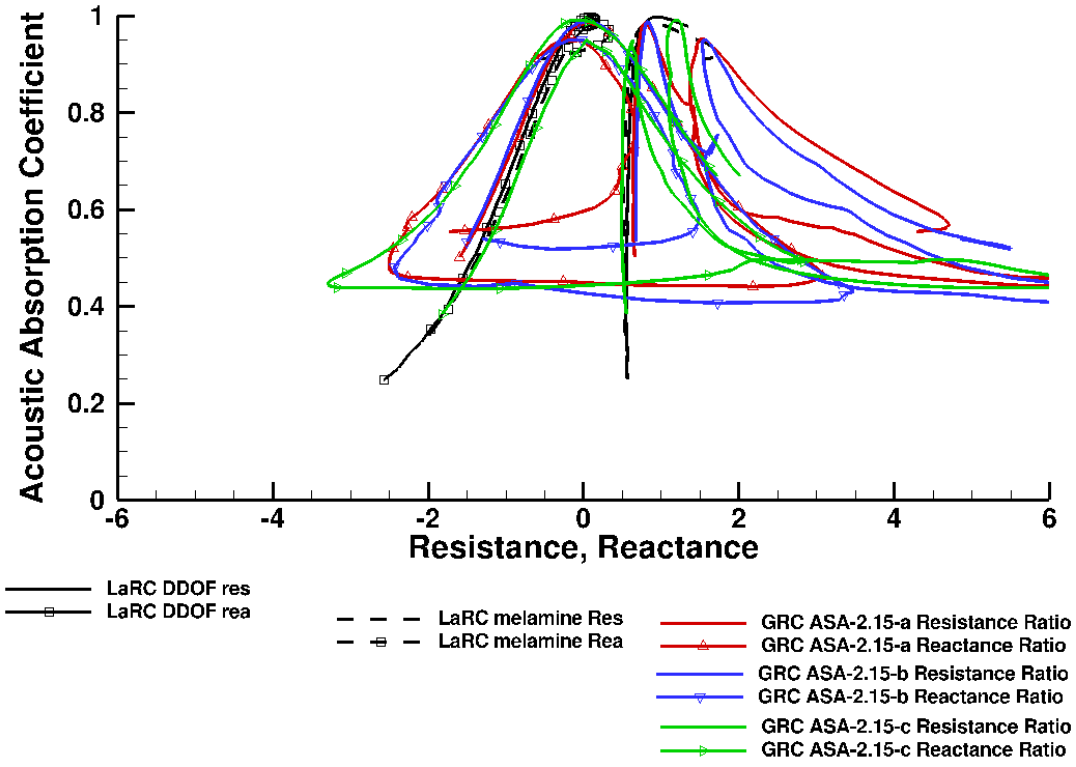

Figure A.53.—Variation of acoustic absorption coefficient with resistance and reactance for prototype ASA-2.15.

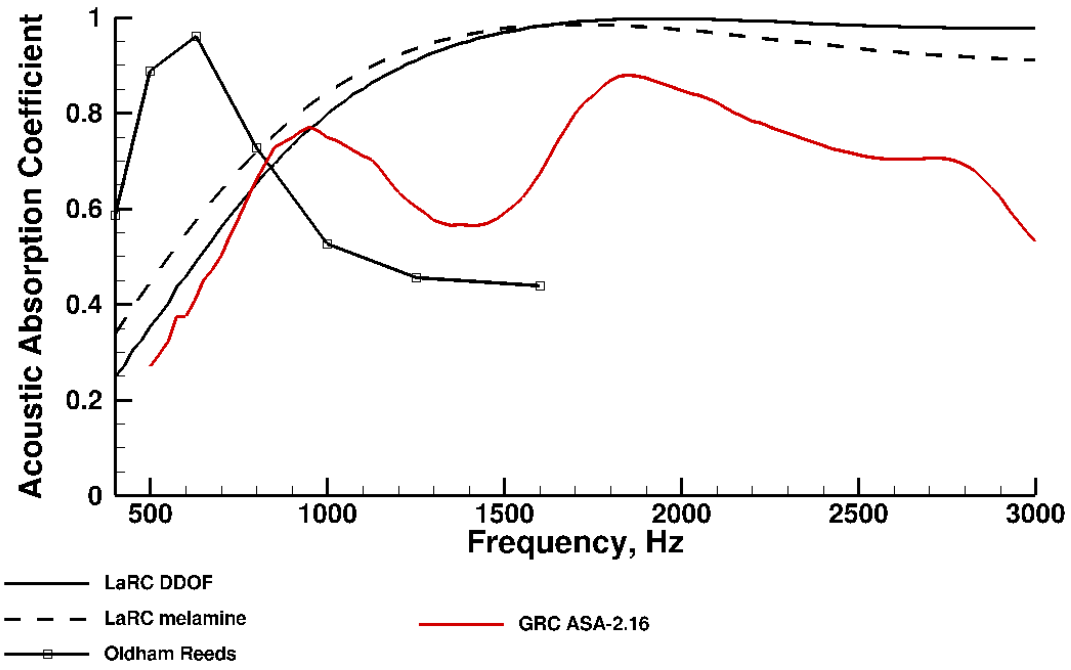

Figure A.54.—The variation of acoustic absorption coefficient with frequency for prototype ASA-2.16.

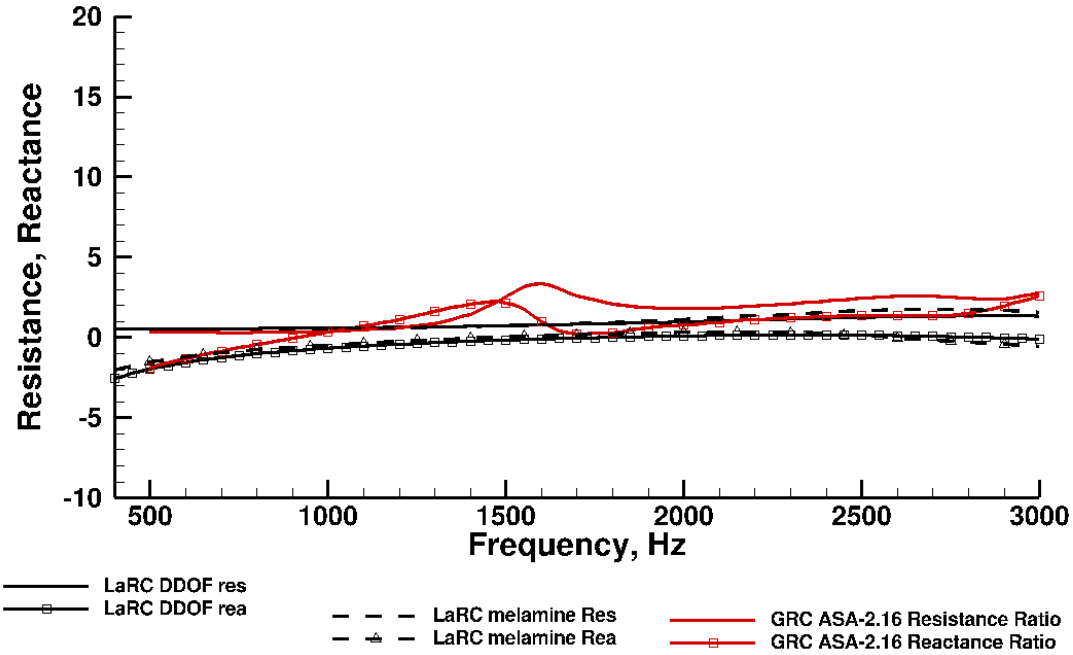

Figure A.55.—The variation of resistance and reactance with frequency for prototype ASA-2.16.

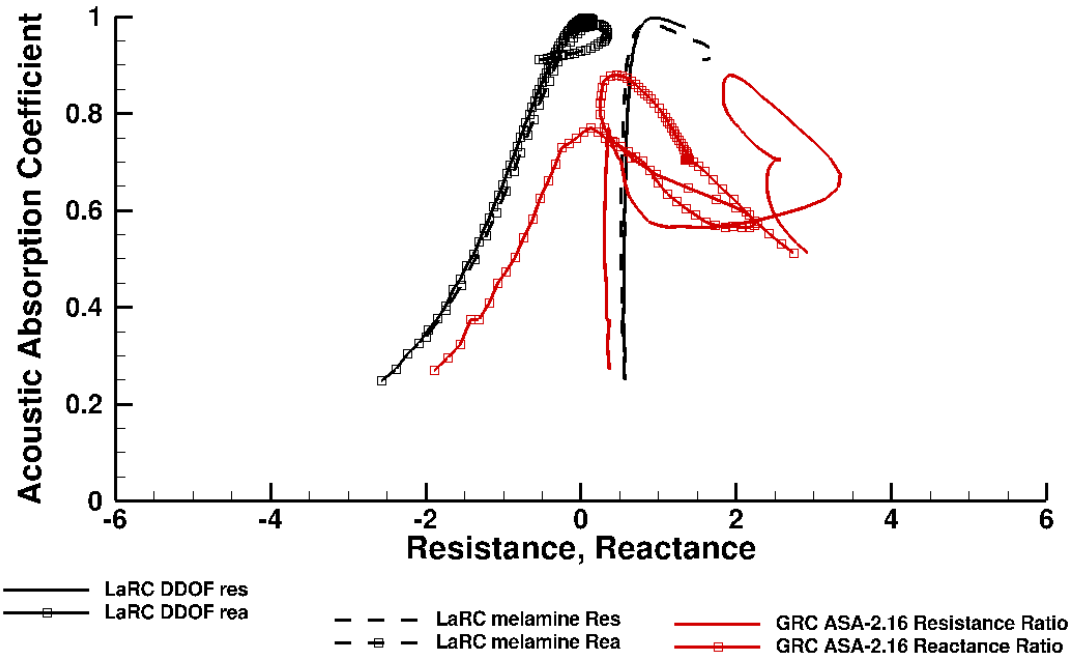

Figure A.56.—The variation of acoustic absorption coefficient with resistance and reactance for prototype ASA-2.16.

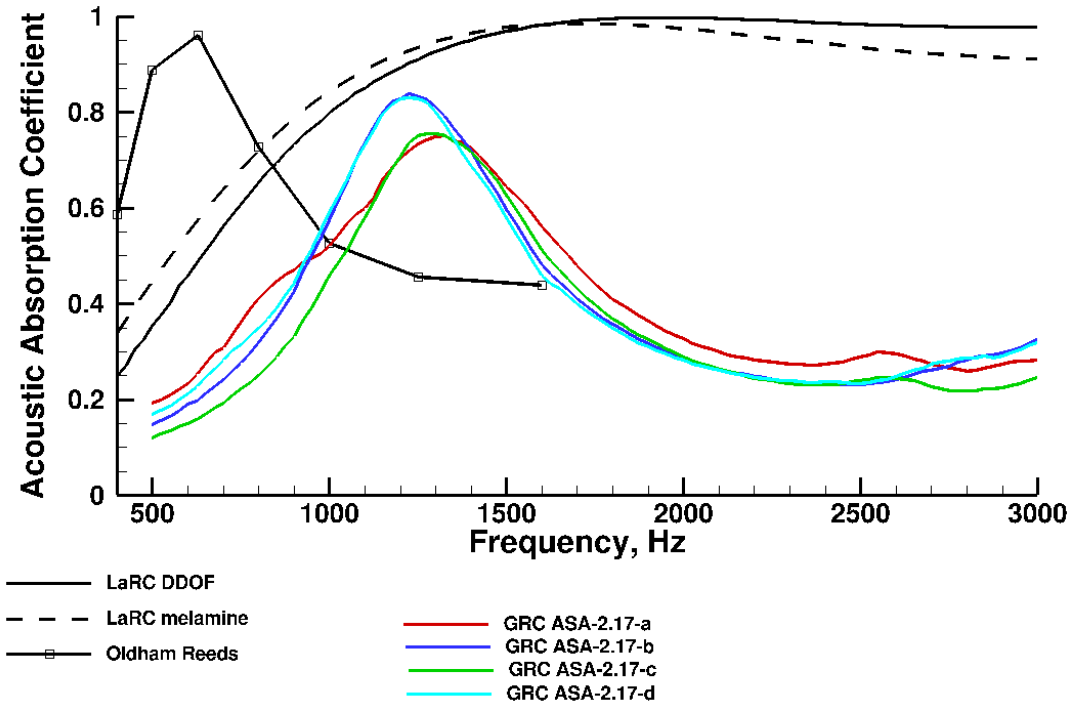

Figure A.57.—The variation of acoustic absorption coefficient with frequency for prototype ASA-2.17.

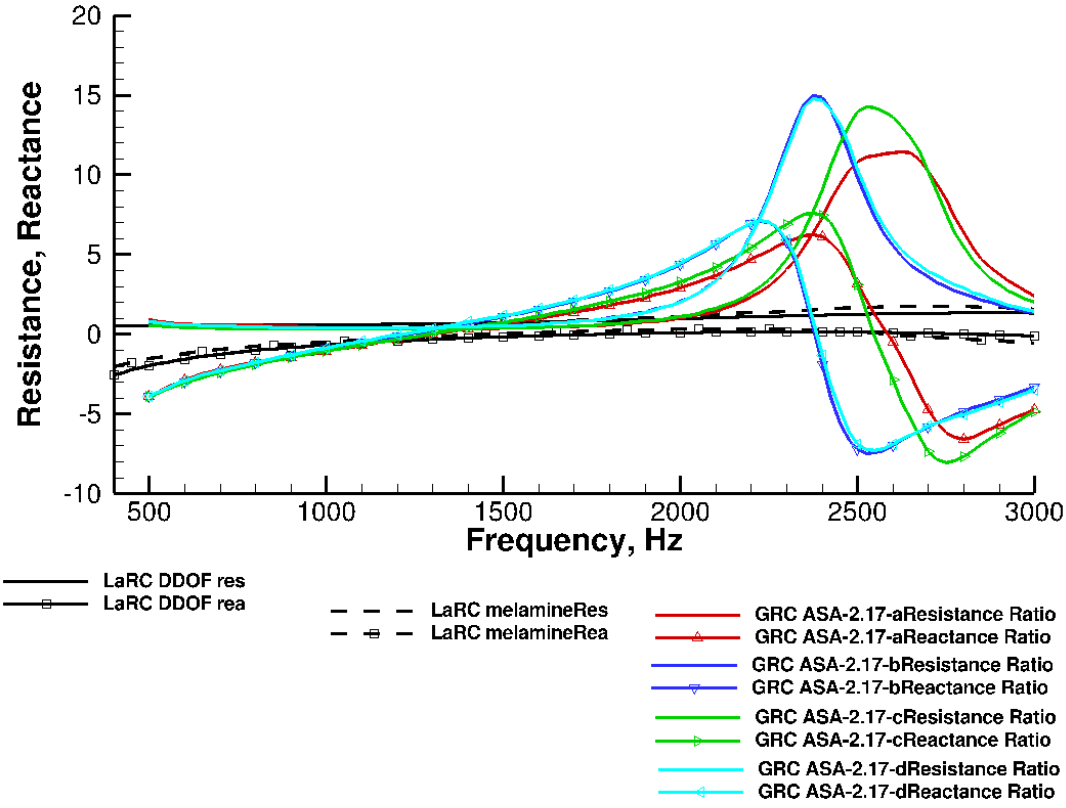

Figure A.58.—The variation of resistance and reactance with frequency for prototype ASA-2.17.

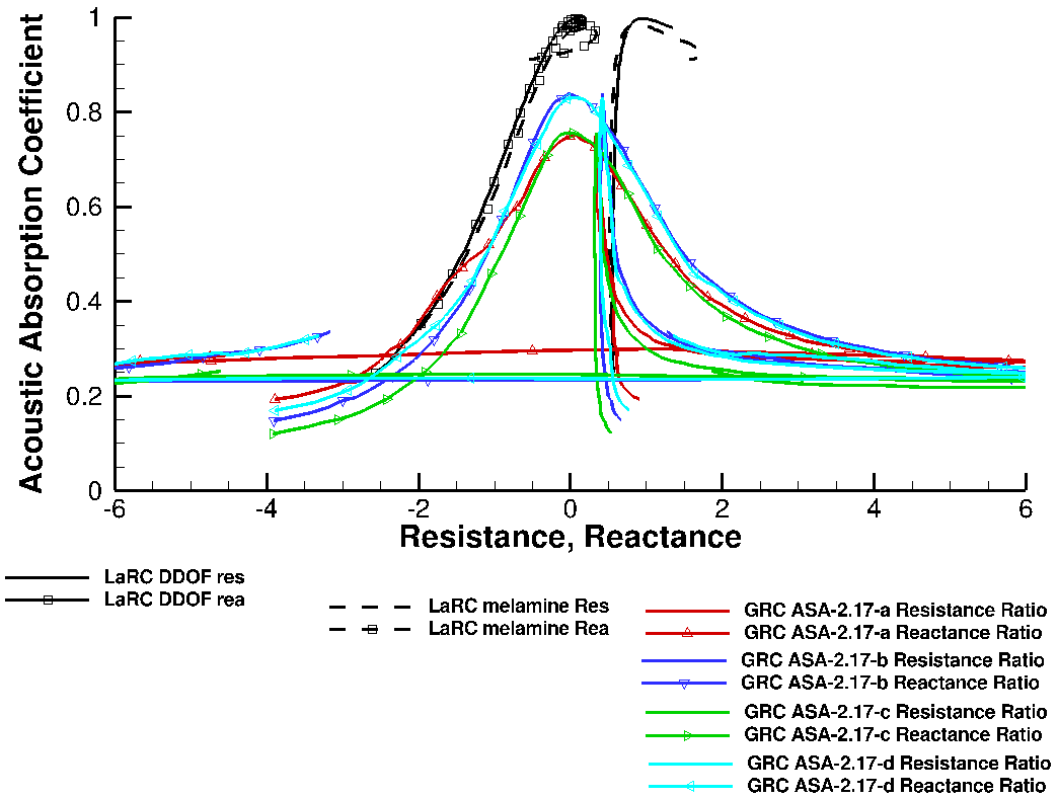

Figure A.59.—The variation of acoustic absorption coefficient with resistance and reactance for prototype ASA-2.17.

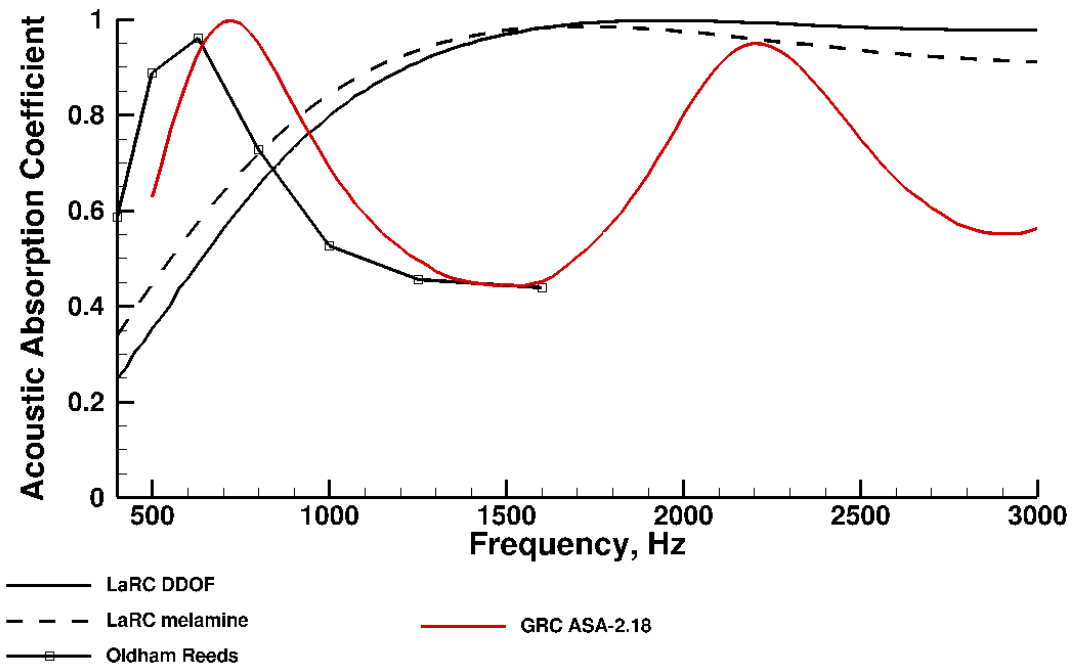

Figure A.60.—The variation of acoustic absorption coefficient with frequency for prototype ASA-2.18.

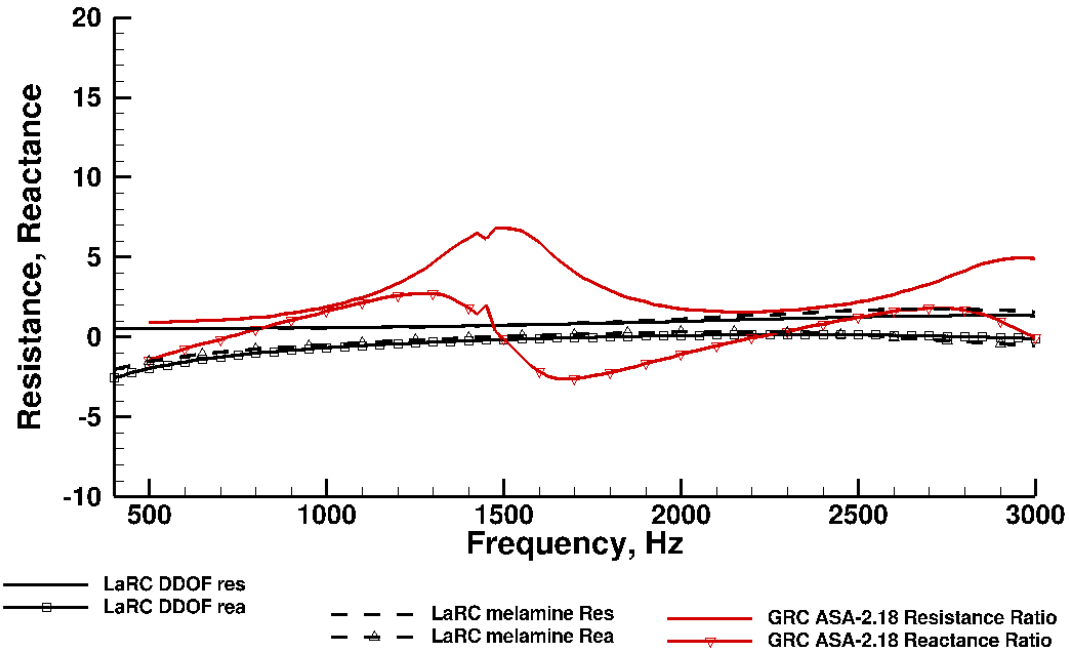

Figure A.61.—The variation of resistance and reactance with frequency for prototype ASA-2.18.

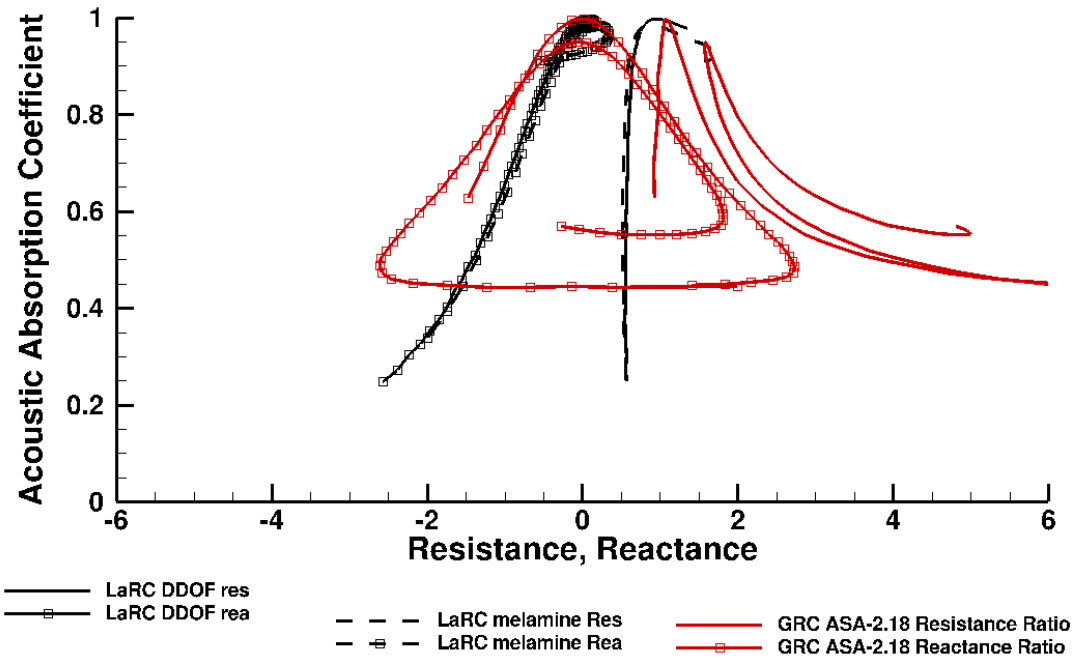

Figure A.62.—The variation of acoustic absorption coefficient with resistance and reactance for prototype ASA-2.18.

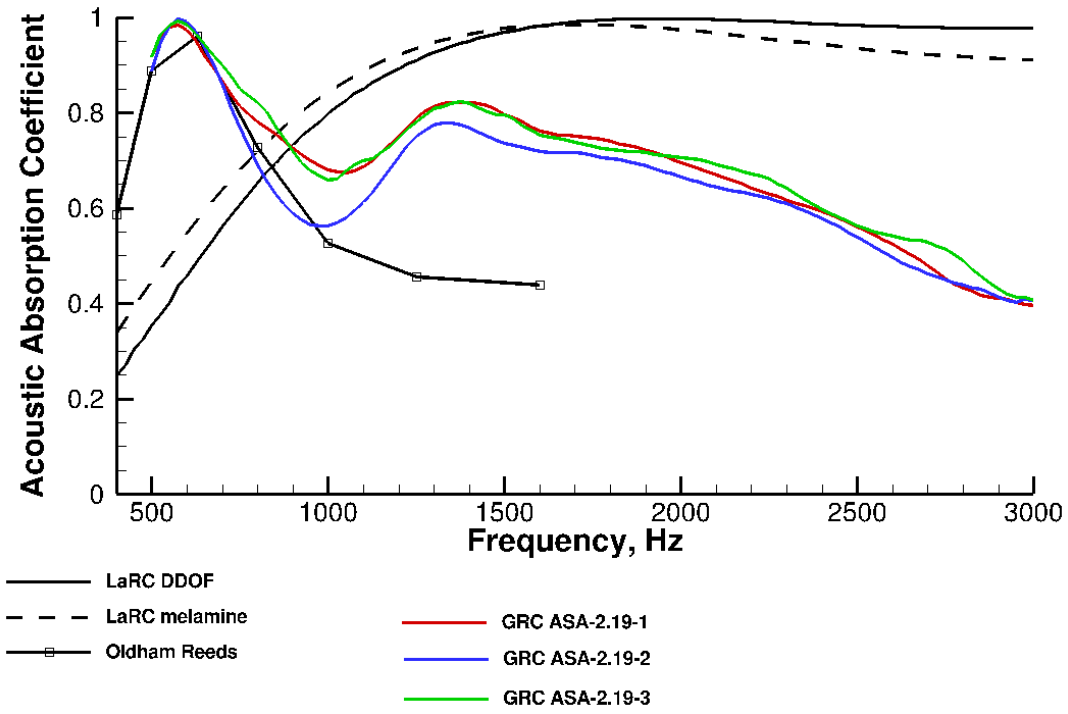

Figure A.63.—The variation of acoustic absorption coefficient with frequency for prototype ASA-2.19.

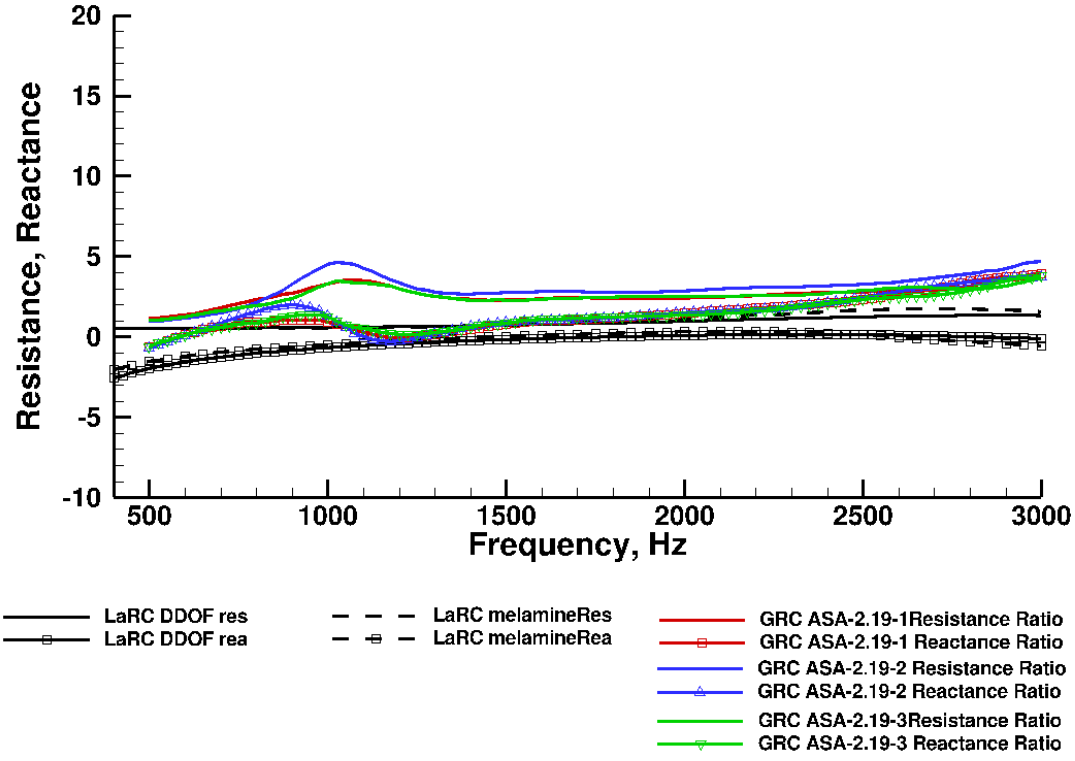

Figure A.64.—The variation of resistance and reactance with frequency for prototype ASA-2.19.

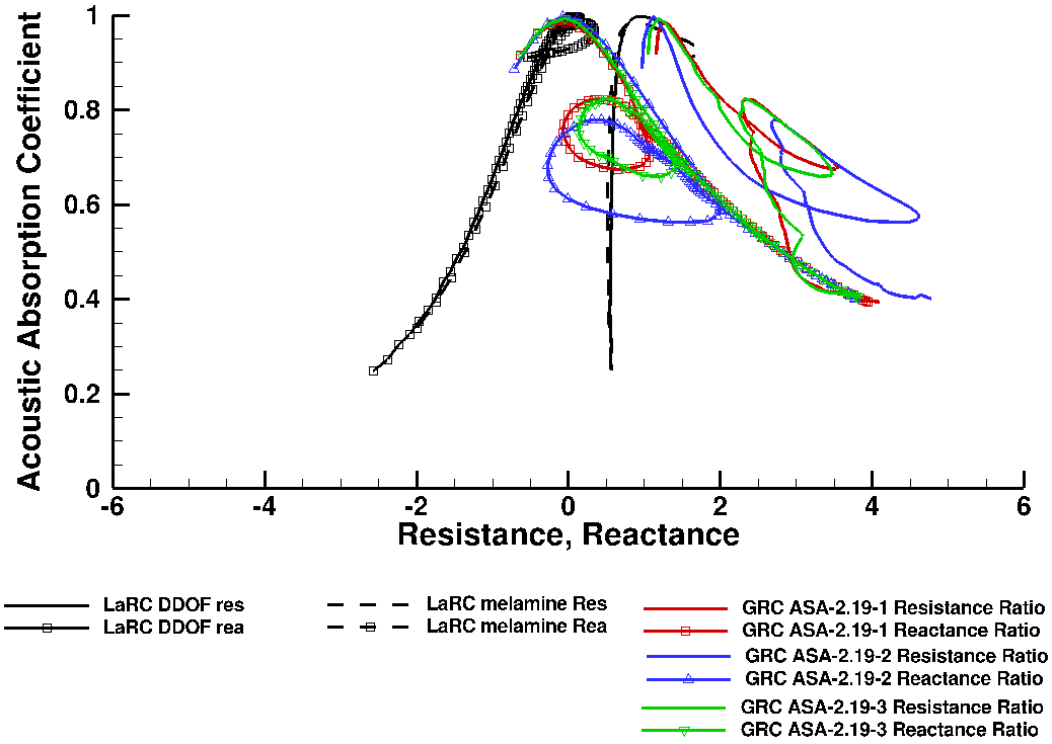

Figure A.65.—The variation of acoustic absorption coefficient with resistance and reactance for prototypes ASA-2.19.

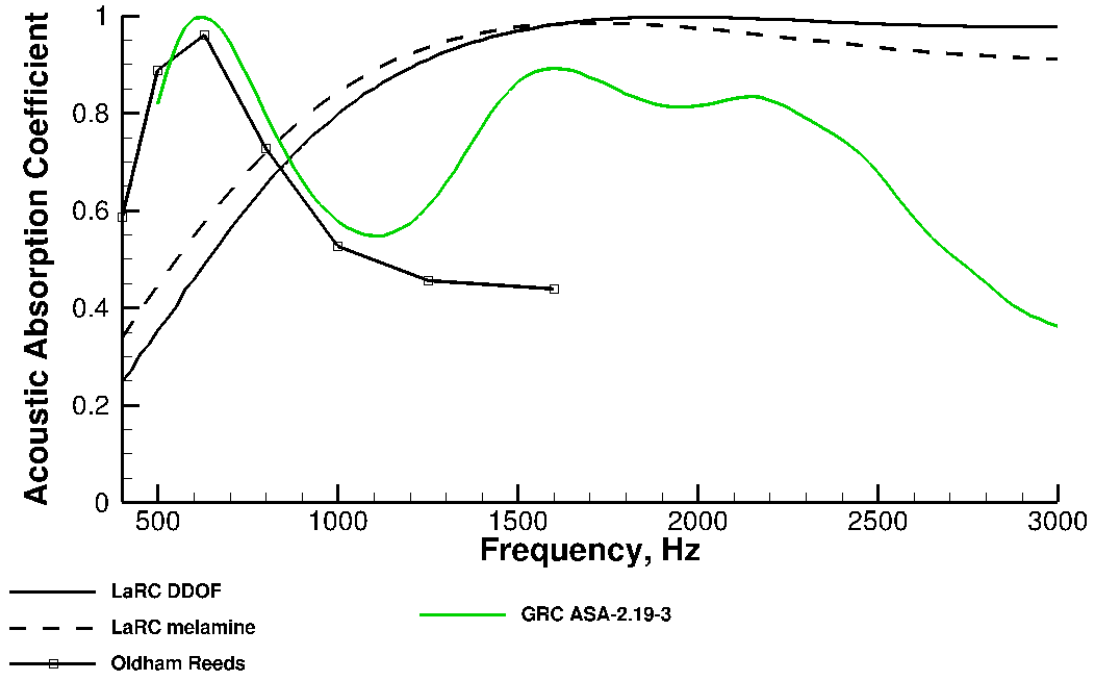

Figure A.66.—The variation of acoustic absorption coefficient with frequency for prototype ASA-2.19.2.

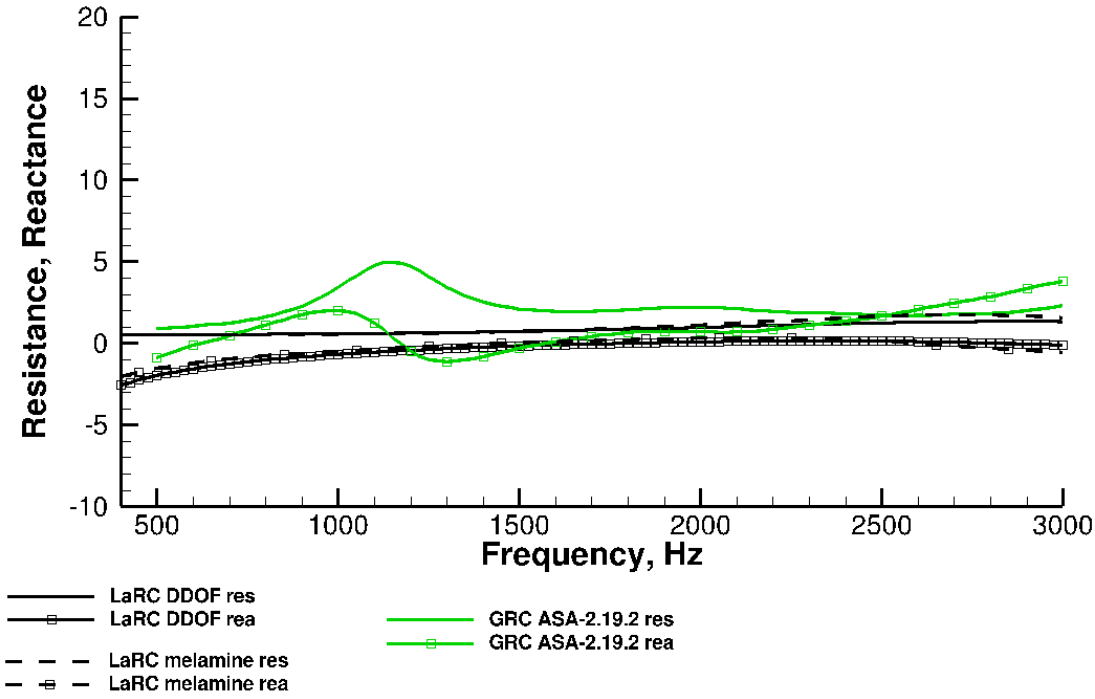

Figure A.67.—The variation of resistance and reactance with frequency for prototype ASA-2.19.2.

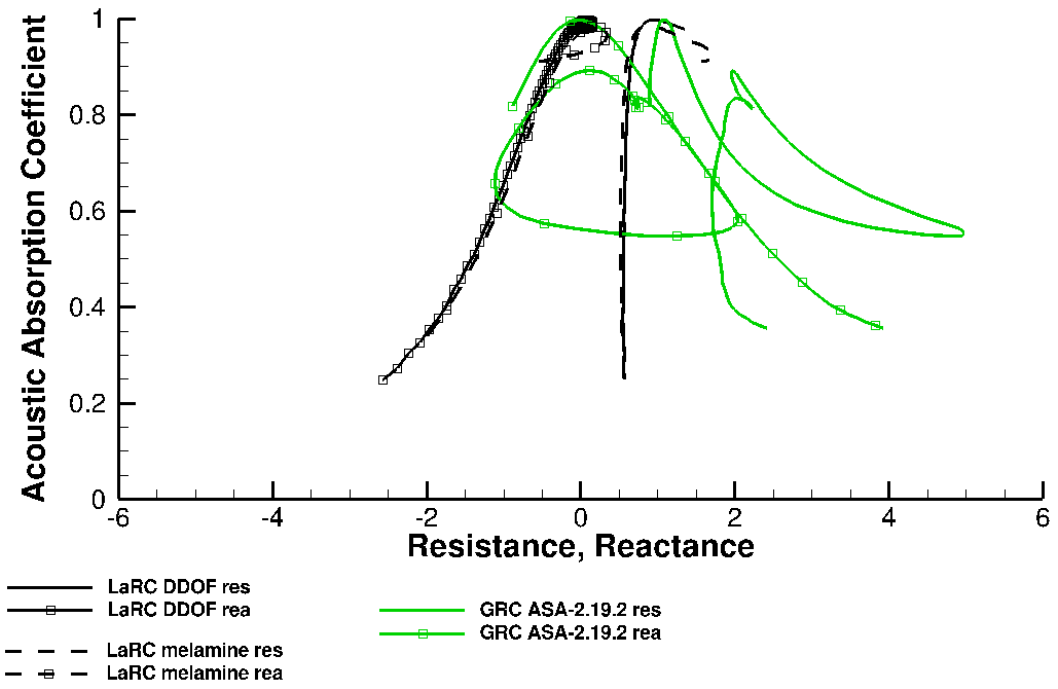

Figure A.68.—The variation of acoustic absorption coefficient with resistance and reactance for prototypes ASA-2.19.

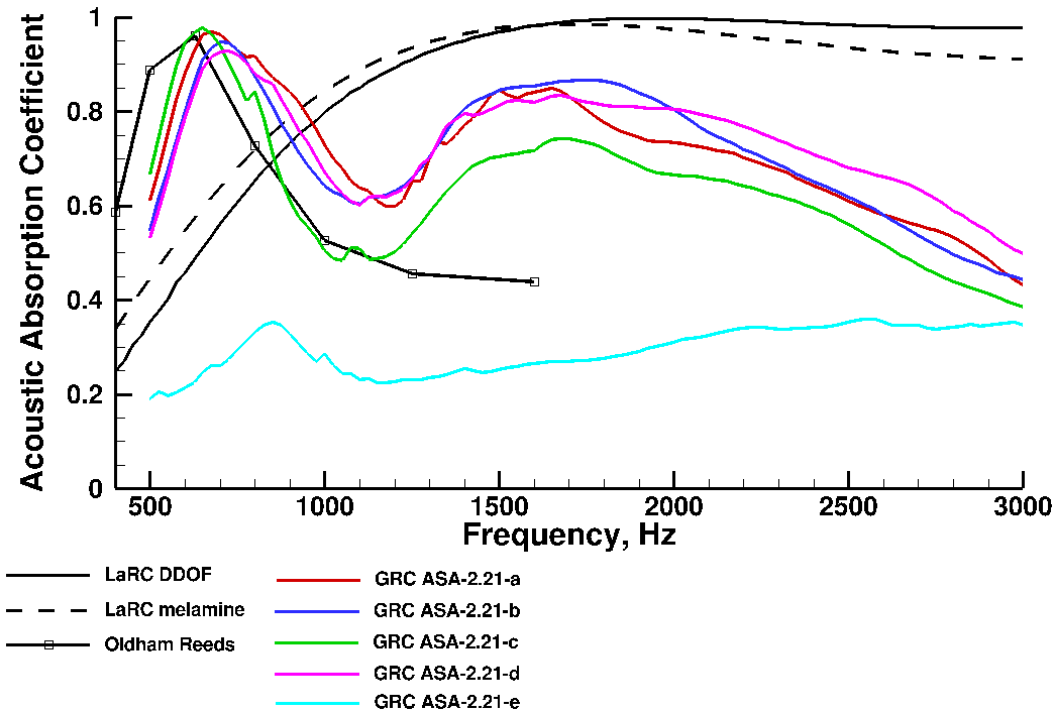

Figure A.69.—The variation of acoustic absorption coefficient with frequency for prototype ASA-2.21.

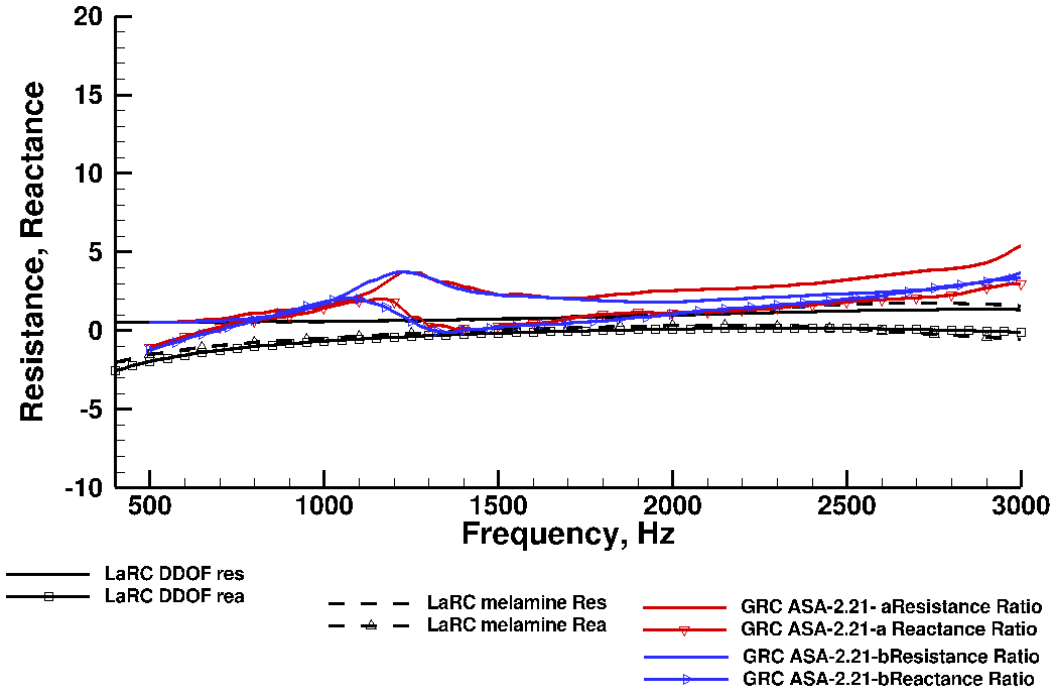

Figure A.70.—The variation of resistance and reactance with frequency for prototype ASA-2.21.

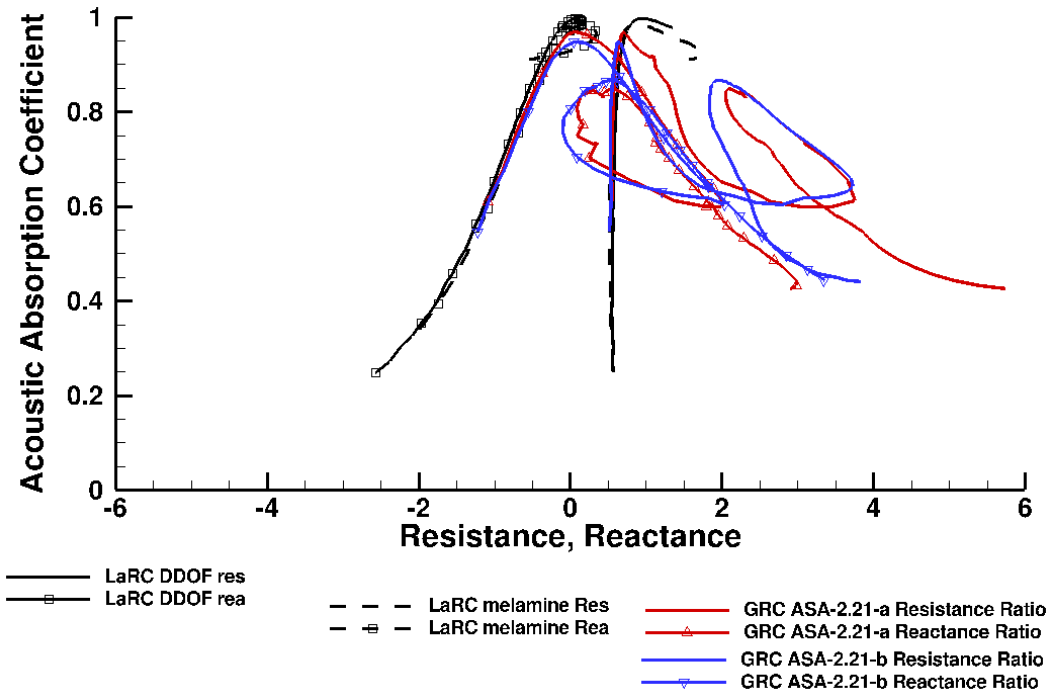

Figure A.71.—The variation of acoustic absorption coefficient with resistance and reactance for prototypes ASA-2.21.

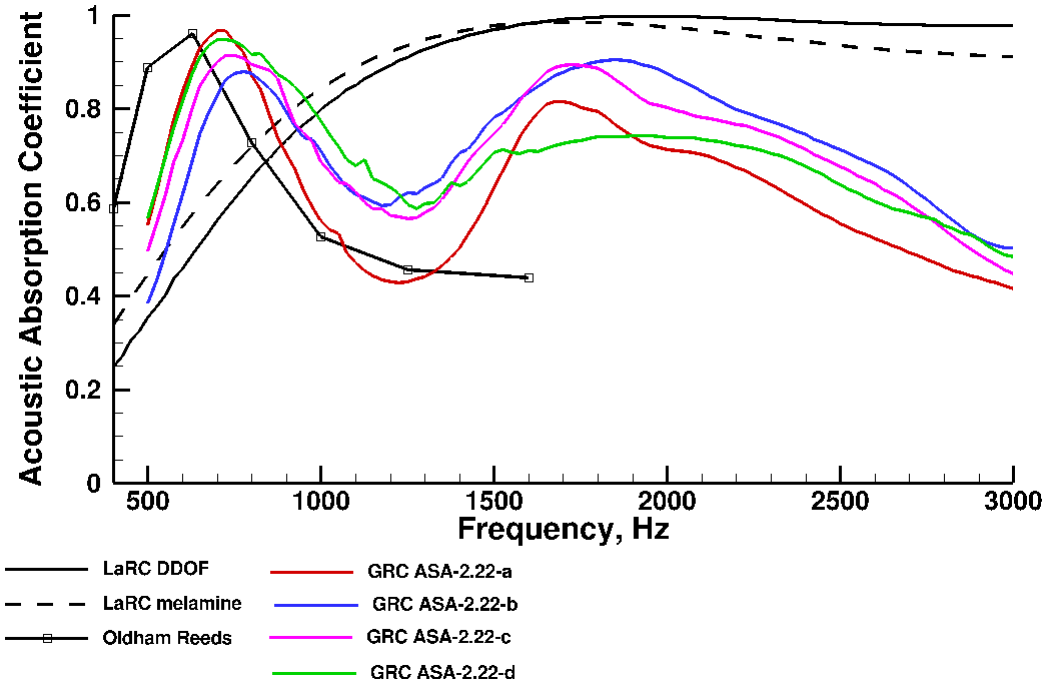

Figure A.72.—The variation of acoustic absorption coefficient with frequency for prototype ASA-2.22.

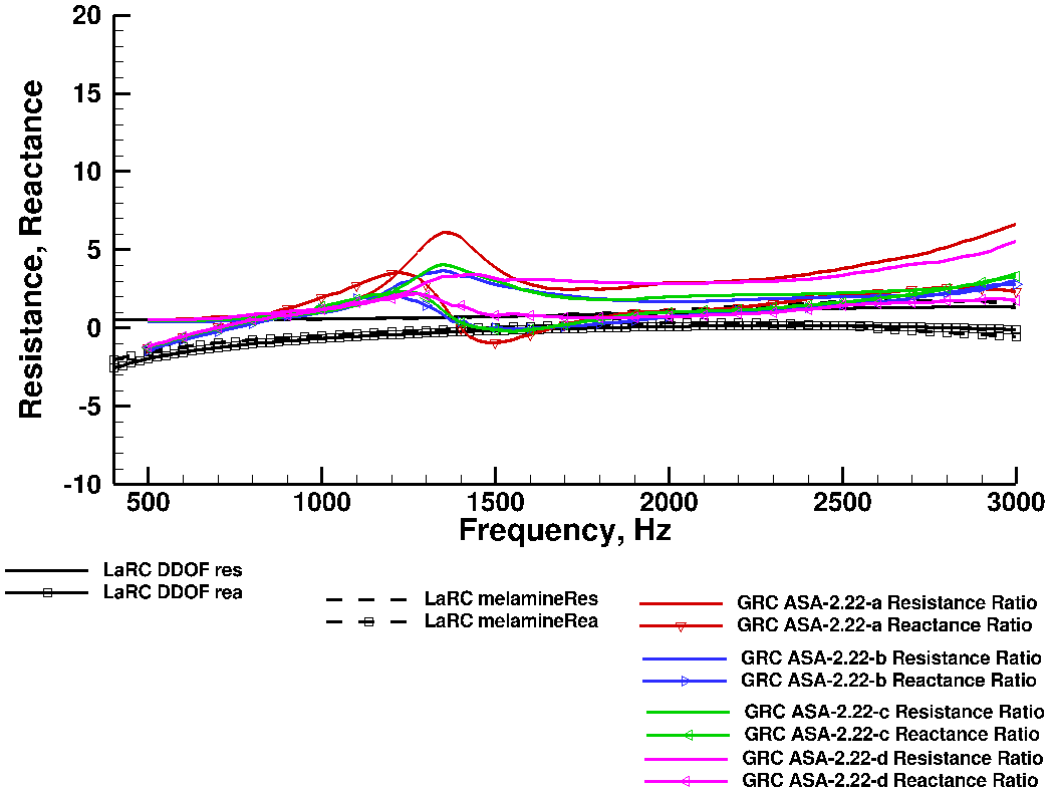

Figure A.73.—The variation of resistance and reactance with frequency for prototype ASA-2.22.

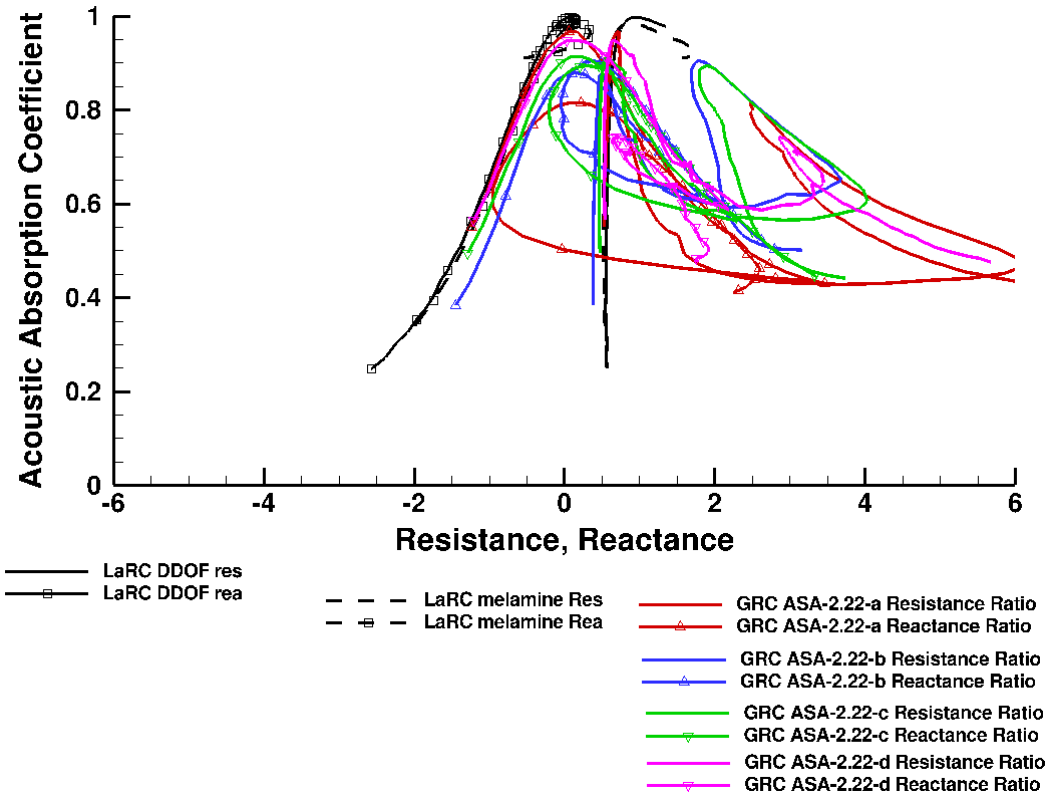

Figure A.74.—The variation of acoustic absorption coefficient with resistance and reactance for prototypes ASA-2.22.

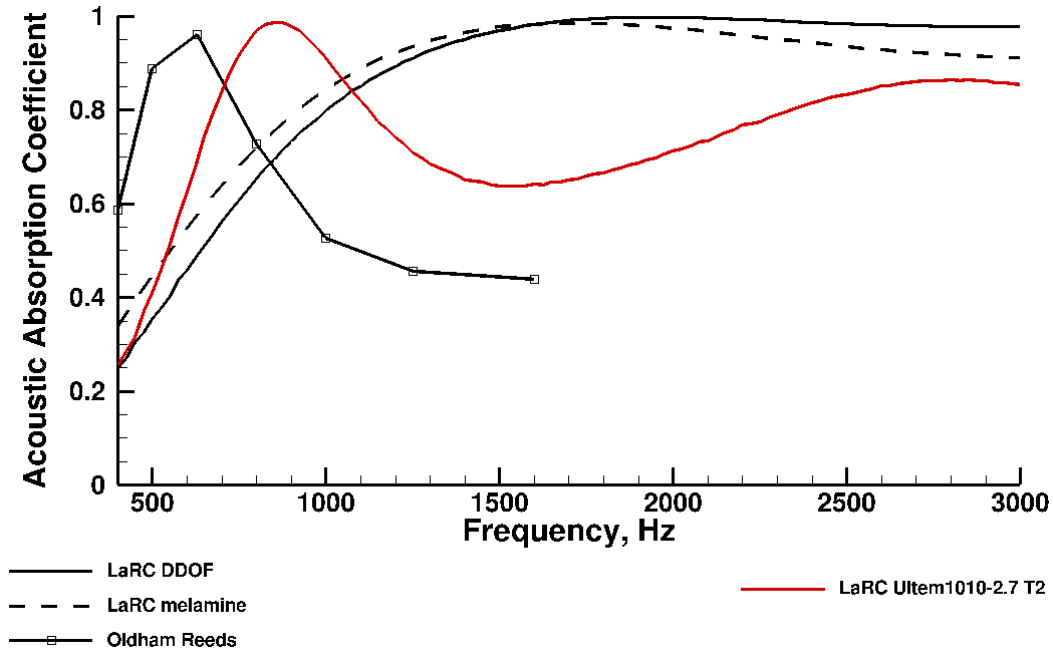

Figure A.75.—The variation of acoustic absorption coefficient with frequency for prototype Ultem 1010-2.7.

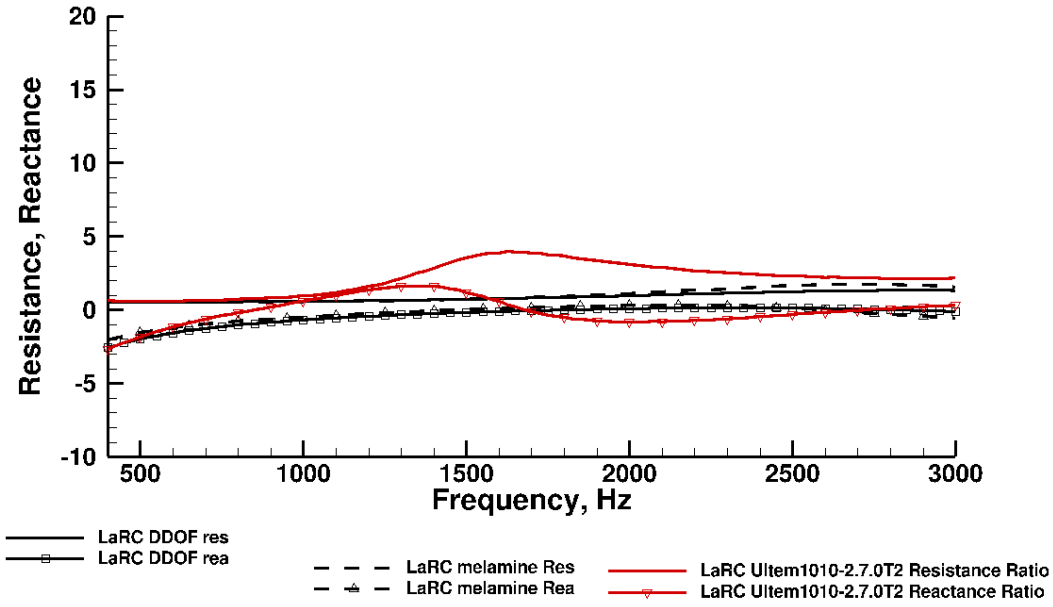

Figure A.76.—The variation of resistance and reactance with frequency for prototype Ultem 1010-2.7.

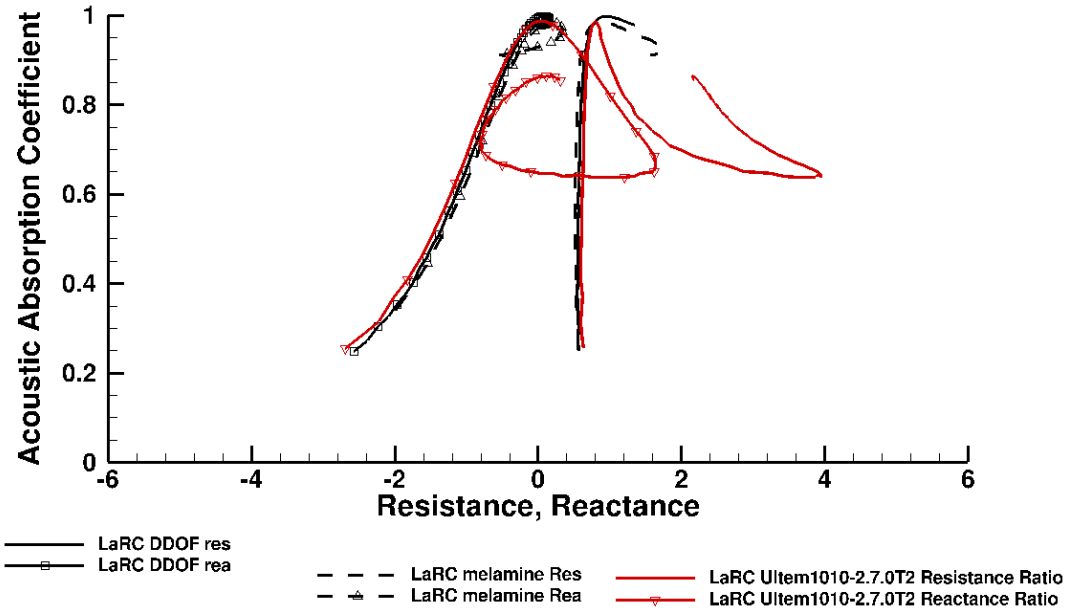

Figure A.77.—The variation of acoustic absorption coefficient with resistance and reactance for prototypes Ultem 1010-2.7.

References

1. U.S. Department of Transportation, Bureau of Transportation Statistics, "Table 1-11: Number of U.S. Aircraft, Vehicles, Vessels, and Other Conveyances." 2019. https://www.bts.gov/content/number-us-aircraft-vehicles-vessels-and-other-conveyances.
2. Falchi, F. et al. "The new world atlas of artificial night sky brightness." *Science Advances*, Vol. 2, No. 6, 2016,
3. Mennitt, D., Fristrup, K. M., Sherrill, K.,Nelson, L. "Mapping sound pressure levels on continental scales using a geospatial sound model." *Proceedings of Internoise 2013*, 2013,
4. United States Department of Transportation, Bureau of Transportation Statistics, National Transportation Noise Map. "National Transportation Noise Map," 2020. https://maps.bts.dot.gov/services/rest/directories/arcgisoutput/Utilities/PrintingTools_GPServer/_ags_bc331eb8eb8a44fa845de8e8879cedbe.pdf. Accessed 04/06/2020.
5. International Civil Aviation Organization, "Annual Report of the ICAO Council: 2018: Presentation of 2018 Air Transport Statistical Results," 2018, https://www.icao.int/annual-report-2018/Documents/Annual.Report.2018_Air%20Transport%20Statistics.pdf. Accessed 04/06/2020.
6. Federal Aviation Administration, "FAA Aerospace Forecast: Fiscal Years 2020-2040," 2020.
7. International Civil Aviation Organization, "Onboard a Sustainable Future: ICAO's Environment Report 2016," 2016.
8. Ozcan, H. K., Nemlioglu, S. "In-Cabin Noise Levels During Commercial Aircraft Flights." *Canadian Acoustics*, vol. Vol 34, no. 4, 2006, pp. 31-35.
9. Brown, M. C., Jones, M. G. "Effects of Cavity Diameter on Acoustic Impedance of Perforate-Over-Honeycomb Liners," AIAA-2017-4189, 2017.
10. Sutliff, D. L., Jones, M. G. "Low-speed fan noise attenuation from a foam-metal liner." *Journal of aircraft*, vol. 46, no. 4, 2009, pp. 1381-1394.
11. Sutliff, D. L., Jones, M. G., Hartley, T. C. "High-speed turbofan noise reduction using foam-metal liner over-the-rotor." *Journal of aircraft*, vol. 50, no. 5, 2013, pp. 1491-1503.
12. Jones, M. G., Watson, W. R., Nark, D. M., Howerton, B. M. "Evaluation of a variable-impedance ceramic matrix composite acoustic liner," AIAA-2014-3352, 2014.
13. Koch, L. D. "Status of NASA's Bio-inspired Broadband Acoustic Absorber," presented at the NASA Acoustics Technical Working Group Meeting, 2020.
14. Koch, L. D. "Investigation of a Bio-Inspired Liner Concept," NASA-E-DAA-TN-41029, 2017.
15. Koch, L. D. "NASA's Bio-Inspired Acoustic Absorber Concept," GRC-E-DAA-TN47193, 2017.
16. Koch, L. D. et al. Broadband acoustic absorbers, U.S. 10,460,714 B1, United States Patent and Trademark Office, 2019.
17. Oldham, D. J., Egan, C. A.,Cookson, R. D. "Sustainable acoustic absorbers from the biomass." *Applied Acoustics*, vol. 72, no. 6, 2011, pp. 350-363.
18. Stratasys. "ASA, A UV-Stable, Production-Grade Thermoplastic for Fortus 3D Production Systems." Stratasys, 2020, https://info.stratasysdirect.com/rs/626-SBR-192/images/Data%20Sheet%20-%20ASA%20EN.pdf. Accessed 08/10/2020 2020.
19. Jones, M. G., Watson, W. R., Nark, D. M., Howerton, B. M.,Brown, M. C. "A Review of Acoustic Liner Experimental Characterization at NASA Langley." 2020,
20. Chung, J. Y., Blaser, D. A. "Transfer function method of measuring in-duct acoustic properties. I. Theory." *Journal of the Acoustical Society of America*, vol. 68, no. 3, 1980, pp. 907.
21. Jones, M. G., Parrott, T. L. "Evaluation of a multi-point method for determining acoustic impedance." *Journal of Mechanical Systems and Signal Processing*, vol. 3, no. 1, 1989, pp. 15-35.